INTERPRETATION OF RADIO ECHO SOUNDING IN POLAR ICE SHEETS

By G. de Q. ROBIN, S. EVANS, AND J. T. BAILEY†
Scott Polar Research Institute, Cambridge

(*Communicated by Sir Edward Bullard, F.R.S.—Received* 4 *September* 1968—
Revised 17 *February* 1969)

[Plates 10 and 11]

CONTENTS

† Died in Dronning Maud Land, Antarctica, 12 October 1965 (see *Nature, London*, **209**, no. 5018, 18–19). From September 1963 to May 1964 Bailey worked with Evans on development of the equipment for use in Greenland. The first half of the 1964 field traverses were carried out by the three authors, then Bailey took over full responsibility for the northern traverse and the return journey from Century to Tuto. He took an active part in the early discussions of the results, when many of the ideas presented in this paper were formed.

Vol. 265. A. 1166. (Price £2. 3*s*.; U.S. $5.60) 44 [Published 18 December 1969

Experimental results are presented from a traverse over the ice sheet of north western Greenland in 1964, during which a continuously recorded profile of ice thickness was obtained for the first time. Interpretation of data from this traverse is consistent with results of subsequent work to December 1967. The parameters of the apparatus are presented briefly, while the details of electronic circuits are being published separately.

Theoretical problems of radio wave propagation in an ice sheet and, in particular, the factors affecting accuracy are discussed. The uncertainty in depth, over a small area, is ± 5 m $\pm 1.5\%$ and this is verified by comparison with the seismic results for a range of depths up to 1.5 km. It is found that the only real uncertainty arises in irregular terrain.

The effectiveness of the radio echo technique is dependent on the absorption of radio waves in ice. Temperature, and to a lesser extent the impurity content of ice, appear to be the main variables affecting field performance. Earlier laboratory results on the variation of absorption with temperature for ice cores from northwest Greenland, together with theoretically predicted temperature distributions throughout the ice mass, have provided estimates of the total loss by absorption. These estimates are reasonably consistent with the observed echo strengths over most of the traverse. Consequently, it is predicted that echoes can be obtained over considerable areas of the ice sheets of Greenland and Antarctica, as has been verified by subsequent observations. The reflexion coefficient at the ice/rock interface is of the order of -15 dB. It could rise to 0 dB for an ice/water interface and one area was found in Greenland where it appeared to fall to -30 dB.

Results from this traverse have shown that local surface slopes on the ice sheet are largely controlled by variations of longitudinal stress along the line of flow. Regional slopes over several kilometres vary with the velocity of movement of the ice, but appear to be less dependent on basal ice temperatures than laboratory results would suggest. The velocity of ice movement increases in proportion to the square or cube of the basal shear stress, but the stress itself shows no obvious dependence on basal ice temperature.

Partially reflecting layers discovered within the ice mass are discussed mainly in terms of small density variations between adjacent layers of ice. One particularly prominent layer is calculated to be about 1000 years old and its variation of depth with position provides evidence in favour of the steady state model of the ice sheet.

LIST OF SYMBOLS

a_n radius of nth Fresnel zone
$\dot{a}$ rate of accumulation (in depth of water equivalent per year)
A total dielectric absorption (dB) for two-way path
b radius of bubble
B ratio of the amplitudes: constant to random component of reflected wave
c velocity of light in vacuum
C constant in the Glen law for the flow of ice
d depth of ice perpendicular to the bed, at a central point
E echo strength (dB above the limit of detectability)
$\mathscr{E}$ electric field strength
f radio frequency
F_1 longitudinal force
g gravitational acceleration
g_b backward-scattering power gain
g_t transmitting aerial power gain
g_i increase in power gain due to refraction
G geometrical factors in echo power equation
h height above the base of an ice sheet
H total vertical thickness of an ice sheet (H_0 at the origin of a flow line)
k thermal diffusivity

l	thickness of an individual ice layer
L	lapse rate; temperature with height above sea level
m	number of bubbles/metre^3
n	refractive index
N	a constant of the ray path on refraction
p_t	transmitted peak power
p_r	received peak power
r	range (r_0 perpendicular range)
δr	range difference
R	reflexion coefficient, power ratio or dB
s_r	absorption cross-section of a receiving aerial
s_s	scattering cross-section
s_b	backward scattering cross-section
S	system performance (dB) (ratio of transmitter peak power to minimum detectable power in receiver)
t	time, since the arrival of the first echo return
t_0	$=2r_0/v$, echo delay from the normal point
t_x	travel time, via x
t_c	correction to travel time due to varying velocity
t_d	difference in travel times
t_p	pulse duration
t_r, t_f	rise time and fall time of pulse envelope
u	horizontal velocity of ice
v	radio propagation velocity
V_p	compressional wave velocity
w	pressure in atmospheres
x	horizontal coordinate measured along a flow line
y	depth from ice surface (dy, thickness of ice stratum)
Y	characteristic value of y in exponent
z	separation of transmitter and receiver
α	slope of the ice surface (suffixes indicate components)
β	small scale slope of the ice bed features
γ	polarizability
$\tan\delta$	dielectric dissipation constant
Δ	density difference from solid ice
ϵ	relative permittivity $= \epsilon' - j\epsilon''$ (suffixes indicate different media)
$\dot{\epsilon}$	strain rate (suffixes indicate components)
θ	temperature (suffixes indicate location)
λ	radio wavelength in the medium of propagation
μ	dipole moment
ν	constant of proportionality between strain rate components
ρ	specific gravity (ρ_i, ρ_s, ice and snow)
$\delta\rho$	difference in specific gravity
σ	electrical conductivity
σ_x^0	$=(\sigma_x - \sigma_y)$ where σ_x and σ_y are the components of longitudinal stress along the flow line, x, and in the vertical, y
τ	shear stress at the base of an ice sheet
ϕ	angle to the normal in ray propagation
ω	angular radio frequency
Ω	solid angles (dΩ elementary solid angle)

1. Introduction

This paper is concerned with a radio echo method of penetrating naturally occurring ice masses to obtain information about the bulk of ice and the nature of the underlying terrain. At present our knowledge of the thickness of the major ice sheets of the world is based on seismic shooting techniques, supplemented by frequent measurements of gravity. These techniques and the results obtained in the Antarctic have been reviewed in many publications, most recently by Bentley (1964). The principal limitations are that seismic reflexion techniques give a sounding of the ice depth at a single location, together with the variation of depth over a distance of half the length of the seismometer spread (commonly 200 or 300 m). Gravity

measurements indicate the average depth over an area whose radius around the point of observation is of the same order as the depth of ice. The calibration of gravity data by seismic reflexion shooting is therefore far from ideal unless the bedrock is flat and uniform in composition. The continuous record of depth obtained by radio echo sounding from a moving vehicle provides a new dimension in the study of ice sheets. The advance may be compared to that which occurred in the study of the ocean floor when continuous echo sounding by ultrasonic means replaced the spot soundings obtained primarily by lead and line methods such as the Kelvin sounding machine. It appears likely that the radio echo sounding technique will prove successful over most areas of polar ice sheets; as yet we have no experience of the application to temperate glaciers and ice caps.

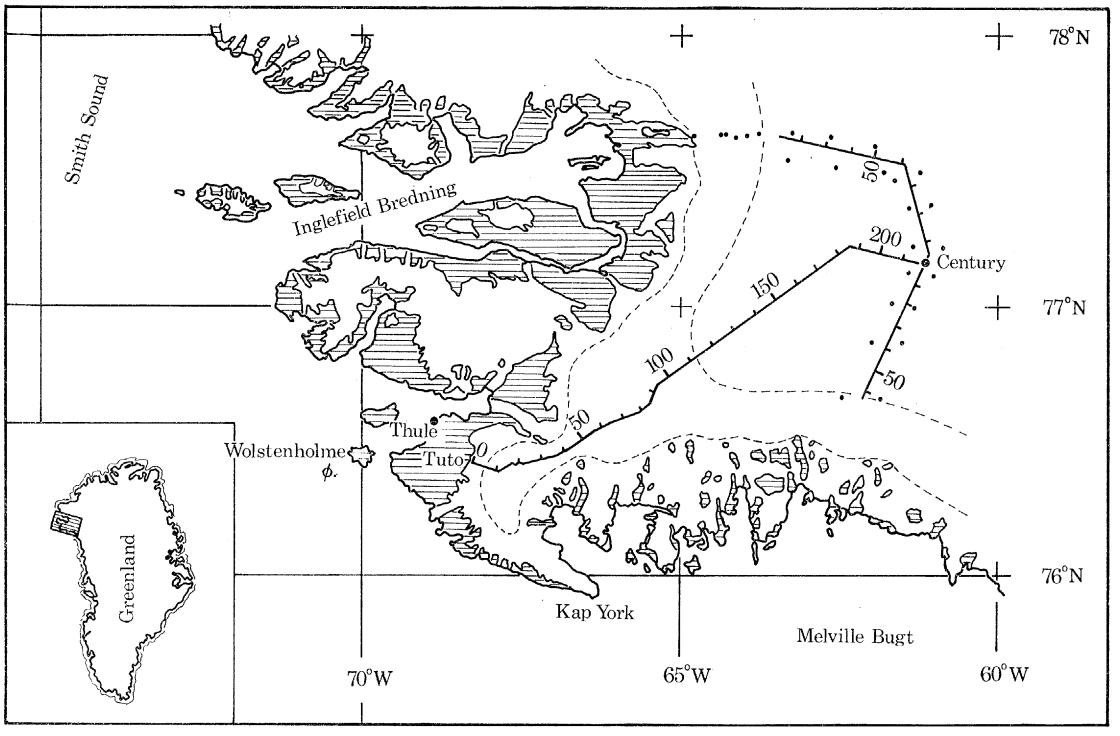

FIGURE 1. Map of northwest Greenland showing the radio echo sounding routes travelled in the summer of 1964. The main trail runs from Tuto to Century and the distance is marked at 10 km intervals from Tuto. The northern and southern traverses are marked in kilometres from Century and the adjacent spots show the position of poles in Mock's strain network. The form lines are at approximately 750 m intervals.

The analogy to echo sounding at sea also applies to the capacity of the radio echo sounding system to detect echoes from small irregularities within the ice mass, particularly within the top few hundred metres. If a particular layer within the ice can be identified over large horizontal distance as reported later, the deformation of such a layer as it flows over irregular bedrock can be used to throw further light on the processes of glacier flow. The same approach may also be useful for multiple layering in the ice which can define the general 'field' of ice movement in a similar manner to the way in which iron filings are used to demonstrate the distribution of a magnetic field.

An earlier paper (Evans 1963) has described how attention was drawn to the technique.

This paper will assess the possibilities and practical limitations as they are at present, will develop some basic equations for the interpretation of records, and discuss results obtained in the field, mainly on a visit to Greenland in summer 1964 (Bailey, Evans & Robin 1964). The operations were the second phase of a cooperative programme of field work designed to evaluate radio echo sounding techniques, to compare results with seismic and gravity surveys,

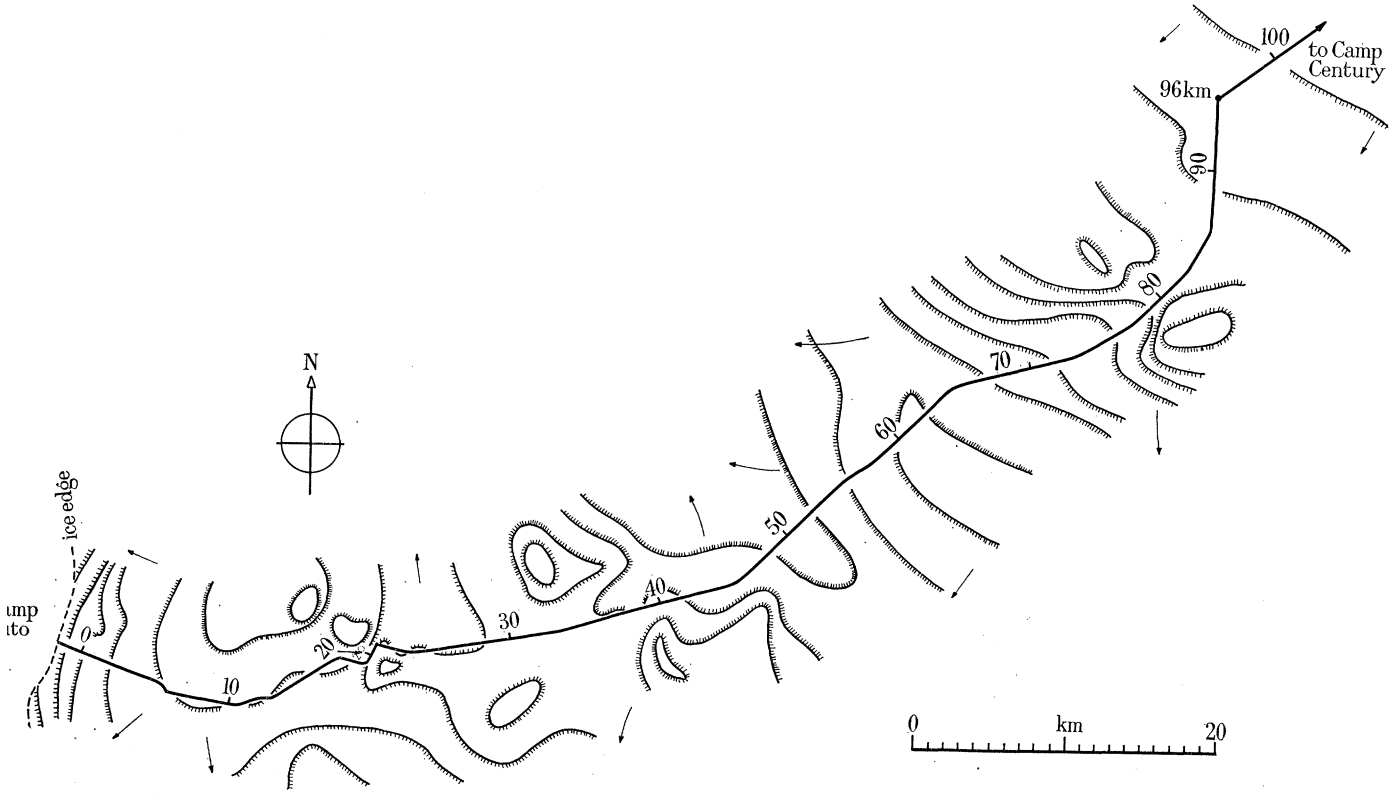

FIGURE 2. Detailed map of the main trail from 0 to 100 km (after J. N. Rinker, U.S. Army C.R.R.E.L. unpublished memorandum dated April 1966). The form lines, at approximately 100 m intervals, are shaded on the downslope side and the main drainage directions are indicated by arrows.

and to continue measurements of strain rate in the ice sheet. All the logistic arrangements were managed by the U.S. Army Research Support Group and information about the field operations, the participating agencies, and personnel has been published by Rinker (1965). Over a part of the journey, Waite (1966) operated radio echo equipment which, while differing in practical arrangement, was the same in principle as the Scott Polar Research Institute (S.P.R.I.) apparatus whose parameters are described below. A recent progress report on radio echo sounding (Evans 1967) lists all known field work from 1963 to 1966 inclusive, and summarizes the main results.

2. Region of operations and navigation

Figure 1 is a map showing the part of northwest Greenland where radio echo observations were made in the summer of 1964. At the edge of the ice sheet near Thule is the U.S. Army Research Support Group Headquarters known as Tuto, and from here the section of the route

referred to in this paper as the main trail, runs inland to Camp Century. The distances are marked in kilometres from the upper end of the Tuto ramp which gives access to the ice sheet. The route was surveyed and marked by the U.S. Army in 1952 and 1953 in a number of straight courses varying from 0.7 to 17 km in length up to 96 km ('Mile 60', 'Station 1–0', 'Point Alpha', or 'Station Morris' in various U.S. Army publications) and straight beyond that. Crevasses were filled by bulldozer. Since that time the trail has meandered, some corners have been cut, and the present route information was compiled with the help of J. N. Rinker of U.S.A. C.R.R.E.L., from air photographs taken in 1963. Figure 2 is a more detailed map of the main trail from 0 to 96 km and it includes form lines at approximately 100 m intervals, taken from the 1953 survey. A number of key positions, shown on the map in figure 1, were originally determined by astrofix and may be assumed accurate now to ± 2 km. The routes which extend each way from Camp Century are referred to in this paper as the northern and southern traverses; the distances are marked from the outskirts of Camp Century and the zeros are separated by about 2 km. These two routes were laid out by Mock in 1962 (Mock 1967) and the positions of glaciological marker poles used for strain-rate measurements are shown by the spots to either side of the northern and southern traverse in figure 1. The relative positions of these poles were remeasured by tellurometer during the 1964 work and they have been used to calibrate the bicycle-wheel odometer with which all intermediate positions have been interpolated in this paper. From the three independent calibrations given in table 1, a constant scale of 2.20 m/revolution has been adopted throughout. Each section was travelled twice, on an outward and return journey. There is a difference of 2 km in the total distance measured, and differences of the same order or less between positions found for survival huts and other recognizable marks. The radio echo apparatus was in operation the whole time. It was carried with separate transmitting and receiving aerials in two 'Polecat' vehicles for 75 km along the main trail on the outward journey, and in heavy tractor trains for the remainder of the distance except the extreme end of the southern traverse where Polecat vehicles were more suited to the snow conditions. On the part of the outward journey made in the tractor train, recordings were taken from the U.S.A.E.L. transmitter in a separate vehicle and the effect on the overall performance is estimated in table 2. The S.P.R.I. transmitter was used throughout the return journey.

TABLE 1. CALIBRATION OF ODOMETER

	distance	revolutions	$\frac{\text{distance}}{\text{revolution}}$
southern traverse, P 42–4 to P 42–9 by tellurometer	36946 m	16 698	2.21 m
northern traverse, P 42–10 to P 42–20 by tellurometer	76121 m	34 773	2.19 m
main trail, using Century and Tuto astrofixes	226 km	101 621	2.22 m

The elevation above sea level was measured by two Wallace and Tiernan surveying altimeters read to ± 1 ft (0.3 m) at 220 m intervals along the trail. The absolute elevations of these points have been calculated by Mock (1965, and private communication 1965) by averaging the

increments for the two instruments and distributing the accumulated differences between these and a few points of known elevation along the trail, essentially derived from the coast-to-coast theodolite levels given by Patterson (1955). Errors in absolute elevation may be ± 25 m, due mainly to uncertainty in correlation with Patterson's points, and there are differences greater than this over short distances between the elevations which have been adopted in our plots and those given in the 1953 U.S. Army survey. The form lines in figure 2 should not be taken for contours though they are arranged to intersect our elevation-profile at 100 m intervals. Differential errors in elevation due to changes in ambient pressure on the other hand should be not greater than ± 1 m/km distance since the vehicles travelled at about 8 km/h, mainly in calm weather.

The accuracy of ice-depth measurement is discussed later in §5, but it will be helpful to describe at this point the main features of the vertical section which has been obtained through the ice; it is illustrated at a 20 to 1 vertical exaggeration in figure 37. There is a major change in the character of the underlying terrain at a distance of 130 km along the main trail. To the coastal side, the bedrock elevations vary from 200 to 1000 m above sea level, but for a distance of at least 100 km further inland the bedrock remains close to 600 m elevation. The character of the radio echoes varies in a related manner, showing that on the small scale, over distances of a few metres, the reflecting surface is rougher in the mountainous region than in the inland plain, as might be expected. The echo strengths were just within the equipment capability in the mountainous region where the ice is near the melting point, but well within the capability for ice depths of the order of 1400 m in the vicinity of Camp Century. The relation of echo strength to the temperature distribution through the ice is discussed in § 6.

As far as may be judged from approximate contours of the snow surface, the southern traverse and north western section of the northern traverse are likely to lie along the ice flow lines, whereas the rest of the routes do not. The main trail lies along the crest of a broad ridge running inland from the Thule peninsula. Thus, in the ice flow studies in § 7, strain-rate and ice-depth measurements complement each other with most profit on the southern traverse and the end of the northern traverse.

Reflexion of radio waves from layered discontinuities within the bulk of the ice is also discussed in §7. It is possible to explain these features by supposing them to be changes in the density of the ice, but much more data about the geographical distribution of occurrence of internal echoes will be necessary to put the hypothesis to a more severe test. The depth of the most prominent, and isolated, layer is shown in figures 36 and 37.

3. Apparatus

A variety of radar systems has been considered and it will help in understanding the choice if our self-imposed requirements are stated; more details of the equipment design are given by Evans & Smith (1969).

The first apparatus was intended to have a sensitivity to detect an echo through as great a thickness of ice as practicable with a range error not greater than 10 m. In the early stages there was great uncertainty regarding the attainable penetration. The overall size, power consumption, and reliability were chosen so that the apparatus could easily be operated on a lightweight oversnow vehicle in motion or in an aircraft, the power to be drawn from the standard vehicle supply.

Pulse modulation of the amplitude of the transmitted wave has been used in the overwhelming majority of commercial applications of radar; possibly the most important reason being that it gathers information rapidly (important in airborne applications) and it can deal with many targets simultaneously. The principle limitations are that it cannot work down to zero range, it cannot reduce the information rate and thereby obtain an increased sensitivity, and in all practical cases it cannot run at as high mean transmitted power as a continuous wave

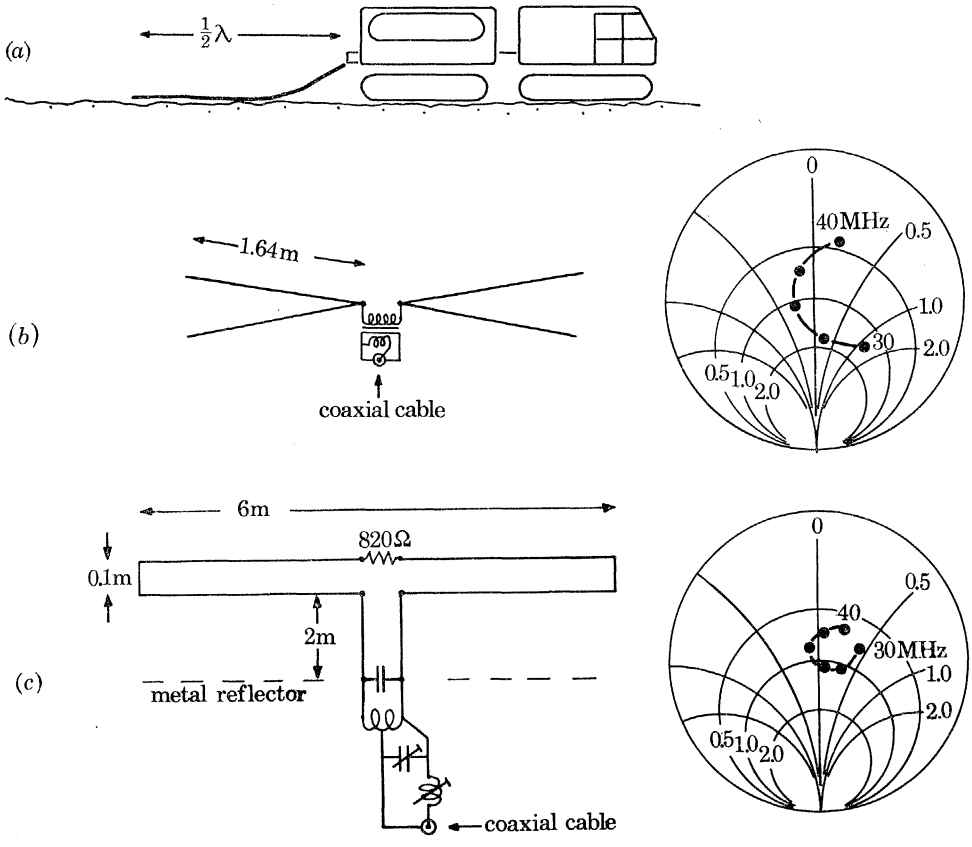

FIGURE 5. Aerial arrangements. (*a*) End-fed wires trailed on the surface behind an oversnow vehicle. Two diverging conductors were used to increase the bandwidth and the unbalanced feed relied on the vehicle frame for a counterpoise. Any trailing arrangement fails to take full advantages of refraction into the denser medium. (*b*) Rigid two-conductor half-wave dipole. The diverging elements consist of copper-cored fibreglass rods having an average characteristic impedance of 150 Ω considered as a balanced transmission line. The resulting free-space admittance at the coaxial feed is plotted to the right on a Smith chart normalized to 20 $m\Omega^{-1}$. The potted matching transformer does not allow essential adjustments to be made after installation close to a vehicle frame. (*c*) Loaded dipole with a tank circuit balun and an adjustable L-match. The forward power gain is greater than for a resonant dipole placed in the same position, in spite of the power loss in the load. An unacceptable fraction of the power is wasted however if the radiators are placed closer than shown to a plane metal reflector. The Smith chart is normalized as in (*b*).

system. The ability of a pulse system to distinguish moving targets is irrelevant in our application. Since details of short range clutter echoes are of considerable interest, the ability to record many targets simultaneously present in the field of view was the overwhelming reason for the choice of a pulse modulated system. The high information rate has to some extent been harnessed in a slow speed photographic recorder which effectively integrates the echoes received during a time interval of the order of one second.

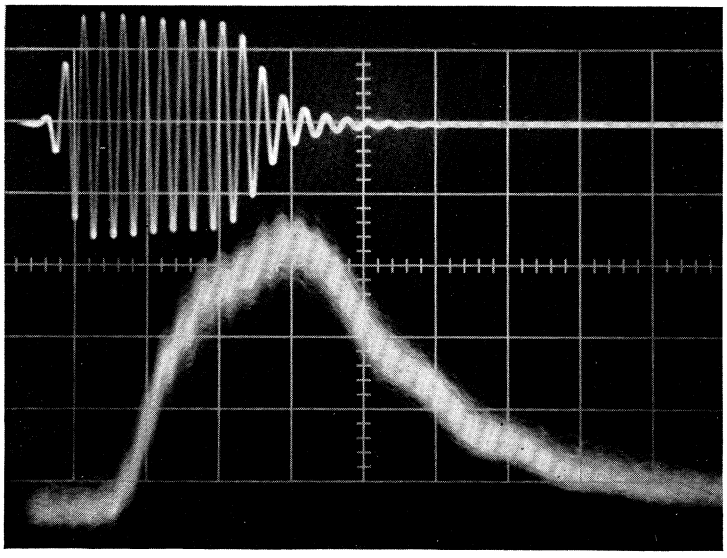

FIGURE 3. At the top, a direct oscillogram of the transmitter output feeding a dummy load. Below: the same pulse, on the same time scale, after attenuation to 15 dB above the input noise level and passage through the receiver. The horizontal scale occupies a total of 1 μs and the vertical scale of volts is arbitrary. The rise time, t_r, is defined as the time for the power to increase from 10 to 90 % of its peak value, and similarly for the fall time, t_f.

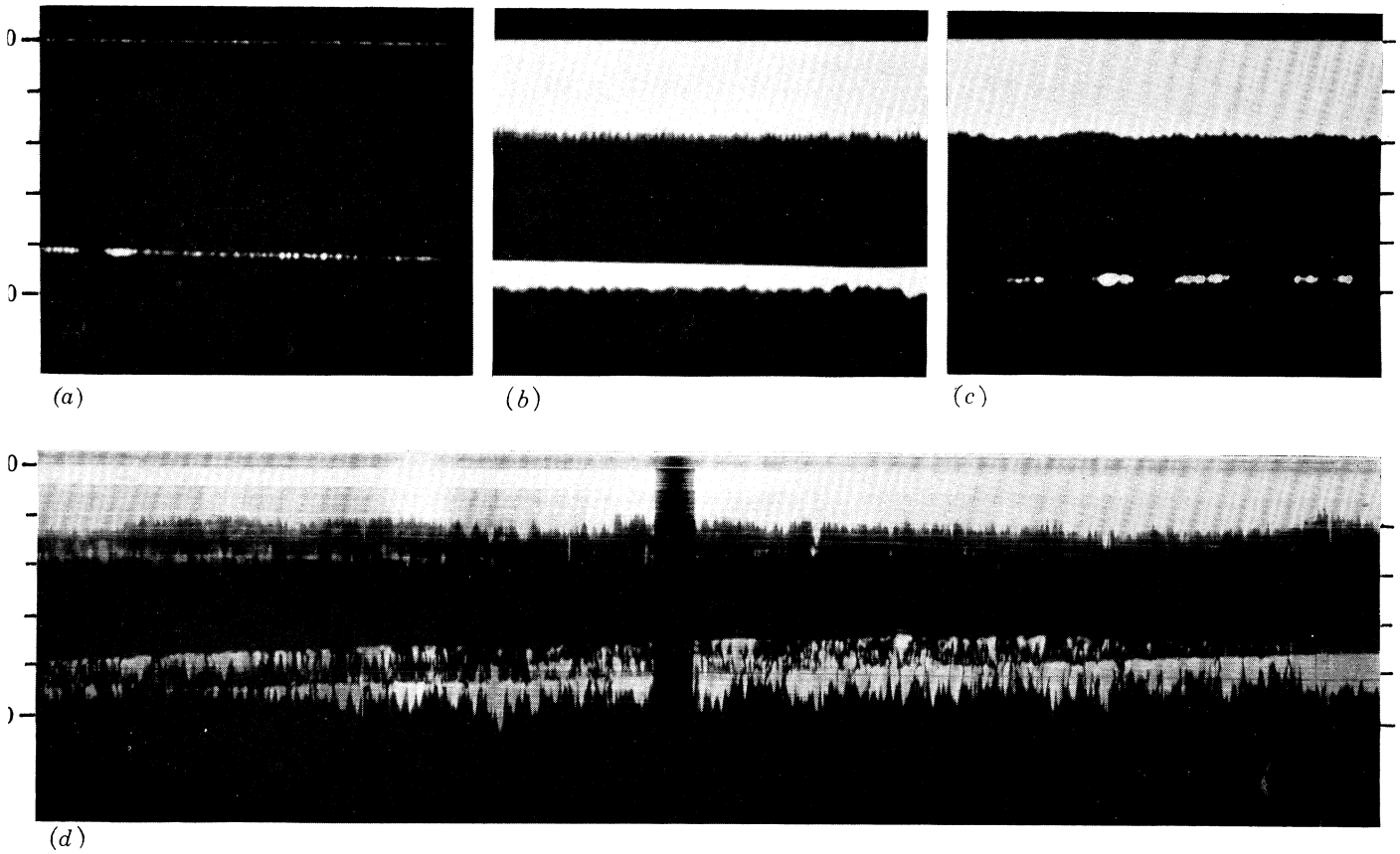

FIGURE 4. Sample echoes recorded on a moving vehicle. Echo delay is measured in microseconds vertically downwards from the zero which marks the arrival of the transmitter pulse at the receiver. (*a*) Single echo at approximately constant range, strength approximately equal to the transmitter break-through. (*b*) Strong clutter echoes following the transmitter pulse, a strong bottom echo showing the sharp leading edge and a varying trailing edge (*c*) Illustrating how a very intermittent bottom echo may be safely recognized by the continuity of the pattern in which it appears. (*d*) A sequence of echoes showing clutter, an isolated layer, and two or more bottom surfaces, both rough, and presumably seen at different angles to the vertical.

(*Facing p.* 444)

The transmitter is a 35 MHz (megahertz) self-oscillating double tetrode, internally neutralized, and designed for 100 W R.F. (radio frequency) output at 600 V h.t. in continuous wave operation. In our apparatus it is driven on the screen grids by free-running trigger circuits to produce 500 W pulse power at 1 kV h.t. The single-tuned tank circuit has a Q of 10 to permit the short pulse rise-time; the resultant output is illustrated in figure 3, plate 10.

TABLE 2. PARAMETERS OF S.P.R.I. MARK II RADIO ECHO APPARATUS

transmitter	
carrier frequency	35 MHz
pulse energy duration	240 ns
rise time, 10 to 90% amplitude	60 ns
peak power, 1964	50W into 50 Ω
peak power, 1968	500W into 50 Ω
pulse repetition interval, 1964	25 μs
pulse repetition interval, 1968	80 μs
total power consumption	4 A. d.c. 12 V
receiver	
pass band (flat ± 2 dB)	28 to 42 MHz
noise figure, 1964	6 dB
noise figure, 1968	3 dB
input attenuators	0 to 120 dB in 1 dB steps
r.f. gain	90 dB
r.f. gain blanked for transmission	0 ± 10 dB
video output noise level:	
a-scope monitor	70 mV r.m.s. into 50 Ω
recorder Z modulation	4 V r.m.s. into 50 Ω
overall receiver sensitivity, S, in dB down on transmitter pulse power:	
1964 A-scope monitor and photo recorder, S.P.R.I. transmitter	140 dB
1964 with U.S.A.E.L. transmitter	146 dB
1968 A-scope monitor	160 dB
1968 photo recorder	166 dB
total power consumption	0.2 A d.c. 12 V
aerials 1964	
(*a*) trailing wire (see §3)	
pass-band for v.s.w.r. less than 2.5	32 to 38 MHz
absolute power gain in air	2 dB
approximate product of vertical gain and absorption cross-section in ice (see §4(*i*))	9 m² (± 3 dB)
(*b*) two-wire half-wave dipoles in air:	
pass-band, including matching device, for v.s.w.r. less than 2.0	30 to 40 MHz
product of vertical gain and absorption cross section in ice	46 m² (± 3 dB)
total weight	4 kg
indicators	
monitor and recorder; Tektronix type 321 oscilloscopes, 6 cm sweep length. Rise-times: Y amplifier: 70 ns, Z modulation: unknown but less than 50 ns	
Shackman AC2/25 35 mm continuous recording camera, 24 mm record width	
total power consumption, all three units: 1.8 A d.c. 12 V	

At the beginning of the operations in Greenland in 1964 an end-fed aerial was trailed on the snow surface behind the vehicle as illustrated in figure 5 (*a*). When the advantages of refraction at the air-snow surface were appreciated, a change was made to folded half-wave dipoles supported in air about 3 m above the surface with a coaxial 'trombone' balun. Rigid two-wire dipoles with a ferrite-cored matching transformer have been used on other occasions (Bailey &

Evans 1968) and most recently the importance of preserving the pulse shape (and thus the range resolution) has led to the use of the loaded dipole arrangement also illustrated in figure 5 (*c*).

The receiver uses two pairs of stagger-tuned transistor amplifying stages at the radio frequency to define the pass-band followed by a linear detector and video filter having a cut-off of 18 dB (decibels) per octave at 7.5 MHz. There is no intermediate frequency amplifier.

There is a conventional 'A-scope' output display for monitoring purposes and a separate recorder cathode-ray tube where the spot is blacked out in the absence of a signal. The video signal from the receiver modulates the brightness up to some maximum level, which is sharply limited to prevent defocusing. The photographic film in the recorder is driven slowly at right angles to the linear time base sweep on the cathode-ray tube so that a single strong echo, constant in range, will produce a single straight line down the length of the film. A second line is produced by the signal which arrives directly from the transmitter at the beginning of the sweep as shown in figure 4, plate 10.

The action on weak signals requires more explanation and it is treated by Evans & Smith (1969), where it is shown that if approximately 1000 sweeps of the time base are superimposed on one part of the film, then it is possible to record echoes which are about 6 dB below the receiver input noise level. This is attained because the output is effectively integrated by the photographic emulsion for the time it takes for the film to advance a distance equal to the diameter of the image of the cathode-ray tube spot. However, it was not attained in 1964 because of defects in the video amplifier. Over longer time intervals, greater than about 0.1 s, there is a further effective gain in sensitivity because of the continuity of the reflecting surface in which we are interested. Hence there is a recognizable element of continuity in the line of blackening along the film, increasing the reliability of interpretation for very weak echoes as illustrated in figure 4 (*c*).

Some of the important parameters of the apparatus are listed in table 2.

4. Reflexion and scattering of radio waves in an ice sheet: theoretical considerations

(*a*) *Plane polished reflector*

The simplest case of echo ranging occurs when we have a point source, an extended plane polished reflecting surface, and a receiver coincident with the source. 'Polished' is borrowed from optics to mean that any departure from a plane surface is small compared to the wavelength in the medium in front of the reflector. The condition is difficult to specify at non-normal incidence, but the difference is unimportant at all angles with which we shall be concerned.

In figure 6 (*a*) we define the radius of the nth Fresnel zone, a_n, by saying that the power received by a narrow annulus of radius a_n differs in phase by $\frac{1}{2}n\pi$ from that received by the perpendicular point S. If λ is the wavelength in the medium, then

$$a_n^2 = \tfrac{1}{4}(2r_0 + \tfrac{1}{4}n\lambda)\, n\lambda \qquad (1)$$

From a large area, which covers a number of zones, the resultant reflected power is the same as that which would be received directly from a similar source at a distance $2r_0$. Thus if p_t is the transmitted power, g_t the aerial power gain in the direction OS, s_r the effective absorption

cross-section of the receiving aerial in the same direction, and R the power reflexion coefficient of the surface near normal incidence, then the received power p_r is given by

$$p_r/p_t = Rg_t s_r/16\pi r_0^2. \quad (2)$$

In order to measure the range r_0, the source at O must be modulated and the velocity of propagation, v, must be known. Consider a transmitted pulse of the type shown in figure 3. At time $2r_0/v$ after the start of the transmitted pulse the echo power rises in an interval t_r. It is

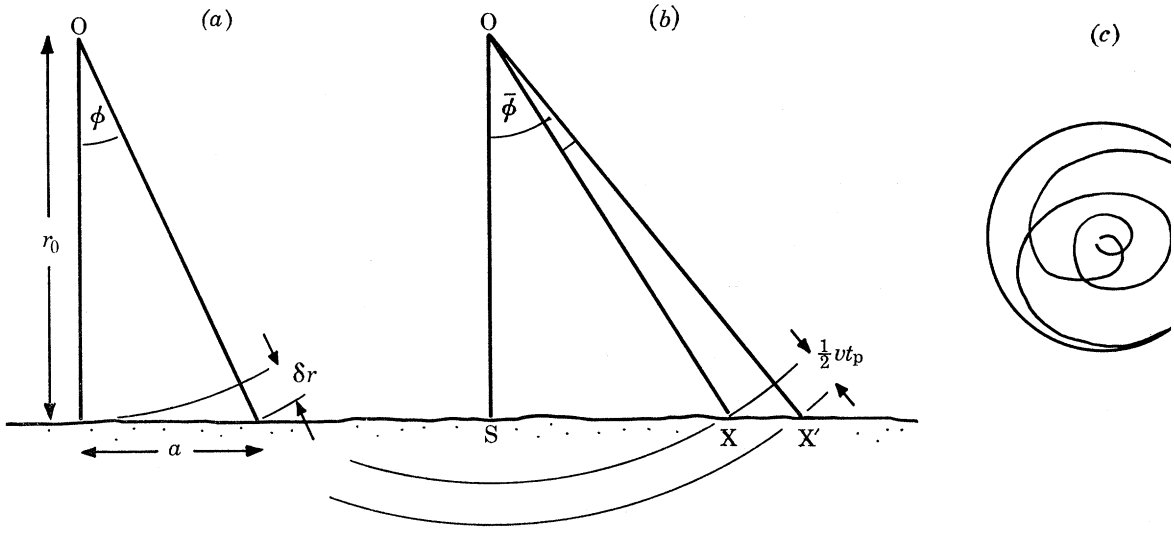

FIGURE 6. (*a*) Defining the variables which determine the size of Fresnel zones seen in a horizontal reflecting surface at a range r_0, by an observer at O. (*b*) To illustrate the annulus XX′ from which power is received at any instant. (*c*) Diagram illustrating the vector addition of wavefront components received by the reflexion of a rounded pulse from XX′. The resultant is almost zero provided the surface is smooth, that is the change of phase from element to element within XX′ is gradual.

less obvious that the echo power falls in an interval t_f after the trailing edge of the pulse has travelled from O to S and back. At any later time power is received by reflexion from an annulus XX′ shown in figure 6 (*b*) but since the times t_r and t_f invariably occupy several cycles of the radio frequency the phase–amplitude diagram for the electric field at O is as shown in figure 6 (*c*) and the resultant is zero. This would not be true if the pulse had any discontinuity, nor if part of the surface were non-reflecting. In this case an echo signal would be observed with a time delay equivalent to that of the non-reflecting patch, or the boundary of the surface if it is not infinite in extent. The surface behaves as if infinite provided that it is larger than the first zone defined above and that, beyond this, the boundary is not too abrupt (that is, it extends over several zones). At 5 m wavelength in ice and 1 km range (typical values for the results considered in this paper), $a_1 = 50$ m.

(*b*) *Isolated targets*

We first define for the target a scattering cross-section, s_s, which is an area such that the incident power density multiplied by the scattering cross-section equals the total power scattered in all directions from the primary beam. If the flux reflected backwards along the line of sight is a factor g_b greater than that which would be reflected by an idealized isotropic scatterer,

then the backward-scattering cross-section, $s_b = g_b s_s$ and it will be a function of the aspect from which the target is illuminated. Thus

$$p_r/p_t = g_t s_r s_b/16\pi^2 r_0^4. \tag{3}$$

This formula (the 'radar equation') is suitable whenever the distance from the source is such that the directional diagram for the scattered power is independent of r_0 but the value of s_b can be calculated only in a few simple cases. For example, a conducting sphere of radius b (a hemisphere is sufficient) reflects all the power incident on the geometrical area isotropically; thus for a sphere, $s_s = s_b = \pi b^2$. When the target dimensions are less than half a wavelength then the approach is to consider the polarizability, γ, in an electric field essentially uniform over the volume of the target. If the electric field in the surrounding medium is $\mathscr{E}$, and μ is the induced dipole moment of the target, then the factor of proportionality is $\gamma = \mu/\mathscr{E}$ and the scattering cross-section

$$s_s = \tfrac{8}{3}\pi 10^{-14}\omega^4\gamma^2 \tag{4}$$

in SI units (metre, kilogramme, second), ω is the angular frequency in radians per second. The backward scattering gain $g_b = \frac{3}{2}$ as for any elementary dipole.

(*c*) *Perfect diffuse reflector*

Without suggesting how it may be realized, we define a perfect diffuse grey surface as one which reflects a fraction R of the incident radiation into a hemisphere according to Lambert's law: the flux per unit solid angle in a direction ϕ to the normal is proportional to $\cos\phi$. In optical terms, the surface has equal brightness from whichever direction it is viewed. The directional diagram should be independent of the direction of illumination, but no real surface would qualify at grazing incidence. Consider the reflexion of a pulse with the same parameters as before. Initially an echo returns to the receiver from the immediate vicinity of the normal point and the power rises with time as progressively greater areas of the surface contribute to the echo. At time t later $\delta r = \frac{1}{2}vt$ in figure 6 (*a*) and an area of radius a contributes to the echo where $a^2 \approx r_0 vt$ provided $vt \ll 2r_0$. The total power reflected from this area is $p_t g_t R a^2/4r_0^2$ During this period while the echo power is rising, ϕ is small and we have ignored the variation of illumination with ϕ. The power reflected from each element of the surface is in random phase relationship with its neighbours and therefore we may add the power received from all the separate elements, allowing a constant factor 4 for the backward scattering gain of a diffuse reflector at normal incidence. (This may be derived by integrating the total power reflected into a hemisphere.) The state of polarization may be affected by reflexion at a diffuse or a rough surface. In general there is a randomly polarized component superimposed on a component having the same polarization as the incident wave and we consider that the reflexion coefficient, R, relates to a specific polarization, the same as the incident wave if no qualification is given. Then

$$p_r/p_t = R g_t s_r vt/4\pi r_0^3. \tag{5}$$

Since the total effect at the receiver is the sum of a large number of random vectors it represents a mean value about which the values for individual positions of O are arranged in a Rayleigh distribution. This fluctuation, or spatial fading, is considered in a later section.

The received power rises linearly until $t = t_p$ after which the effective scattering area is approximately constant for small ϕ and we expect an echo of the shape OAB in figure 7. The sharp corners are rounded over intervals t_r and t_f. The way in which the trailing edge of

the echo decays with time may be imagined in terms of an effective reflecting annulus of width XX′ limited by the transmitted pulse duration as shown in figure 6(*b*). By considering Lambert's law and simple geometry the factor $g_t s_r$ ($\phi = 0$) in equation (5) is found to be replaced by

$$g_t s_r(t) = g_t s_r(\bar{\phi}) \cos^5 \bar{\phi} \quad \text{where} \quad \cos \bar{\phi} = (1 + v\bar{t}/2r_0)^{-1}. \tag{6}$$

The quantities $\bar{\phi}$ and $\bar{t}$ refer to mean values for the annulus, and an approximate result of this equation is that the echo falls from its maximum to half power during a time equal to 15 % of the initial echo delay, $2r_0/v$.

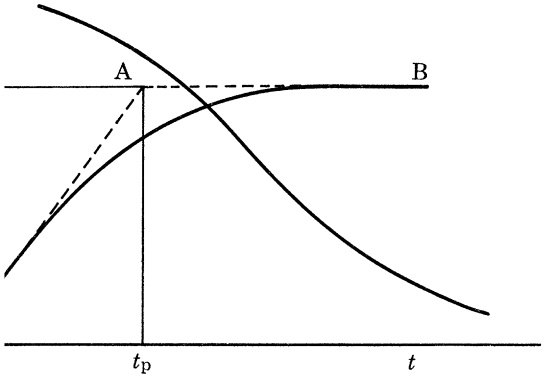

FIGURE 7

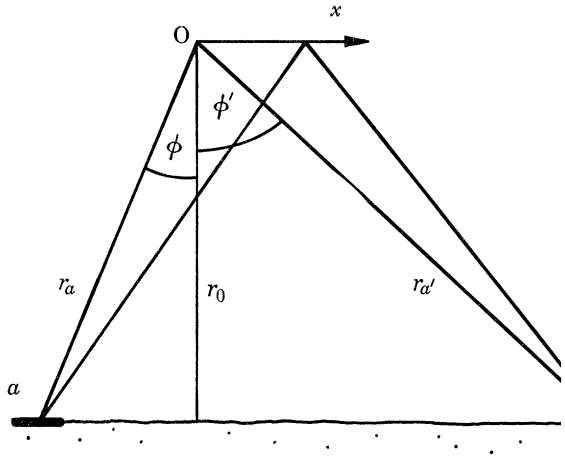

FIGURE 8

FIGURE 7. Two factors influencing the shape of an echo received from a diffuse surface. The rising curve shows that the power increases for a time of the order of the total duration of the pulse, t_p (not its rise-time, t_r, as for a smooth surface). The falling curve, shown in an arbitrary position here, represents the combination of increasing ϕ, and increasing r which eventually conspire to reduce the power to zero, much more slowly however than for a smooth surface.

FIGURE 8. To illustrate the change in the relative phase of echoes received from a and a' as the observer at O moves in the direction x.

(*d*) *Extended rough surfaces*

An extensive literature is devoted to the problem of reflexion of electromagnetic waves from rough surfaces (see Beckmann & Spizzichino 1963) because of the many types of surface which may be considered and because of the number of parameters required fully to describe the reflected wave. However, our problem is restricted in a way which permits many simplifications to be made to the general problem. First, for each element of the reflecting surface we are interested only in backward scattering in the direction of incidence; secondly, we are not concerned with grazing incidence; and lastly, it seems likely in glacierized terrain that the local surface slopes are not too precipitous, that is to say the vertical scale of the irregularities is not greater than the horizontal scale. For mathematical convenience there are two favoured approaches to the model of a rough surface. One supposes that local departures of the actual surface from a mean plane are distributed according to a probability law, usually Gaussian. There is an independent auto-correlation distance in the plane of the surface which, for convenience in terminology, we assume to be horizontal. The other model supposes that the local surface slopes are distributed according to a specified law, in particular they may be uniformly

distributed up to some specified maximum slope. Many elaborations, for example, those involving hemispheres, cylinders or cones, distributed on a plane, have also been used but it is invariably found (Beckmann & Spizzichino 1963, p. 410) whether by analysis, computation, or experiment, that the directional diagram of the scattered radiation is scarcely affected by the type of model which is chosen within the limits stated above (near-normal incidence and no precipitous slopes).

We shall therefore refer when necessary to the model in which the surface slopes, β, are uniformly distributed up to some maximum value $\beta_{\max}$, because it allows the use of the simplest mathematical methods and contains one parameter whose physical meaning is readily visualised. Segments of cylindrical surfaces with their axes lying in the mean plane, have this property; segments of spherical surfaces have a higher proportion of steep slopes.

When the maximum departures from the plane surface are small compared to the wavelength in the medium in front of the reflector, then it behaves as discussed in §4 (*a*). When the surface consists of random irregularities of all sizes down to $\lambda/2\pi$ or less in the horizontal plane then, within our limitations, it was shown by Booker, Ratcliffe & Shinn (1950) that the surface behaves like the Lambert's law reflector treated in §4 (*c*). Since this is a statistical result based on the average contribution from a large number of irregularities there is an upper limit to their size also.

When the smallest horizontal dimension of the irregularities becomes appreciably greater than the wavelength then it is no longer a problem in diffraction and we consider geometrical reflexion by elementary facets of the surfaces. For an uninterrupted source we imagine, by analogy with optics, a 'glistening surface' defined by $\phi \leqslant \beta_{\max}$. (The area over which sunlight is reflected from a rough water surface is a familiar example.) We suppose that the power received from each facet is in random phase relationship with its neighbours and the average total power received is the sum of the individual powers. If pulse amplitude modulation is considered, the whole glistening surface may not be effective in returning power to the receiver at any instant and we consider an annulus limited by the transmitted pulse duration as in §4 (*c*). The power received from the elementary annulus XX′ in figure 6 (*b*) is given by

$$\delta p_r/p_t = R\lambda^2 g_t^2(\phi) \cos\phi \, d\phi/64\pi^2 r_0^2 \beta_{\max}. \tag{7}$$

If the total effective area is not limited by the pulse length, that is if $t_p/t_0 \gtrsim \frac{1}{2}\beta_{\max}^2$, where $t_0 = 2r_0/v$ (the echo delay time from the normal point), then the total received power is given by

$$p_r/p_t = \frac{R\lambda^2}{64\pi^2 r_0^2 \beta_{\max}} \int_{\phi=0}^{\beta_{\max}} g_t^2(\phi) \cos\phi \, d\phi,$$

which may be written

$$p_r/p_t = \frac{R\lambda^2 \overline{g_t^2}}{64\pi^2 r_0^2} \left(\frac{\sin\beta_{\max}}{\beta_{\max}}\right), \tag{8}$$

where $\overline{g_t^2}$ is a mean square aerial gain over the range of integration. The second factor in (8) is always near unity and may be ignored; note then the similarity with (2) for a polished surface. For a pulse duration of 0.2 μs and a range of 1 km in ice, this formula will apply if $\beta_{\max} < 0.18$ (or 10°). To calculate the initial echo maximum for a short pulse, we integrate (8) from $\sin\phi = 0$ to $\sqrt{(vt_p/r_0)}$, then

$$\frac{p_r}{p_t} = \frac{R\lambda^2 \overline{g_t^2}}{64\pi^2 r_0^{2.5}} \frac{\sqrt{(vt_p)}}{\beta_{\max}}. \tag{9}$$

After this peak value, the power decreases with time approximately proportional to $\sqrt{t}$ until $t/t_0 = \frac{1}{2}\beta_{\max}^2$ when it decreases abruptly, since we have postulated a surface with no slopes greater than $\beta_{\max}$.

Thus, for all types of surfaces which we have considered the variation of echo power follows an r^{-2}, $r^{-2.5}$ or r^{-3} law and it is fortunate that for the pulse length and ranges with which we are principally concerned, there is no very great numerical difference in the geometrical factors involved in calculating echo powers. In §6(*d*) all these factors (not including R, the power reflexion coefficient) are grouped in the symbol G, indicating 'geometry'.

(*e*) *Fading range and fading rate*

For a uniform plane polished reflector the echo power is clearly the same at all points equidistant from the plane. In radio terminology the signal does not fade with position, or time. An isolated target gives rise to an echo power which varies slowly as the range changes and perhaps more rapidly with aspect.

If two separate targets which are not resolved in range give rise to echo amplitudes a and a' then the resultant amplitude will vary with position from $(a+a')$ to $(a-a')$ according to their relative phase. On a decibel scale their fading range is $20 \lg (a+a')/(a-a')$. In figure 8, consider an observer at O to move a distance x on a line parallel to aa'. Then $\delta r_a = \sin\phi\delta x$. If the two are not resolved $\phi \approx \phi'$ and the fading rate in cycles per unit distance is

$$\frac{1}{\lambda}\left(\frac{\delta r_a + \delta r_a'}{\delta x}\right) = \frac{2\sin\phi}{\lambda}. \tag{10}$$

In §§4(*c*) and 4(*d*) we have referred to the average echo power obtained by summing a large number of random vector components of the field strength. Note that this is an average value and, provided the assumptions are valid, the echo amplitudes at individual points (all equidistant from the average surface) will be Rayleigh distributed. The fading range may be described by considering two power levels, one above which 90 % of the observations lie, and the other above which only 10 % lie. The ratio of the two is expressed by saying that the 10 to 90 % fading range is 13.4 dB for a Rayleigh distribution, from -8.3 to $+5.1$ dB of the median value. Consider the various assumptions involved in turn. The requirement for a large number of component vectors is usually met since departures from the Rayleigh distribution are very small if the components are six or more in number. Rayleigh's original analysis of the two-dimensional random walk problem was restricted to component vectors all of the same amplitude and with the phase uniformly distributed over $-\pi$ to $+\pi$. The distribution may be shown to remain Rayleigh if the vectors are of random amplitude and clearly any phase distribution of width much greater than π is equivalent to Rayleigh's assumption. If the phase is distributed over a narrow range corresponding to a reflecting surface which is almost smooth, the fading range is less than Rayleigh. An intermediate model, easily visualized, consists of a surface which is smooth over part of its area, giving rise to a constant ('unfading' or 'specular') component, but having irregularities here and there giving rise to a Rayleigh-distributed component of the echo signal. The resultant distribution was found by Rice (1945) in another connexion. If B is the ratio of the amplitude of the constant component to the root mean square (r.m.s.) Rayleigh component then the 10 to 90 % fading range is 11.7 dB for $B = 1$ and 7.4 dB for $B = 2$. Thus we gain little information from the fading range except a rough estimate of the ratio of specular to fading components.

The fading rate fills a spectrum which may be deduced from (10). The highest fading frequencies are produced by those areas of the reflector farthest from the perpendicular in the plane containing the direction of motion. The effective angle may be limited by the aerial polar diagram, by the absorption of the signal over the greater path, or by the pulse length. If not, then the highest fading frequency, in cycles per unit distance, is

$$2 \sin \beta_{\max}/\lambda. \tag{11}$$

To summarize: it is expected that average echo duration beyond the transmitted pulse length will give the clearest indication of the range of angles to the normal from which the echo is received, but if this range is small, the fading rate may be an appropriate method of estimating the parameter $\beta_{\max}$.

The problems which have been discussed are similar to those encountered in the interpretation of aircraft radio altimeter returns, except that in the altimeter case the terrain may be much more complicated (by the presence of vegetation or city buildings). Edison, Moore & Warner (1960) compared measurements at 0.7 m wavelength made with radio altimeters carried in aircraft, with the backward-scattering polar diagram to be expected for a Gaussian rough surface. For eleven types of terrain except forest he found that the r.m.s. deviation for the distribution of surface slopes was $\tan \beta_{\text{r.m.s.}} = 0.16$ to 0.19, but the uniform model used above with $\tan \beta_{\max} = 0.3$ would fit the results equally well (within a factor of 2). They also found the effective slopes to be somewhat greater at higher frequencies; and the converse is likely to be true but no measurements at lower frequencies have been found. Thus, on glacierized terrain, at metre wavelengths, we expect $\tan \beta_{\max}$ to be less than, or of the order of, 0.3.

Beckmann & Spizzichino (1963, p. 410) also report that the cross-polarized component of the reflected power is invariably small compared to the scatter in measurements of the in-line component.

(*f*) *Reflexion coefficient of the bottom surface*

The quantity R which appears in §§ 4(*a*) to 4(*d*) is the power reflexion coefficient of an element of the surface. Though we are concerned with angles of incidence other than perpendicular to the average surface, yet locally the incidence is always perpendicular for backward scattering and a single value of R may be calculated for the boundary between any two media from

$$R = \left(\frac{\sqrt{\epsilon_2} - \sqrt{\epsilon_1}}{\sqrt{\epsilon_2} + \sqrt{\epsilon_1}}\right)^2. \tag{12}$$

Let us deal with the properties of ice first. The real part of the relative permittivity, ϵ', is discussed in § 5. At the bottom of an ice sheet it may be assumed that $\epsilon' = 3.17 \pm 0.07$ (Evans 1965 and §5(*b*)). The imaginary part is discussed in §6 where it can be found that at radio frequencies, under the conditions at the bottom of a natural ice sheet, $\tan \delta$ is always much less than unity. In nature, this is likely to be untrue only for ice formed from frozen sea water, so that $\tan \delta$ has a negligible effect on the reflexion coefficient.

The dielectric properties of the rock beneath the ice cannot be specified accurately. It is supposed from outcrops that most of the rocks of Greenland and Antarctica are largely granites or sandstones. The value found for ϵ' is 7 to 10 in the v.h.f. radio frequency range for various samples of these material (Kaye & Laby 1959, p. 94; Von Hippel 1954, p. 313; Parkhomenko 1967, p. 38). Loss tangents may be as great as 0.03, but not usually greater, and again we may ignore their effect on the normal reflexion coefficient. Naturally occurring sands have

permittivities of the order of 2.5 when very dry. This low value is assumed to be due to the included air since quartzite and sandstones have a permittivity of about 4.5. Thus although loose sand may occur beneath an ice sheet in erosion shadows it is not likely to contain air and 4.5 is considered a lower limit to the permittivity even if it contains a small proportion of ice. Thus we expect the reflexion coefficient to be about -14 dB at ice/rock interfaces, or as low as -22 dB locally for quartz-based materials. Probably the most important materials about which we have no information are the clays, shale and mudstone; it would be desirable to know the relevant properties in both the frozen and unfrozen state. Note that quartzite and even uncemented quartz sands if less that 5 % water, or if frozen, have small loss tangents and a useful penetration by v.h.f. radio waves may be expected. The possibility should be borne in mind in the interpretation of ice-sounding records and the properties of a limited range of rock types should repay further investigation in this connexion (see Cooper 1948).

The reflexion coefficient of an ice/water interface is essentially unity if the water is deeper than the skin depth,

$$1/2\pi\sqrt{(0.1f\sigma)}, \tag{13}$$

where σ is the conductivity in mhos per metre and f is the frequency (MHz). In the v.h.f. range the skin depth is of the order of centimetres for sea water, and metres for fresh water. Any layer less than this in thickness is transparent in the sense that more than half of the power passes through, but the fraction reflected may be easily detectable.

(*g*) *Scattering by air bubbles*

Imagine the medium of propagation to consist of clear solid ice containing a distribution of spherical air bubbles. The total scattering cross-section s_s of an isolated bubble of radius b in ice of relative permittivity ϵ_i may be derived from the polarizability

$$\gamma = 4\pi b^3\epsilon_0\epsilon_i(1-\epsilon_i)/(1+2\epsilon_i) \quad \text{(Stratton 1941, p. 206)} \tag{14}$$

and (4).

If there are m similar bubbles per cubic metre then the density of the resultant ice is

$$\rho_s = (1-4\pi b^3 m/3)\rho_i. \tag{15}$$

For a sparse, random distribution of bubbles the total scattering cross-section is ms_s but if the spacing between bubbles becomes comparable with their diameter (that is $\rho_s \lesssim 0.85$) then the electric field due to the incident electromagnetic wave is not accurately calculable in the vicinity of each bubble. We have considered a bubble radius of 1 mm to be the upper limit in an ice sheet and the straight line portion of the graph in figure 9 showing the total scattered power may be scaled at the rate of $+40$ dB per decade in radio frequency (Rayleigh's fourth power scattering law) or $+60$ dB per decade in bubble radius, provided the bubble density is not too great (density greater than 0.8).

There are two aspects of the scattered power of interest. The first is the loss of power from the primary beam and its effect on the overall sensitivity. Some values are marked in the upper left portion of figure 9 from which it is clear that for bubbles of 1 mm radius or less the loss is not of practical significance at radio frequencies less than 1 GHz.

However, we may enquire if the scattered power is detectable as an echo. At any instant after the transmitter pulse, the received power is returned from anywhere within a shell of thickness $\frac{1}{2}vt_p$ metres, the 'space pulse length', and each scattering centre as an elementary dipole, has a backward scattering gain of about $+2$ dB. Echo power is returned from the whole scattering

volume and, to take a numerical example, if $\frac{1}{2}vt_p = 20$ m, and $m = 10^7$ bubbles of 1 mm radius per cubic metre, then at 35 MHz the reflexion coefficient is $-110+13+2 = -95$ dB and there are situations in which this is readily detectable.

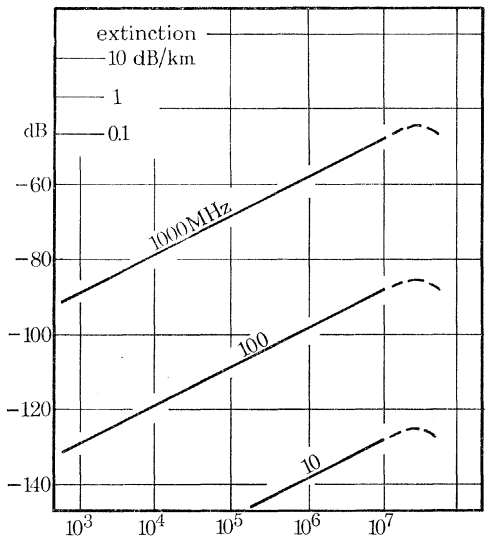

FIGURE 9

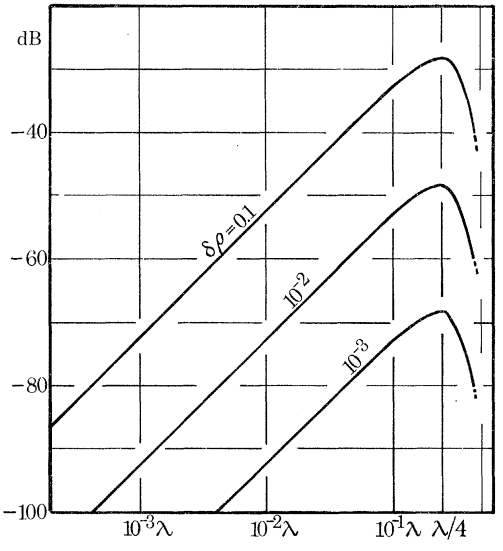

FIGURE 10

FIGURE 9. The ratio of incident power to the power scattered per metre path in an ice medium containing spherical air bubbles; the ordinates express this ratio in dB. Alternatively these ordinates may be expressed by the reduction in strength of the primary beam, and three representative values are plotted in the top left corner. The number of bubbles per cubic metre is m and they are assumed to be 1 mm in radius. The straight line relation breaks down when the relative density of the ice/air mixture falls below 0.8; above this, the effect of changing the bubble radius is +60 dB/decade.

FIGURE 10. The reflexion coefficient in dB for a layer of thickness l and density different from that of the surrounding medium by an amount $\delta\rho$. The wavelength in the medium is λ.

(*h*) *Horizontal layering*

The stratified distribution of snow density with depth is another known glaciological feature which may cause scattering. For a transmitting source in air, the major discontinuity occurs at the snow surface where the power reflexion coefficient is given by equation (2) putting $\epsilon' = 1$ for air and $\epsilon_2 = \epsilon_s$ for snow. Maximum and minimum values are -11 dB for solid ice and -18 dB for snow of density 0.3; thus the loss to the forward wave is unimportant but the echo is of easily detectable strength. Note that the duration of the surface echo is determined by the considerations of §§4(*a*) to 4(*d*) and that thought should be given to the height of the transmitter and receiver above the snow surface if the surface echo is not to overlap with wanted echoes from below. Thus if the sounding apparatus is carried in an aircraft at an altitude of, let us say, 1 km above the snow surface and if the surface behaves as a Lambert's law reflector (as seems likely from our recent observations) the echo will be -10 dB of its maximum strength for 350 m beyond the first return on the range scale, and above -40 dB for 1 km beyond that (equations (5) and (6)).

Below the top surface, large variations in snow density may take place in a vertical distance much less than $\frac{1}{4}\lambda$ and each discontinuity will have a power reflexion coefficient given by (12). Substituting from (20) in the next section, if $\delta\rho$ is the change in density (positive or negative),

the power reflexion coefficient is approximately $(0.24\ \delta\rho)^2$ or -52 dB for $\delta\rho = 0.01$. If more than one such discontinuity is within the space pulse length at one time, they may be in some regular phase relationship and an estimate of the total reflected power is rather uncertain, but -40 dB is the order of magnitude if one assumes 40 random layers each having $\delta\rho \sim 0.01$ within the space pulse length. This is a reasonable situation in the top 100 m of a polar ice sheet (see, for example, Schytt 1958). This type of echo, which in radar terminology is referred to as short range clutter, decreases with depth mainly because the possible range of variation $\delta\rho$ becomes less. At great depths we may imagine there will occur isolated layers, of thickness l, within which the average density is different from the surrounding material. By analogy with the reflexion from a short section of transmission line inserted into a long line of different characteristic impedance and with the same substitutions as before, it can be shown that the power reflexion coefficient is

$$R = [\pi\delta\rho(l/\lambda)]^2, \tag{16}$$

and some numerical results are plotted in figure 10. When the layer becomes of the order of, or greater than $\frac{1}{4}\lambda$ in thickness (say 1 m), the total reflexion coefficient is dominated by interference between the waves reflected at the top and bottom faces and this formula does not apply.

(i) Refraction

It is convenient for the transmitting and receiving aerials to be carried in air, at a height of the same order as the radio wavelength, if on surface vehicles, or at low aircraft altitudes if flying. The latter case may be treated as a simple problem in geometrical optics. The total deviation of the ray OX in figure 11 is given by Snell's law and the refractive index of the medium at X is $\sqrt{\epsilon_1}$. The power radiated into the solid angle $\mathrm{d}\Omega$ (between the cones of semi-angle ϕ and $\phi+\mathrm{d}\phi$) is refracted into the solid angle $\mathrm{d}\Omega'$. Thus if g_1 is the increase in the power gain due to refraction into ice

$$g_1 = \mathrm{d}\Omega/\mathrm{d}\Omega' = \epsilon_1 \cos\phi'/(1-\epsilon_1 \sin^2\phi'). \tag{17}$$

For substitution in the expressions given in §§4(*a*) to 4(*d*) we consider refraction at the snow surface to a part of the properties of the aerial system, that is to say, we substitute the total power gain, g, the absorption cross-section, s, and the wavelength, λ, appropriate to the combination of source and surface refraction seen from within the ice. Equation (17) is an inconvenient analytical form but two limits may be simply stated. Close to the normal to the top surface, $g_1(0) = \epsilon_1$, there is a power gain of $+5$ dB in the vertical gain (but no significant effect on the absorption cross-section) due to refraction, assuming the material above X to be solid ice. The critical angle $\phi'_c = \sin^{-1}\epsilon_i^{-\frac{1}{2}} = 34°$ on the same assumption, but this requires grazing incidence on the snow surface and as a working rule we may say that the total gain due to refraction is approximately ϵ_1 until it decreases abruptly for angles of refraction of about 30°, somewhat dependent on the height of the source above the surface.

No exact theory can be given for an aerial which is close to the surface. It is clear that there is no power gain if the source is within the ice and therefore it should be carried as high as is convenient. However, if we imagine the aerial to generate a wavefront which is initially plane over its effective radiation or absorption cross-section then the wavefront will tend to be spherical at distances much greater than the linear extent of this area ($\sim 0.4\ \lambda$ for a half-wave dipole). Thus there will be little advantage in carrying an aerial at a much greater height than this.

During the first part of the 1964 Greenland traverse described in §§2 and 3, an end-fed wire aerial was trailed on the snow surface behind the vehicle. We have assumed in calculating the approximate performance given in table 2 that the snow in the top 5 m was of average density 0.7 and thus there was only a small power gain due to refraction into material of greater density.

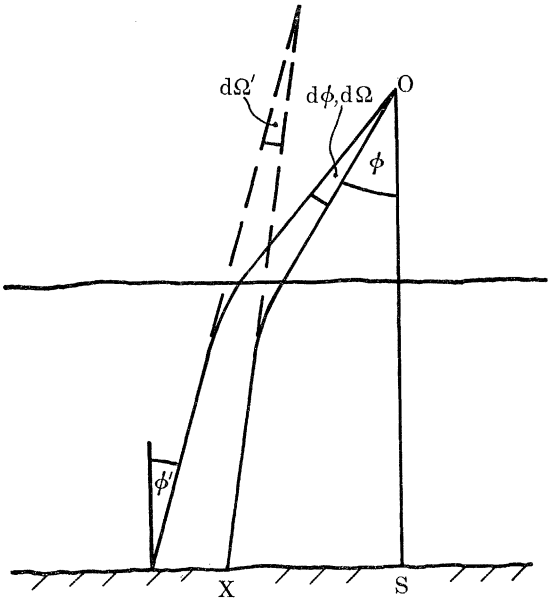

FIGURE 11

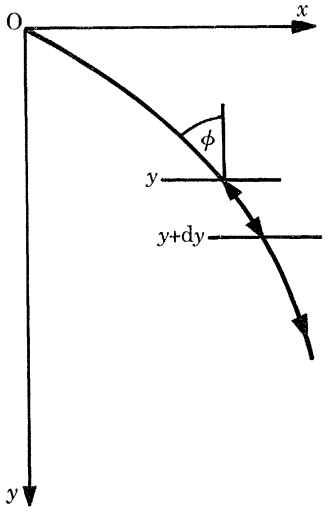

FIGURE 12

FIGURE 11. Refraction and increased gain on entering a denser medium. The power radiated into the solid angle $d\Omega$, between the cones of semi-angle ϕ and $\phi+d\phi$, is refracted into the solid angle $d\Omega'$.

FIGURE 12. Defining the variables in equation (25), if n is the local refractive index (a function of y only) then $n \sin \phi = N$, a constant defining the ray path.

5. ACCURACY OF DEPTH DETERMINATION

Two quantities are required to determine the range of a given echo from the observer: the time delay and the velocity of propagation of the signal through the intervening medium. Considering the time measurement first, there are proportional systematic errors due to the use of a reference time scale which is inaccurate and there are fixed errors: systematic if, for example, they are due to an unrecognized time delay in the system, and random if set by the instrumental time resolution. The errors in velocity arise from incomplete knowledge of the state of the ice at any location and uncertainty in the effect of variations in the temperature, density, crystal size and orientation. The effect of temperature is fortunately small, the effect of crystal orientation is not well known, and density is dealt with separately below.

These considerations affect the accuracy of range measurement to a chosen echo; there remains the problem of identifying the echo with the ice/rock interface in which we are chiefly interested. It is possible to receive echoes from other directions, or from objects above the snow surface, but in considering mistakes in interpretation we have found that the picture presented by the continuous film record is the greatest safeguard because of the visible form and continuity of the bottom echo. Furthermore, by this type of record an effective means is provided for averaging during a time interval, or a definite forward movement of the observer, though we

allow that the ultimate accuracy of any such average is limited by the real depth variations which occur within the area averaged. Echoes of uncertain origin have been found to be of short duration and never to be confused with the virtually continuous bottom trace; the exception being in terrain with very steep slopes where it seems likely that specular echoes are received from facets of the bottom surface widely separated from one another and it becomes difficult to specify a single depth. An example of this situation is shown in figure 4 (*d*).

At the end of this section we compare radio echo depth determinations with seismic determinations made at the same locations and this is probably the most satisfactory and wholly independent check of either technique that we are likely to find.

(*a*) *Timing accuracy*

The time base used to measure echo delays may be controlled by a quartz crystal oscillator which will have an entirely negligible error, of the order of twenty parts per million over long periods and over wide temperature ranges. In the S.P.R.I. mark II displays used in 1964, the sweep speed was calibrated from time to time by an external crystal oscillator but it is more satisfactory to have a number of regular crystal-controlled timing marks on the permanent record and this obvious improvement has been added since. The display and recording arrangements permit the position of the oscilloscope spot to be measured to ± 1 part in 200 of the sweep length employed, namely ± 0.3 mm on a 60 mm monitor display or ± 0.1 mm on a 24 mm photographic record of the type shown in figure 4. This uncertainty accounts for a minimum error of ± 2 m depth on the shallowest scale (400 m) rising proportionally to ± 8 m on the 1.6 km scale, or ± 20 m on the 4 km scale.

The speed of response, or overall 'rise time', of the apparatus is illustrated in figure 3 which has a photograph of the receiver output on the monitor display when the transmitter pulse is fed via a suitable attenuator to the receiver aerial input. The separation of this pulse from a similarly shaped echo pulse may be measured to ± 50 ns, equivalent to ± 4 m range in ice, and this error is independent of the sweep speed. However, the echo may be different in shape (see §§4 (*a*) to (*d*)) and it is certain to be very different in amplitude; possibly this introduces a greater uncertainty into the measurement of time differences in the intensity-modulated display. The receiver input is blocked for large signals with semiconductor diodes arranged back-to-back, and the receiver gain is blanked for a short period, with the result that the transmitter pulse is of the same order as, or less than, the echo signal at the receiver output. We have made laboratory measurements of the delay suffered by pulses passing through the receiver in the blanked and unblanked condition. The total delay is 120 ns for a barely detectable signal, reducing to nearly zero as the signal power increases by 100 dB, a much greater range than will ever occur in practice. In the blanked condition the change in delay is less.

It is not possible to measure time differences by taking the instants at which the signal has risen to (say) half amplitude because many signals will saturate. The method suggested for the highest accuracy is to extrapolate the steeply rising section of the leading edge of the pulse back linearly to zero amplitude. This method has been used for the velocity measurements in §5 (*d*), but it is not possible with the intensity modulated display used for continuous recording. It is also essential to accuracy that all signals enter the receiver at the aerial and do not leak into the feeders or later stages of the receiver, so that effective screening and filtering are important to accuracy as well as stability. With separate transmitting and receiving aerials (figure 13*a*), the arrangement used in Greenland in 1964, the time delay for the direct path

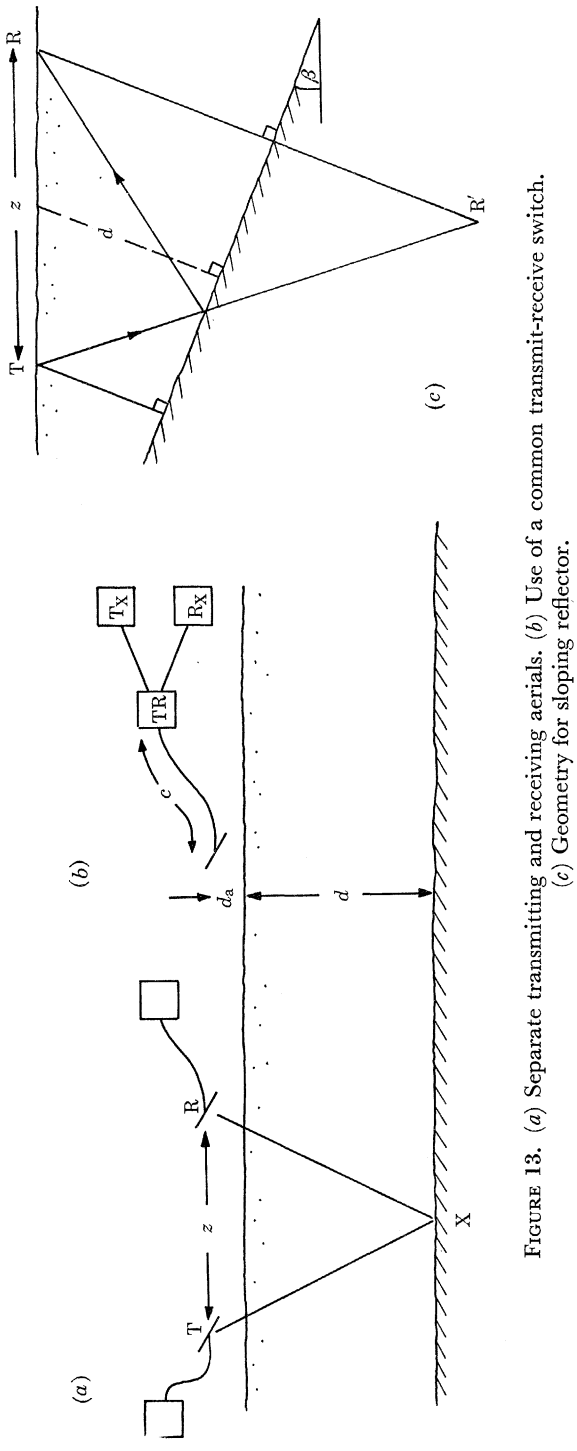

FIGURE 13. (*a*) Separate transmitting and receiving aerials. (*b*) Use of a common transmit-receive switch. (*c*) Geometry for sloping reflector.

from T to R is included in the measured time delay. This and the height of the aerials above the snow surface are allowed for in calculating the ice depth. There were several changes in the arrangement of the aerials and apparatus within the vehicles—affecting the overall sensitivity, but not the accuracy of depth measurement. The transmitting and receiving aerials were mounted in separate vehicles and a fixed spacing was maintained by trailing a rope from the forward vehicle. If a common aerial arrangement were used, as in figure 13 (*b*), the travel time for the cable length c and the height d_a should be subtracted from the measured time delay.

(*b*) *Velocity of propagation of radio waves in solid ice*

In a few isolated cases it will be possible to calibrate radio echo depth soundings by direct comparison with depths measured in drill holes. However, we expect the velocity of propagation of a radio pulse to depend on snow density, and slightly on temperature and structure, and thus it is important to be able to calibrate soundings at many points or to know how the velocity depends on the physical state of the snow and to have sufficient knowledge of the physical state. Let us see how accurate this knowledge needs to be.

The dielectric properties of naturally occurring ice and snow have been reviewed by Evans (1965). Experimental measurements of ϵ', the permittivity of polycrystalline ice samples in the laboratory are summarized in figure 14 (*a*). At centimetre wavelengths there is excellent agreement between three independent authorities: Von Hippel (1954, p. 301), Cumming (1952), and Lamb & Turney (1949). At low frequencies, the results due to Auty & Cole (1952), Kuroiwa (1956), and J. G. Paren (recent and unpublished) are derived from measurements in the range 50 Hz to 50 kHz fitted to a Debye relaxation spectrum and extrapolated to the asymptotic value of ϵ' at much higher frequencies. Other authors using this technique have derived values of ϵ' ranging from 2.2 to 7.5 but we are satisfied that, in this frequency range, extreme care is necessary with the electrode surfaces, the purity of the water, the crack and bubble content, and the elimination of strain to obtain absolute results. In the centre of the figure the results due to W. B. Westphal (private communication, 1963) were obtained on samples of ice of density $\rho = 0.90$, taken by A. H. Waite from the Tuto tunnel, in the ablation zone of the Greenland ice sheet near Thule. The permittivity of solid ice ($\rho = 0.917$) is expected to be approximately 2% greater (see next section). We can include the results in figure 14 (*a*), their estimated errors, and temperature coefficients, by saying that the relative permittivity of pure polycrystalline ice is $\epsilon' \equiv 3.17 \pm 0.07$, independently of temperature, in the frequency range from 10 to 10^5 MHz.

When dispersion and absorption are negligible, the velocity, v, and refractive index, n, are related to the permittivity by

$$v = c/n = c/\sqrt{\epsilon'}, \tag{18}$$

where the velocity of light *in vacuo*, $c = 300$ m/μs. In a dispersive medium, the signal velocity is close to the group velocity except in regions where n decreases steeply with increasing frequency ('anomalous dispersion'). There is no simple expression for the signal velocity (see Stratton 1941, p. 333) and to estimate the magnitude of any possible error we use the expression for the group velocity v_g in terms of the phase velocity v_p:

$$\frac{1}{v_g} = \frac{1}{v_p} + \frac{f}{c}\frac{\mathrm{d}n}{\mathrm{d}f}. \tag{19}$$

If we take 5×10^{-4} MHz^{-1} as the maximum possible gradient between 10 and 100 MHz in figure 14 (*a*), the difference $(v_g - v_p)$ is less than 2 m/μs; it is likely to be an order of magnitude

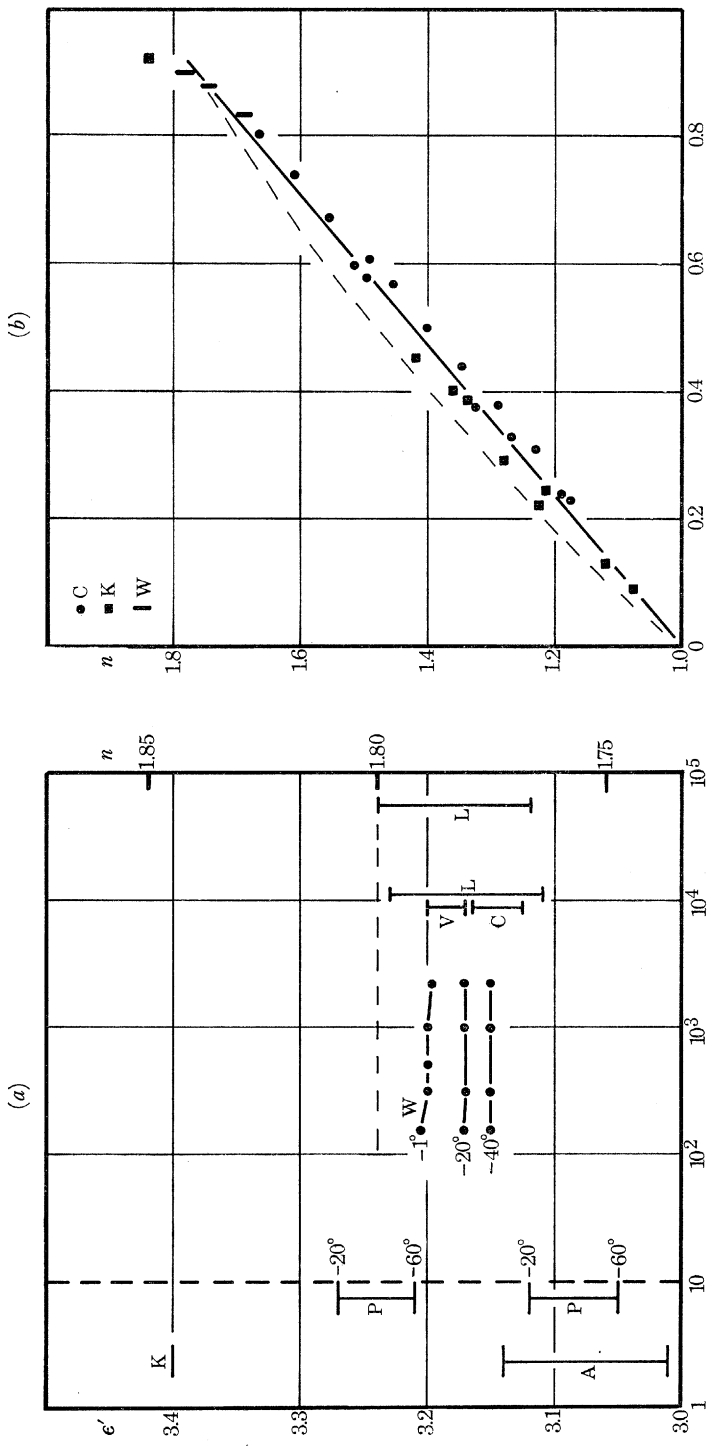

FIGURE 14. (*a*) Permittivity, ϵ', of ice samples of relative density greater than 0.90, against frequency. The values obtained by extrapolation from measurements of the relaxation spectrum at lower frequencies, are plotted to the left of the 10 MHz ordinate. Temperatures are marked in degrees Celsius where a significant temperature coefficient has been observed. (*b*) Refractive index of snow, n plotted against density ρ, according to three independent authorities.

K, Kuroiwa (1956) −1 to −15 °C; A, Auty & Cole (1952) −11 °C; P, Paren (private communication, 1968). Out of six different natural-ice specimens, all having similar temperature coefficients, the two extreme examples are shown here (upper, from Tuto tunnel; lower, from 480 m depth in central Greenland); W, Westphal (private communication, 1963) (Tuto tunnel sample); V, Von Hippel (1954), −12 °C; C, Cumming (1952), −18 °C; L, Lamb & Turney (1949), 0 to −190 °C.

less than this and we shall ignore the distinction and use equation (18). The effect of absorption on the velocity is even less (see Evans 1965, appendix C). Thus the refractive index, $n = 1.78 \pm 0.02$ and the velocity, $v = 169 \pm 2$ m/μs, over the temperatures and frequencies of interest in this paper.

(*c*) *Snow density distribution*

The relation between refractive index, n, and ρ, the relative density of snow, is summarized in figure 14(*b*). The values of n are scattered over the range to be expected from variations in snow structure (see Evans 1965), but none of them deviates more than ± 0.05 from the simple linear relation

$$\sqrt{\epsilon'} = n = 1 + 0.85\rho \tag{20}$$

shown by the solid line in the figure. The linear relation for permittivity

$$\epsilon' = 1 + 2.36\rho \tag{21}$$

shown by the broken line in figure 14(*b*) is less accurate, but may be more convenient in other applications. Thus, where the density is low, there will be a maximum uncertainty in the velocity of propagation of $\pm 5\,\%$ due to possible variations in snow structure, and an additional uncertainty about the density distribution itself which we shall now examine.

The density distribution in polar ice sheets has been studied extensively, for example Benson (1962) and Robin (1967*a*) present summaries of results from Greenland and Antarctica respectively. In the ablation zones, the specific gravity of the ice rarely falls below 0.88, even close to the surface, except for the temporary cover of winter snow. Over the major part of the accumulation zones of both the Greenland and Antarctic ice sheets, the mean density of the uppermost 2 m of firn lies between 0.32 and 0.45 at almost all locations but where surface elevations are below 500 m, the effects of summer melting and percolation cause irregular variations in density so that in northwest Greenland the average density of the top 2 m is 0.50 ± 0.10 (Benson 1962). Except in this zone, where percolation of meltwater is important, the processes of change from lower density firn into ice of maximum density do not vary greatly from place to place. The density of firn is governed primarily by the stress to which it is subjected, normally the weight of overlying snow, although longitudinal stresses in the ice can modify the normal density–depth relation—most markedly in the upper 50 m. Variations in the depth–density relation are affected by temperature, and to a lesser extent by the rate of accumulation at the surface. Smoothed depth–density curves are shown in figure 15 for three representative situations: the South Pole (-51 °C mean annual temperature); Maudheim (-17 °C) and 'Site II', Greenland (-24 °C).

Consider a density deviation at depth y defined by $\Delta(y) = \rho_{\mathrm{ice}} - \rho(y)$. Consider a thin stratum of thickness $\mathrm{d}y$; the travel time for a vertical one-way passage is $\mathrm{d}t = n(y)\,\mathrm{d}y/c$. Let the 'reference time' be that for a solid ice layer of the same thickness. Then the correction to the reference time is given by $\mathrm{d}t_{\mathrm{c}} = [n_{\mathrm{ice}} - n(y)]\,\mathrm{d}y/c$, substituting from equation (20)

$$\mathrm{d}t_{\mathrm{c}} = 0.85\,\Delta(y)\,\mathrm{d}y/c. \tag{22}$$

The total correction on passing once through the whole density distribution may be obtained by graphical integration of Δ, equivalent to the area between one curve in figure 15 and the value $\rho = 0.918$ for solid ice, using a planimeter. Alternatively one may assume that the curve is approximately exponential:

$$\Delta(y) = \Delta(0)\exp(-y/Y),$$

when $$t_c = 0.85 Y \Delta(0)/c. \quad (23)$$

Substituting $\Delta(0) = 0.45$ and $Y = 38$ m, which define the exponential fitted by Schytt (1958, p. 122) to the Maudheim density distribution, we find $t_c = 48$ ns. A probable maximum value of t_c (for the South Pole or central Greenland) is 100 ns.

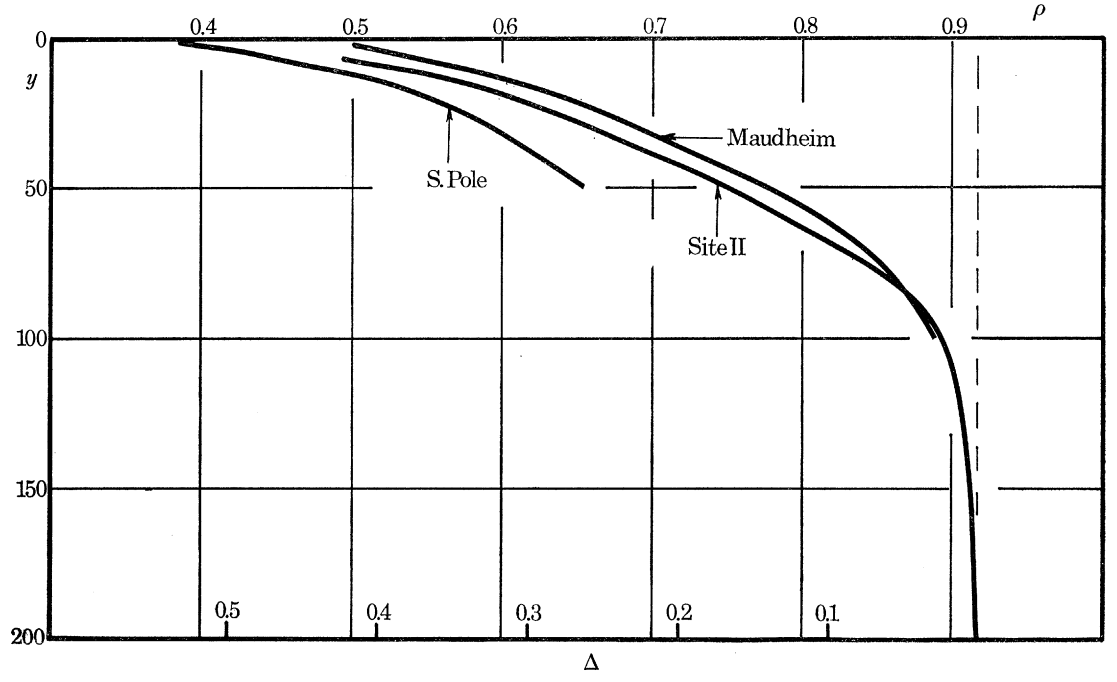

FIGURE 15. Density, ρ, plotted against depth, y (metres), observed in boreholes at three locations: South Pole (Giovinetto 1960), 'site II' north central Greenland (Langway 1967) and Maudheim, Dronning Maud Land (Schytt 1958). The parameter Δ is the difference between the observed density and that of solid ice.

The ice thickness is calculated from the echo delay time, t, and the velocity of propagation, $v_1 = 169$ m/μs for solid ice, and in the ablation zone the range of the echo is $\frac{1}{2}tv_1$. In the accumulation zone a correction $t_c v_i$ should be added to the depth; the probable value is $+8$ m at -20 °C, it may be as great as $+16$ m under very cold polar conditions but rarely less than $+6$ m except close to the ablation zone. Having made this estimate, the total depth error due to density variations in polar firn should not be greater than ± 4 m and this includes the uncertainty in the relation between ρ and n.

(*d*) *Measurement of velocity in the field*

The velocity of propagation may be derived from field measurements using separate transmitting and receiving aerials, T and R in figure 13 (*a*) if the height above the snow surface is small compared to z, the distance apart. They should, however, be higher than the effective linear electric dimensions of the aerials so that a radio signal may travel freely from T to R in time z/c. For a first approximation, the snow is assumed to be a uniform medium in which the radio velocity is v; a signal travels the path TXR in a time given by $v^2 t_x^2 = (z^2 + 4d^2)$ and the difference in the arrival time of the two signals at R is t_d, which may be measured directly on an oscilloscope.

Then v may be calculated from a series of values of t_x^2 plotted against z^2. Random error in the result due to error in the measurement of z is likely to be insignificant compared to that due to error in t_d.

There are two principal systematic errors to be guarded against in the use of this technique. First, the bottom may not be parallel to the top surface in the area of reflexion; the geometry is shown in figure 13 (*c*), d is the depth at the central point and β the bottom slope. Applying the cosine rule to TRR′

$$v^2 t_x^2 = z^2(1-\beta^2) + 4d^2. \tag{24}$$

Thus a slope of $\beta = 0.1$, if it is ignored or is unknown, produces an error of only $\frac{1}{2}\%$ in v and any slope of this magnitude or greater should easily be detected by vertical sounding, with T and R coincident, along the length of the baseline.

A second source of systematic error is introduced by refraction at the snow surface and within the upper layers if these are of lower specific gravity than the bulk of the material. The only safe rule is not to use spacings, z, greater than 1.2 times the depth, d, otherwise the ray will enter the surface at grazing incidence some indeterminate horizontal distance from the aerial itself. The restricted range of z limits the measured time difference, and hence the proportional accuracy of the result for v as will be seen by the example in the next section. The correct remedy is evidently to make many measurements within the narrow range of spacings allowed.

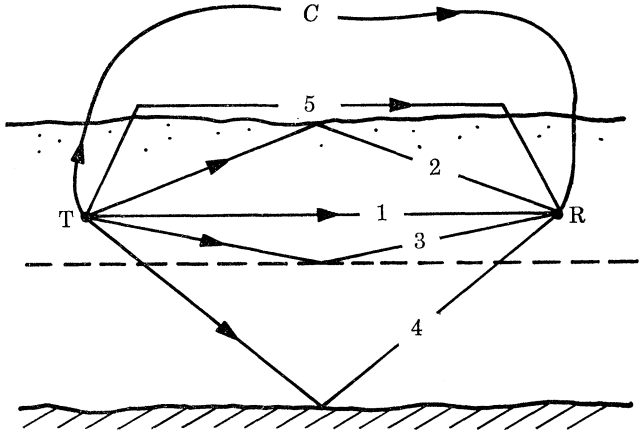

FIGURE 16. Illustrating alternative paths of propagation between buried aerials at T and R.

It may appear a practical proposition to overcome the above limitation by burying the aerials in the snow to a depth comparable with the aerial dimensions. The object is to utilize rays nearer to the horizontal than the critical ray so that larger aerial spacings, and longer time differences may be used for a given depth. However, there is a danger of confusion among the several pulses which arrive at the receiver. In figure 16 the ray paths 1, 2, 3, 4 and 5 are of unknown time delay and thus a zero reference pulse must be taken by cable *C*. The length and velocity of propagation in the cable must be sufficiently accurately known, it must have accurately matched attenuators at each end to prevent multiple reflexions, and some means (such as a variable attenuator) must be provided to identify which of the received pulses has travelled via the cable.

Refraction within the upper layers of snow, and its effect on the ray path and travel time, must be considered in either arrangement. In figure 12 the travel time from depth y_1 to y_2 is given by

$$[t]_{y_1}^{y_2} = \int_{y_1}^{y_2} n^2(y)\,\mathrm{d}y/c\sqrt{\{n^2(y) - N^2\}}, \tag{25}$$

where $n \sin \phi = N$ which, by Snell's law, is a constant defining the angle of entry or emergence. Consider two extreme models: (*a*) in which the refractive index increases exponentially, with $Y = 38$ m, from a value 1.31 at the snow surface to 1.78 at depth, as at Maudheim; and (*b*) in which the medium is solid ice of refractive index 1.78 throughout. Then the travel times from the top surface to 100 m depth are in table 3; the displacement in the last column is the difference in the horizontal component of the path travelled. Thus, even with buried aerials, angles greater than 45° or spacings greater than 1.4 times the depth may not be used in the accumulation zone though in principle the density distribution could be computed from results at a sufficient number of spacings. In the ablation zone, or wherever the surface densities are not too low, wider spacings may be used and more accurate results obtained thereby.

TABLE 3. RESULTS OF RAY PATH CALCULATION

angle of emergence below 100 m depth	travel times (ns)		(*a*) minus (*b*) (ns)	displacement, Δz (m)
	model (*a*)	model (*b*)		
vertical	530	590	−60	0
30°	650	680	−30	+10
45°	890	840	+50	+34
60°	∞	1180	+∞	+∞

(*e*) *Measurements at Tuto East*

A spaced aerial experiment was conducted near Tuto East, northwest Greenland on 6 August 1964. The position, 76° 23′ N 68° 03′ W, 6 km from the head of the Tuto ramp, appeared from direct sounding to have an average bottom slope of the order of $\tan^{-1}$ 0.05 though small irregularities contained slopes up to $\tan^{-1}$ 1.0. In this area the mean specific gravity of the top 2 m of snow is 0.40, but by extrapolation of the data given by Benson (1962) for 'station O-6' nearby, it is likely that the specific gravity reaches 0.90 at 20 m depth so that refraction in the upper layers is much less serious than in model (*a*) in §5(*d*) above. Half-wave dipole aerials were carried at a height of 2.5 m above the snow surface and their horizontal separation was measured by steel tape. Seven different positions were set up along a fixed straight line, in each case the aerials were equally separated about a fixed central point, and an A-scope display and timing waveforms were photographed, in some cases for more than one input attenuator setting. Time differences, measured by projecting the rising edge of the pulse back to zero, are given in table 4. A linear relation has been fitted by computer to the values of t_x^2 against z^2 for the least square error in t_x^2. The observations have been considered in two groups and the results are given in table 5. It is clear that the random error in measuring the time difference does not explain the change in the result when the widest separations are included. In the determining of the gradient of t_x^2 against z^2 it is unfortunately true that much greater weight is given to larger values of z, which are subject to systematic error, and a mistaken impression of the true accuracy is gained from the random error in the gradient.

In the same area in 1963, with spacings up to 400 m, Evans (unpublished) obtained

172 ± 12 m/μs and in the following year with spacings up to 520 m (A. H. Waite, J. Hryckowian & A. L. Zanella, private communication, September 1964) obtained 153 m/μs with no standard deviation quoted.

TABLE 4. ECHO TIMES FOR SPACED AERIALS

station	separation z (m)	time difference t_d (μs)	travel time t_x (μs)
9	100	3.46	3.79
8	200	3.24	3.91
8	200	3.19	3.86
7	300	3.17	4.17
7	300	3.13	4.13
6	400	3.09	4.42
6	400	3.09	4.42
5	500	3.29	4.96
5	500	3.25	4.92
4	600	3.31	5.31
3	700	3.54	5.87

TABLE 5. RESULTS OF SPACED STATION OBSERVATIONS

	velocity (m/μs)	ice depth (m)
all stations	154 ± 2	282
stations 9 to 6 incl.	166 ± 4	306

(*f*) *Measurements in Antarctica*

The most satisfactory and extensive spaced aerial measurements have been made at 30 MHz by Jiracek (1965; see also Bentley & Jiracek 1965) with the University of Wisconsin Antarctic field programme in the 1964/5 season. The observations were made in three different areas and several determinations were made in each.

On the McMurdo ice shelf, to the south of Ross Island, three baselines were occupied and their orientations with respect to the surface strain direction are known. In this area, Jiracek recorded signals which had travelled from top to bottom of the ice shelf more than once and independent determinations of the velocity of propagation may be made from each of these multiple echoes. In one case fourth-order echoes were used and altogether a total of sixteen values of the velocity was obtained, some in an ice depth of the order of 170 m and some in a depth of 320 m. The arithmetic mean velocity is 180 ± 5 m/μs, though this spread will include the real variations of velocity from one baseline to another. For an individual baseline Jiracek gives values of the standard error from ± 1 to ± 4 m/μs.

Two baselines were measured on the Skelton Glacier in an area of almost solid ice of depth 760 m. The mean of the two results here is 168.5 m/μs. Lastly, two baselines were measured on Roosevelt Island in depths of 500 and 800 m and the mean result is 174.8 m/μs. No multiple echoes were recorded at these other locations.

Jiracek discusses the results for each baseline separately in terms of the mean snow density, and there is excellent agreement with the laboratory measurements of permittivity referred to in the earlier part of this paper and with figure 14 in particular. One should not expect a precise quantitative relation with average snow density since it is not obvious what average will be obtained with a curved ray path in a varying medium. However, the result is satisfactory because the variation in density is not very great; the lowest average value is 0.82.

On the Skelton glacier the velocity obtained is in excellent agreement with that to be expected for solid ice of relative permittivity 3.17.

Measurements in Antarctica have also been made by Walford (1965) on the Brunt ice shelf, but problems with the apparatus have resulted in rather large uncertainties in the values obtained and they do not add materially to those already given here.

(*g*) *Comparison with seismic soundings*

Seismic reflexion shooting on the traverse in Greenland in 1964 was supervised by Clarke (1966) with the object of comparing ice depths measured by two independent techniques. The accuracy of seismic soundings at some shallow depths, up to 200 or 300 m, has been checked from boreholes. At greater depths accurate measurements have depended almost entirely on the seismic technique since it is by this technique that the results obtained from measurements of the variation in gravity are calibrated. The comparison of depths obtained from seismic shooting and those from radio echo measurements therefore provides the first real check of the validity and accuracy of all our values for the thickness of polar ice sheets. We must first discuss the accuracy of the seismic technique.

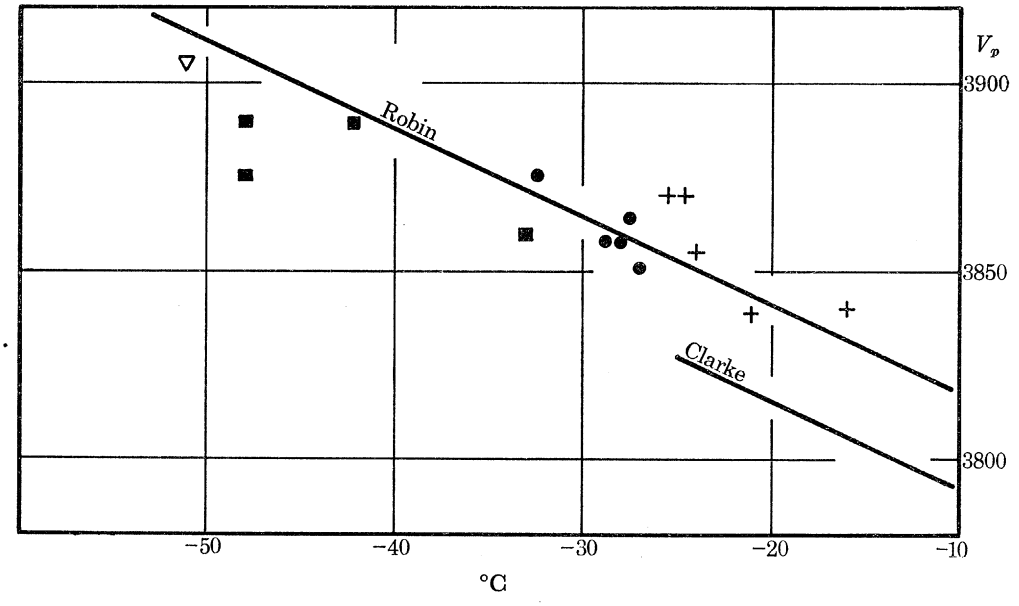

FIGURE 17. Seismic compressional wave velocity, V_p (metres per second), as a function of 10 m temperature (after Bentley 1964). The lower line shows the velocities used in reducing the seismic shooting on the 1964 Greenland traverse (Clarke 1966).

The velocity of seismic *P* waves in a polar ice sheet depends on density, temperature, crystal structure and orientation, but owing to our inadequate knowledge of the latter in deep ice sheets only the effects of density and temperature are normally considered. Robin (1958) has discussed the errors in general and studied the effect of density and temperature by laboratory measurements giving the following relation between wave velocity, V_p (m/s), relative density ρ, and the temperature, θ (°C):

$$V_p = 10^4(\rho - 0.059)\,(1 - 6.1 \times 10^{-4}\theta)/2.21. \qquad (26)$$

At Camp Century, where the temperatures and densities are known from measurements in a borehole, Clarke compared the results of his refraction shooting with this formula. The

values obtained fitted closely down to 100 m depth where the specific gravity is 0.892, but were too high for higher densities. The relation between velocity and 10 m firn temperature adopted by Clarke is shown in figure 17, the remainder of this figure coming from Bentley's (1964, p. 342) discussion of the seismic shooting results in Antarctica. The points plotted from field measurements are the maximum wave velocities in the Antarctic inland ice sheet determined by refraction shooting. The maximum is found in the top few hundred metres of the ice sheet, below which the increase of temperature with depth will cause lower velocities. If the temperature distribution at Camp Century is as calculated in §6(*c*) then the maximum velocity from Robin's formula would be 3850 m/s and the mean value over the total depth of ice would be 3842 m/s compared to a value of 3826 m/s adopted by Clarke for this station. The effect is that, on the basis of Robin's laboratory values of velocity, the ice depth would be 5 m greater. There could be no appreciable errors in the corrections which Clarke has applied for the effect of the low density layers near the surface and these will not be discussed further. Clarke puts his maximum uncertainty in the final results at ± 10 m due to the error in reading the arrival time on the records, and $\pm 2\,\%$ in velocity due to errors in the density and temperature. It is reasonable to suppose that the standard errors will be less than half these amounts except in a zone near the coast, where the ice thickness is less than 500 m and we believe the 10 m temperatures to be about 10 °C higher than estimated by Clarke (see §6(*b*)). For an ice thickness of 300 m this higher temperature would decrease the seismic results by 2 or 3 m.

In table 6 we show comparative depths obtained at a number of locations on the Tuto to Century trail and on the northern and southern traverses. Station names, such as 'mile 45', refer to survival huts whose actual distance from the Tuto ramp may differ by several miles from the nominal value but they are identifiable positions to which the seismic and radio echo depths refer, irrespective of errors in navigation. Stations such as P 42–10 refer to Mock's permanent glaciological stakes whose positions were surveyed by tellurometer-theodolite for strain-rate measurements. Radio echo depths are included in the table only when the position of the seismic line was marked on the radio echo record at the instant the vehicles passed. The radio echo depths are calculated assuming a constant velocity of propagation of 169 m/μs and to the depth obtained a 'firn correction' (see §5(*c*)) of 8 m has been added to obtain the depth tabulated. This correction is estimated on the basis of density distributions published by Schytt (1955) and Benson (1962) which show that the mean specific gravity of the top 2 m is 0.40 ± 0.05 for the whole area covered, with the exception of station 'Baker'. Where radio echo depths were available from measurements on both the outward and return journeys we have taken the mean value, and the difference between all seismic and radio echo depths is plotted in figure 18.

The seismometers were normally laid out on a line at right angles to one side of the trail used by the heavy vehicles so that the reflexion point is likely to lie about 100 m from the line of radio echo soundings. Though this may introduce error into the comparison there does not appear to be much correlation between the dip of the bedrock along the seismic line and the differences in depth found in the table. The mean difference in depth, without regard to sign, for the 27 points in figure 20 is ± 15 m and this is a measure of the uncertainty in a single observation. Taking account of the sign, the mean is 9 ± 3 m. This indicates that there is probably a systematic difference between the two techniques but, since most of the depths are greater than 1000 m, it is less than 1 %. If, instead of using Clarke's velocities, we used those of Robin in figure 19, and the temperature distributions derived in §6(*c*), then the mean

TABLE 6. COMPARISON OF RADIO ECHO AND SEISMIC DEPTHS

station	seismic results slant depth (m)	seismic results dip (deg)	radio echo results ice depth (m) outward	radio echo results ice depth (m) return
Able	167	7	—	—
Baker	255	1	265	222
Mile 7.5	293	2	309	—
Mile 17	254	7	242	—
Mile 30	579	30	no echo	no echo
Mile 45	352	4	386	306
Mile 60	735	7	722	722
Mile 75	910	2	939	924
Mile 90	969	2	996	965
Mile 105	1024	5	1040	1035
Mile 125	1292	1	1317	1297
P 42–4	1080	4	1095	1080
P 42–5	1098	11	1095	—
P 42–6	1175	7	1185	1141
P 42–7	1261	1	1286	1317
P 42–8	1281	1	1286	—
P 42–9	1335	3	1337	1362
P 42–10	1340	1	1387	1367
P 42–11R	1308	3	—	1337
P 42–12R	1328	1	—	1347
P 42–13	1317	2	1337	1325
P 42–14R	1333	11	—	1325
P 42–15	1389	5	1387	1394
P 42–16	1274	5	1300	1276
P 42–17	1227	26	1255	1248
P 42–18	1155	1	1152	1173
P 42–19	1113	2	1116	1132
P 42–20	1053	1	1076	—
P 42–21	891	2	924	906
	borehole depths			
Camp Century	1370 m to the silt 1387 m to the till		1379	1361

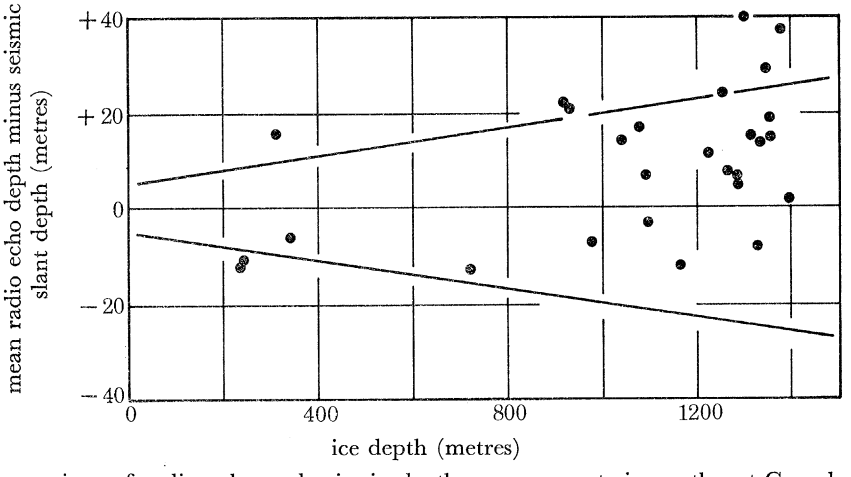

FIGURE 18. Comparison of radio echo and seismic depth measurements in northwest Greenland. Each solid circle refers to the measurements on a single seismic base-line; the straight lines represent a difference of ±5 m ±1.5 %.

systematic difference between the two techniques would be reduced to 4 ± 3 m. The straight lines in figure 20 represent a difference of ± 5 m $\pm 1.5\,\%$ which we estimated earlier to be the errors in radio echo sounding and they are approximately the same as the standard errors of seismic shooting. We can see that these estimates of errors appear to be generous. The maximum difference of any individual radio echo sounding from the seismic result is 52 m at 'mile 45' where the thickness was varying rapidly along the trail and positional errors are likely.

There is one further important comparison. Deep core drilling by U.S.A. C.R.R.E.L. at Camp Century reached the bottom of the ice sheet in July 1966 (Hansen & Langway 1966) and therefore we have accurate, unambiguous, information at this one point. Ice containing silt bands and small pebbles was encountered at 1370.5 m and after drilling through 16.9 m of this material, frozen till was reached at 1387.4 m from the ice surface. Some 3.6 m of the till was also recovered.

The radio echo vehicle approached within 300 m of the borehole position and the depths recorded on the outward and return journeys are entered at the end of table 6. It is conceivable that the top and bottom surfaces of the morainic material would be resolvable on the radio echo record but we can find no convincing example of it and we expect the ice/till interface to be the major reflecting discontinuity. Our average radio echo depth is 17 m short of the borehole depth to the till. Independent measurements of radio echo delay times in the vicinity of Camp Century have been compared with the borehole depths by Pearce & Walker (1967).

For other areas the implications of the findings in this chapter are that careful estimates of the errors in seismic reflexion shooting should be considered reliable. For example, Bentley's (1964) conclusion, that the maximum errors of ice thickness measurement by seismic reflexion method should not exceed $2\frac{1}{2}\,\%$ in East Antarctica and $1\frac{1}{2}\,\%$ in West Antarctica, is strengthened by the results in this paper.

6. Attenuation and ice temperature

Attempts to use a radio echo method for sounding the thickness of a glacier were made as early as 1948, but the initial uncertainty of success, and particularly the inadequate knowledge of the factors governing the attenuation, held back developments of the technique. Evans (1965) reviewed the available measurements of dielectric loss in ice and the results are summarised in figure 19, together with more recent measurements on Greenland cores by J. G. Paren (unpublished). Attenuation is seen to rise rapidly with increasing radio frequency above a few hundred megahertz and over the whole range the losses are markedly reduced as the temperature is lowered. Walford (1968) has shown that the losses in the 3 to 300 MHz band are approximately proportional to the amount of ionic impurity, above one part per million, in the ice. In figure 19 the data by Westphal cover a large part of the v.h.f. and u.h.f. frequency range and indicate the losses to be expected in our area of operations in Greenland since the measurements were made on ice samples taken by A. H. Waite from the Tuto ice tunnel at the edge of the ice sheet where our traverse started. Paren's measurements are further removed from the relevant frequency range but have the impurity content of the inland ice sheet of Greenland and there is close correspondence with Westphal's 150 to 300 MHz values. In the Antarctic, Brocas & Delwiche (1963) determined the quantities of ionic impurity in the ice. They concluded that the concentration of sodium and chlorine ions decreases from the

coast to the interior of the continent, although the potassium concentration seemed roughly constant. The total concentrations inland were of the order of $1/10^6$. Thus smaller losses than those indicated in figure 19 seem possible towards the centre of the Antarctic ice sheet, but in coastal areas losses could reach an order of magnitude higher. In radio echo experiments on the Brunt ice shelf, Antarctica, Walford (1964) and Bailey & Evans (1968) found that the attenuation varied greatly over distances of a few hundred metres. They suggested that the effect was due to the percolation of sea water into the ice, or that parts of the ice shelf were formed by the freezing of sea water. In this situation the losses were more than an order of magnitude greater than is indicated in figure 19, but this result is probably not typical of most Antarctic ice shelves.

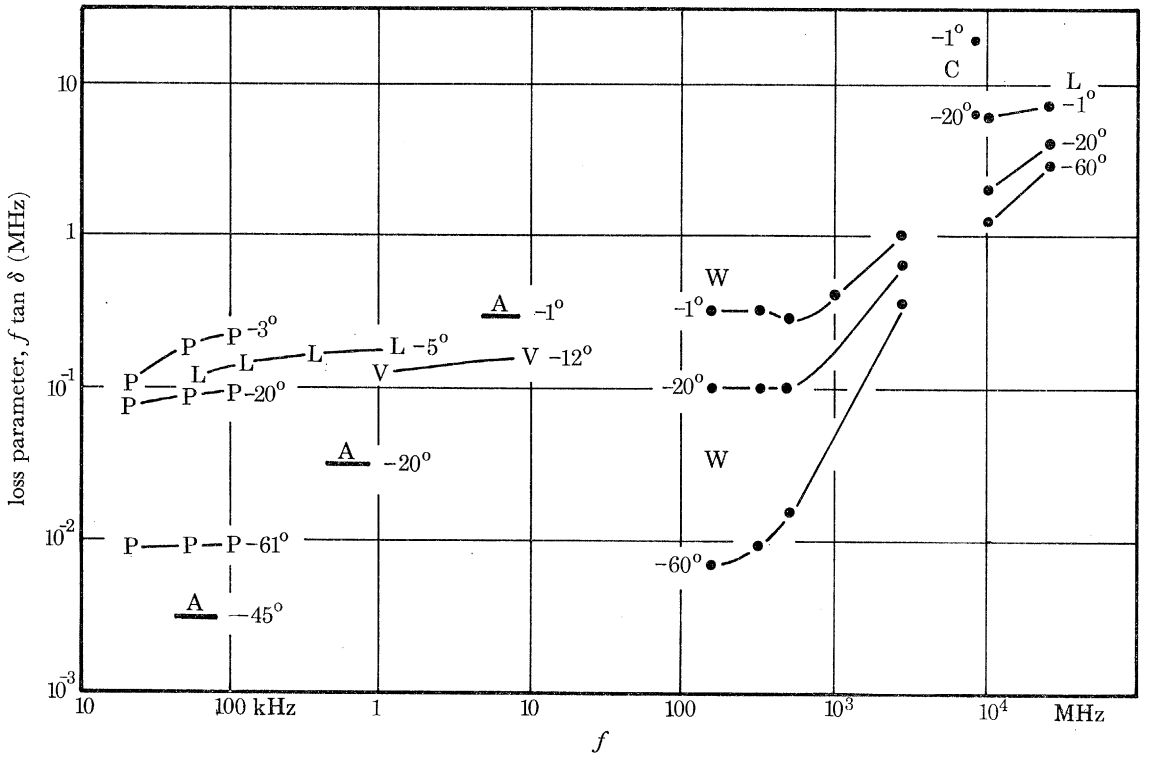

FIGURE 19. Loss tangent of ice against radio frequency, f. The quantity plotted vertically is $f \tan \delta$ where f is the frequency (MHz). The attenuation of a radio wave passing through the medium is given by $9.10 \sqrt{\epsilon'} f \tan \delta$ dB per 100 m path. Temperatures are marked in degrees Celsius. A, Auty & Cole (1952), limiting values extrapolated from the parameters of the observed relaxation spectrum; C, Cumming (1952); L, Lamb (1946) and Lamb & Turney (1949); P, Paren (private communication 1968), core from 100 m depth, 'site II' Greenland, density 0.89; V, Von Hippel (1954); W, Westphal (private communication 1963), Tuto tunnel Greenland, density 0.90.

In general, for radio waves in ice the lower the frequency, the less will be the dielectric absorption per unit path length. At 0 °C, the variation with frequency from 1 to 500 MHz is uncertain and it may be negligibly small but in 1962, when our work began, it was considered advisable to design apparatus to work at as low a frequency as practicable. At the lowest ice temperatures there is some advantage to be gained in using the lowest possible frequency and the band from 30 to 40 MHz was chosen. At even lower frequencies we expect interference from long distance communications, and furthermore the desired range accuracy could not be achieved using pulse amplitude modulation.

(a) Temperature distribution in ice sheets: general considerations

Numerical estimates based on figure 19 show that the feasibility of using radio echo methods for sounding ice thickness depend critically on the temperature distribution throughout the ice sheet. If the temperatures are near the melting point, as is usual in temperate glaciers, echoes are unlikely to be obtained through more than a few hundred metres of ice, while the presence of liquid water is likely to decrease performance still further. On the other hand, it will be possible to obtain echoes through several kilometres of ice if the temperature is below −20 °C. The maximum depths of ice so far measured by seismic sounding are 3.1 km in Greenland and 4.3 km in Antarctica. At the time at which these investigations were undertaken, the greatest depth at which the temperature had been measured in an ice sheet was 400 m (Hansen & Landauer 1958). Beyond that depth, temperatures had to be estimated on theoretical grounds, as described by Robin (1955) for the central portions of ice sheets which are in equilibrium: that is, the temperature, movement, surface form, and the rate of accumulation on the surface are all assumed to be invariant with time. The difference between the temperature θ_h at a height h above the base, at the centre of an ice sheet of thickness H and surface temperature θ_H is given by

$$\theta_H - \theta_h = \left(\frac{\mathrm{d}\theta}{\mathrm{d}h}\right)_{\text{base}} \frac{\sqrt{\pi}}{2} \sqrt{\left(\frac{2Hk}{\dot{a}}\right)} \left[\operatorname{erf}\sqrt{\left(\frac{\dot{a}}{2Hk}\right)} H - \operatorname{erf}\sqrt{\left(\frac{\dot{a}}{2Hk}\right)} h\right], \tag{27}$$

where $\dot{a}$ is the rate of accumulation at the surface, k is the thermal diffusivity of ice, and $(\mathrm{d}\theta/\mathrm{d}h)_{\text{base}}$ the temperature gradient in ice at the base of the ice sheet. This solution applies to the case where the temperature at the base is below the melting point. Zotikov (1961) has given the full solution in the presence of bottom melting, and Jenssen & Radok (1961, 1963) have applied digital computer techniques to some non-steady-state solutions. The temperature versus depth curves calculated from equation (27) predict isothermal conditions in the upper parts of thick ice sheets (2000 m or more) when a moderate accumulation rate exists. Observed temperatures at depths from 150 to 400 m at 'Site 2' and Station Centrale in Greenland, and at Byrd Station, Antarctica, all confirm the presence of a thick, approximately isothermal layer under such conditions.

Additional factors which govern the ice temperature are climatic changes, and departures from the assumption of equilibrium, such as changes of the surface elevation of the ice sheet with time. Also, away from the centre of the ice sheet, colder ice from further inland moves out beneath the warmer surface acccumulation and tends to produce a negative temperature gradient whose maximum value close to the surface is

$$\alpha u L/\dot{a} \quad \text{(Robin 1955; Radok 1959).} \tag{28}$$

The surface slope is α, u is the horizontal velocity of the ice, and L the gradient of mean annual surface temperature against elevation (approximately 1 °C/100 m). An analysis by G. de Q. Robin (in press) shows that for three deep boreholes, this movement effect and the generally accepted pattern of climatic change over the the last 500 a (years), are sufficient to explain the observed temperature gradients in the upper 500 m of polar ice sheets. The change of ice thickness with time does not appear to be sufficient to modify the temperature gradients appreciably.

Most of the present data have been obtained on or near the long sloping ridge which runs from the Thule Peninsula to Century. Horizontal ice motion on this ridge is likely to be low,

as shown by measurements of Mock (see Weertman 1968) which give a movement of 3.3 m/a at Century. Hence equation (27) is likely to give a reasonable guide to temperature variations with depth in the area in which this work was done. We have sufficient data to estimate the various parameters in equation (27) along our routes, including the critical quantities, θ_H and $\dot{a}$. Uncertainty in the temperature gradient at the bottom of the ice is much bigger than errors which may be introduced by neglecting corrections for bottom melting, or climatic change. The temperature gradient at the bottom was assumed to be 3 °C/100 m. This is equivalent to a geothermal heat flux of 50 mJ m^{-2} s^{-1}, which is around the mean value for the other continents, but could be considered as including a small additional heat supply due to basal friction.

In 1966, the borehole at Camp Century penetrated the ice to bedrock at a depth of 1390 m, and provided a full temperature–depth curve (Weertman 1968). This is compared in figure 20 with our previously calculated curve based on equation (27). The difference between the calculated and observed curves are significant in relation to the theory of heat flow in an ice sheet, but for the practical purpose of calculating the total absorption of radio waves, the difference is only 1 dB in the two-way path. We have therefore used the Robin equation (27) without any corrections, at a number of points along the Tuto to Century trail, even though our estimated heat flow at bedrock was 20 % greater than that observed at Camp Century.

(*b*) *Temperature and accumulation in northwest Greenland*

Apart from ice temperatures measured to a depth of 410 m at 'Site 2', and to bedrock at Camp Century (as shown in figure 20), the information available is limited to the uppermost 10 m of ice. In order to apply equation (27) we need to know the mean annual ice temperature at the surface, and this is most easily measured by taking the ice temperature at a depth of about 10 m where seasonal effects are negligible. On polar ice sheets the 10 m temperature is close to the mean annual air temperature provided there is little surface melting: the process governing the temperature at 10 m is then primarily thermal conduction. However, if meltwater percolates into porous firn it may raise the temperature to the melting point at depths greater than 10 m even though the mean annual air temperature may be some degrees lower. Below the firn line where the surface layers consist of non-porous ice, the summer meltwater runs off as surface streams and the ice temperature at 10 m depth is again approximately related to the mean annual air temperature.

In figure 21 we have plotted observations of mean annual temperature (approximate 10 m temperatures) as a function of elevation above sea level. The observations were all made in Greenland between latitude 76° 20′ N and 77° 20′ N by various workers during the period 1954 to 1963. Some scatter is to be expected because observations were made in different seasons and most of the values due to Benson are based on measurements at about 4 m depth, while the others come mainly from observations at 8 or 9 m depth. The crevasse temperature is an exception and it was measured at 30 m depth.

Some surface melting of the ice is known to take place up to elevations of 2100 m (Benson 1962), but the trend in figure 21 indicates that above 1300 m elevation meltwater does not modify the 10 m temperature appreciably. However, its effect becomes increasingly important below 1300 m and at 800 m elevation the temperature had risen to the melting point at 9 m depth in late August 1954 (Schytt 1955). Note that the three temperatures from non-porous

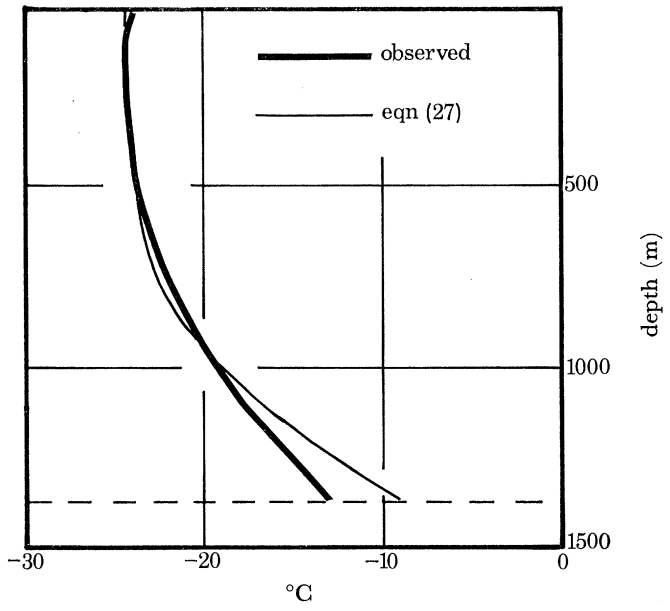

FIGURE 20. Temperature against depth at Century. The observed curve has been published by Weertman (1968). The parameters used for the theoretical curve are given in the text, y is the depth in metres.

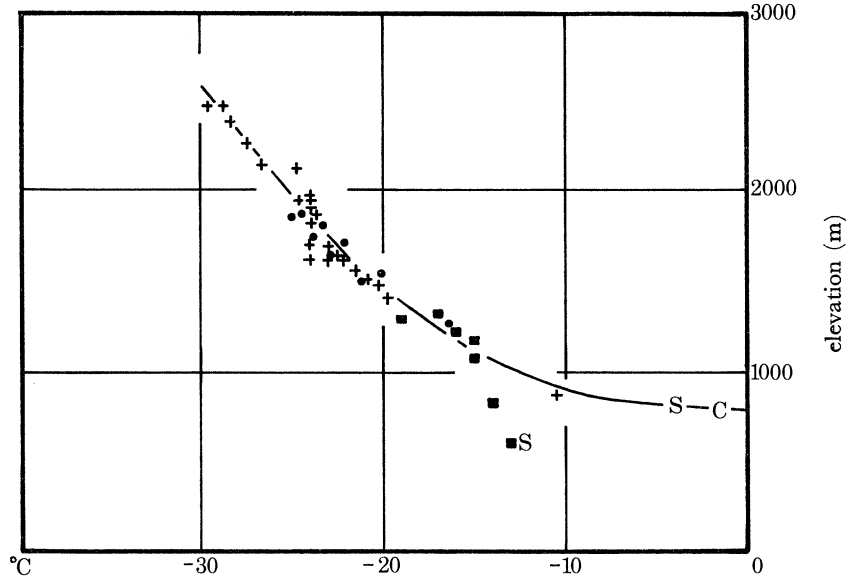

FIGURE 21. Mean annual ice temperature plotted against elevation above sea level near latitude 77° N in Greenland. +, Benson (1962); ●, Mock (1965); ■, Nobles (1960); S, Schytt (1955); C, Crevasse (Rinker, private communication July 1964).

ice below the firn line lie near the extrapolated temperature/elevation trend from the higher, and drier, firn zone.

The largest variations in 10 m temperature are likely to occur between 800 and 1000 m elevation in the firn zone where meltwater has the maximum effect. Even here, the trend of measurements by different observers is reasonably consistent so that there is justification in using the mean curve to interpolate the 10 m temperature at any elevation.

For the higher parts of the ice sheet dealt with in this paper, accumulation measurements

have been presented by Mock (1968) and Benson (1962). Net accumulation in the area is greater than 60 cm of water equivalent per year on southward facing slopes and approximately 30 cm/a on northerly slopes in the northern area. The firn line near Tuto lies at 700 m elevation (Schytt 1955), but a little farther north on the Nuna ramp it appears to lie at 900 m. Benson (1962) also gives 700 m as the height of the firn line on southward facing slopes in this region. His detailed pit studies along the route inland from Tuto show clearly that, apart from the Tuto ramp area, the whole inland trail lies within the firn zone including the section which falls to an elevation of 700 m near the 50 km point on the main profile (figure 37). The accumulation data used later in ice temperature calculations for specific locations, are based on the reports by Schytt (1955), Mock (1968) and Benson (1962).

(*c*) *Calculated absorption*

Since the route from Tuto to Camp Century roughly follows the crest of a broad ridge we suppose that ice is unlikely to flow from distances far inland, and equation (27) should present a reasonable approximation to the temperature distribution in these areas. Using a temperature gradient of 3 °C/100 m we have calculated the temperature distributions at seven points on the Tuto to Century trail on the basis of the available 10 m temperatures and accumulation data. The results are illustrated in figure 22. At the 48 km point (not illustrated) we have assumed that the whole column is at between -1 °C and the melting point, owing to the percolation of meltwater.

Once the temperature distribution is known, the total radio wave absorption is estimated by applying the numerical value of tan δ appropriate to the temperature at each depth. Field measurements of dielectric absorption in firn have been given by Yoshino (1961) and Walford (1968), using transmission line techniques; Walford also derived some values from echo strengths at 30, 100 and 440 MHz observed in the Brunt ice shelf. The uncertainties of field measurements are thought to be greater than the best laboratory measurements, but Walford's results indicate absorption of similar magnitude to those obtained by Westphal at 150 MHz, but higher absorption at 440 MHz. We have used the Westphal values at 150 MHz (figure 19) as the best indication of the absorption at our frequency rather than attempting any interpolation between the results of different workers at different frequencies. This is done for three reasons.

First, Westphal's data relates to samples from the Tuto ice tunnel within our area of operation. Secondly, Westphal's results show no appreciable change of absorption with frequency from 150 to 500 MHz at -1 and at -20 °C, and only a small effect at -40 °C. Thirdly, the results at lower frequencies (except for Paren) were obtained on ice from distilled or conductivity water. The difference in absorption between Westphal's measurements at 150 MHz and those marked A, L and V (below 10 MHz) may be due to variations in ionic impurity content rather than to a variation of absorption with frequency. The absorption curve used for calculating the attenuation is shown in more convenient practical units in figure 23, derived from Westphal's measurements at 150 MHz (curve W). For comparison, a curve obtained by extrapolation from Auty & Cole's measurements on pure ice at lower frequencies is shown by curve A.

Alongside each of the temperature distributions in figure 22 is shown the variation of attenuation in dB per 100 m, and for each location the total absorption of a radio wave in the two way passage from top to bottom and back, has been obtained by graphical integration of the area to the left of the attenuation curve. Note that the total absorption is expected to be less at

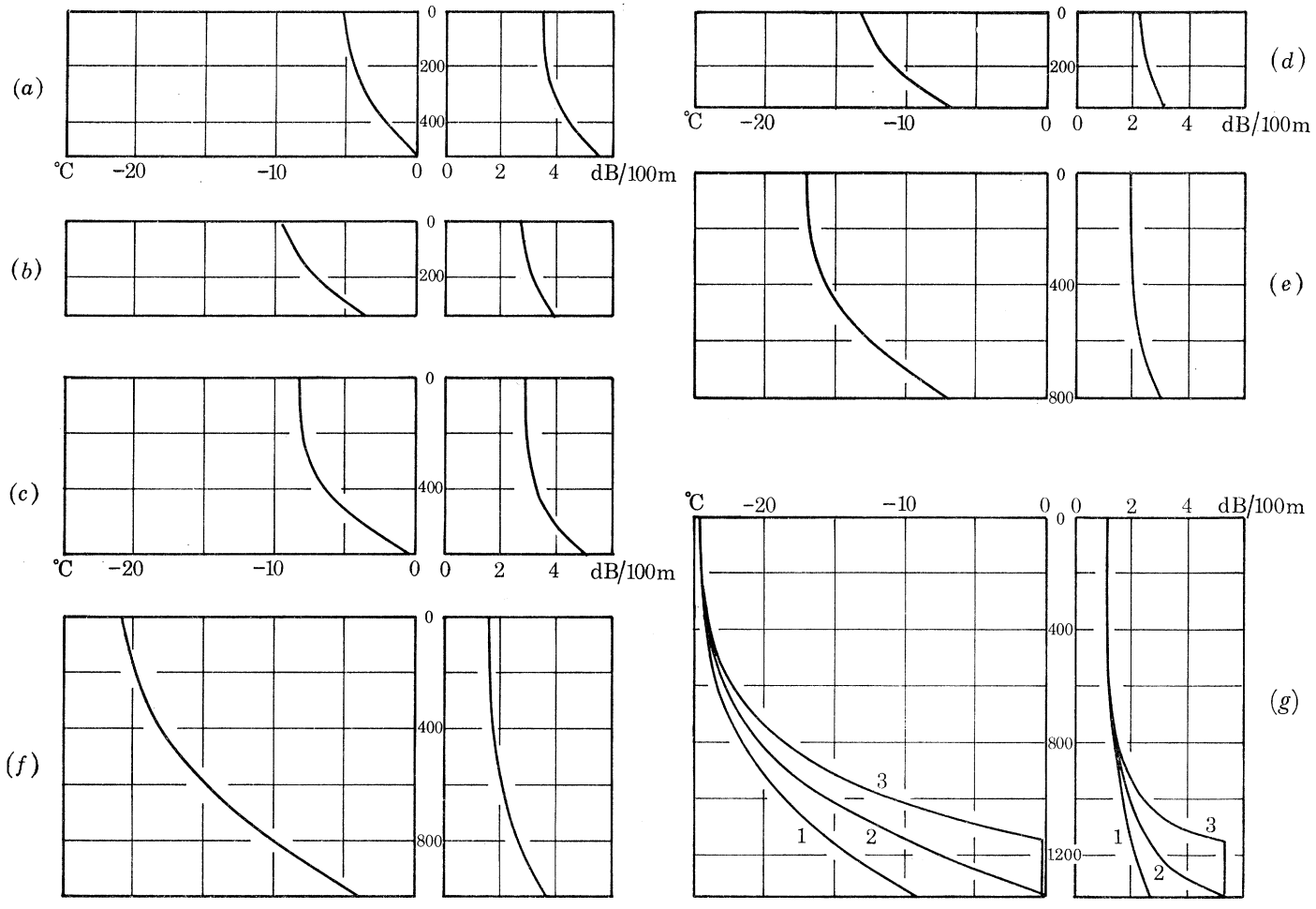

FIGURE 22. Calculated temperature profiles, and absorption plotted against depth, at seven points on the Tuto to Century trail. For each location the temperature profile is plotted to the left in degrees Celsius, and absorption to the right in dB per 100 m. The depth is scaled from the top surface downwards and the grid lines are at 200 m intervals. At the 48 km point, the temperature is assumed to be −1 °C throughout the whole depth.

	position on main trail (km)	elevation (m)	attenuation (dB) two-way total
(*a*)	32	840	46
—	48	690	56
(*b*)	61	950	21
(*c*)	68	930	42
(*d*)	76	1100	18
(*e*)	96	1340	34
(*f*)	144	1560	42
(*g*)	Century	1885	(1) 42 (2) 50 (3) 60

Camp Century, where the ice depth is 1370 m, that at the 48 km point where the depth is 550 m. At Camp Century we have also calculated the absorption for two other cases: if the temperature rose to pressure melting point at the bottom, and for the case where it rose to the melting point 200 m above the bottom, being isothermal in the intervening layer.

(d) Absorption estimated from echo strengths

The setting of the input attenuator on the receiver was recorded in the operational log from time to time and these settings can be used to estimate the total absorption which occurred in the field. Since the echo amplitude fluctuates by approximately 20 dB as the vehicle moves along the trail the attenuator setting was chosen so that echoes of maximum strength just saturated the recorder display and this is approximately 20 dB above the setting at which the

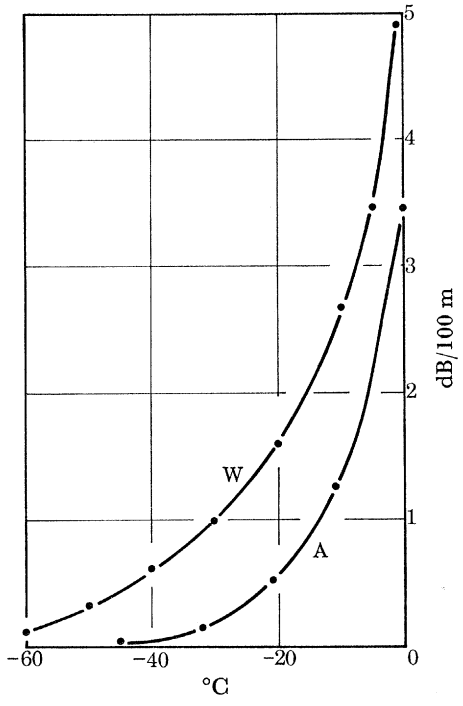

FIGURE 23. Absorption of radio waves in ice. A, Auty & Cole (1952), extrapolated from relaxation spectrum of pure ice; W, Westphal (private communication 1963), Tuto tunnel sample at 150 MHz.

echo would be lost in the noise. In order to estimate the average strength of the echo above noise power before attenuation we have therefore added 10 dB to the setting recorded in the log. An uncertainty of ± 5 dB remains in a single observation. In future it is clearly desirable to record regularly the input attenuator setting necessary to reduce the echo to a fixed level, probably the noise level, and to check occasionally the total attenuation required to reduce the transmitter pulse, fed directly into the receiver, to the same level. The difference is an absolute measure of the echo strength, independent of any parameters of the apparatus, except attenuator calibration.

In figure 24 we show all recorded echo strengths plotted against ice thickness. Most of the observations were recorded during the outward journey from Camp Tuto to Camp Century and on the southern traverse. The few points recorded during the return journey give confidence that no great change in equipment performance took place during the field work. Since the aerial system and transmitter were changed several times during the operations, all the echo strengths have been standardized to the performance when using dipole aerials and the U.S.A.E.L. transmitter, which was the arrangement when most of the echo strengths were recorded.

In order to discuss figure 24 it appears desirable to divide the data into two groups, one in which the ice mass is likely to be nearly isothermal and close to the melting point throughout, and a second group in which the temperature distribution is likely to fit equation (27). The 10 m temperature data in figure 21 suggests that the dividing line should be drawn for a surface elevation close to 800 m, but the echo strength data in figure 24 is best divided at 1000 m surface elevation. Thus, the circles show all data below 1000 m (the highest elevation being 922 m) and the crosses relate to all observations above 1000 m (the lowest being 1068 m), and we shall discuss these two regions separately.

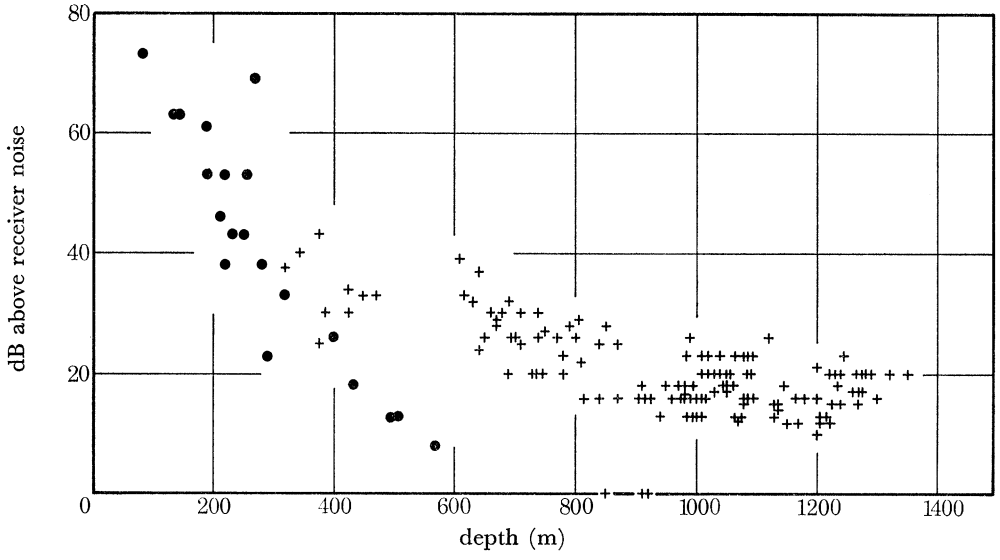

FIGURE 24. Echo strength measurements. Solid circles refer to places below 1000 m surface elevation, crosses refer to higher surface elevations and lower mean annual temperature.

(i) *Isothermal ice mass, surface elevations below* 1000 m

Referring to the circles in figure 25, the broken line represents an absorption loss of 4.5 dB/100 m for a plane wave while the two full curves show the effect of adding to this the loss by spreading, due to either an inverse square law, equation (2), or an inverse cube law, equation (5). The difference between the two is not very great and it is concluded in §4 that the real behaviour lies somewhere between these two limits. Thus, taking account of the scatter of points, we estimate the mean absorption for this ice mass to be 4.5 dB/100 m. The estimate is dependent on two assumptions only: that the equipment performance, and the reflexion coefficient at the bottom surface, were constant throughout the observations. The limited scatter of points gives confidence in these assumptions. For comparison, Westphal's laboratory measurements on an ice core from this area (curve W in figure 23) showed an absorption of 4.9 dB/100 m at -1 °C. We therefore conclude that for surface elevations below 922 m the main bulk of the ice is within two degrees of the melting point, in spite of the evidence on 10 m temperatures in figure 21.

In order to compare the absolute measured echo strengths with estimates of absorption made in §6(*c*) we need to consider the following factors:

S the system performance, being the ratio of the transmitter power to that which can just be detected by the receiver (146 dB with the U.S.A.E.L. transmitter in 1964);

R the power reflexion coefficient of the ice-rock interface beneath the glacier;

A the total dielectric absorption of a plane wave travelling from top to bottom of the ice and return.

G geometrical factors which take account of the aerial dimensions, refraction effects in the upper snow layers and spreading of the wavefront (equation (2) or (5));

E the observed echo strength, above the limit of detection.

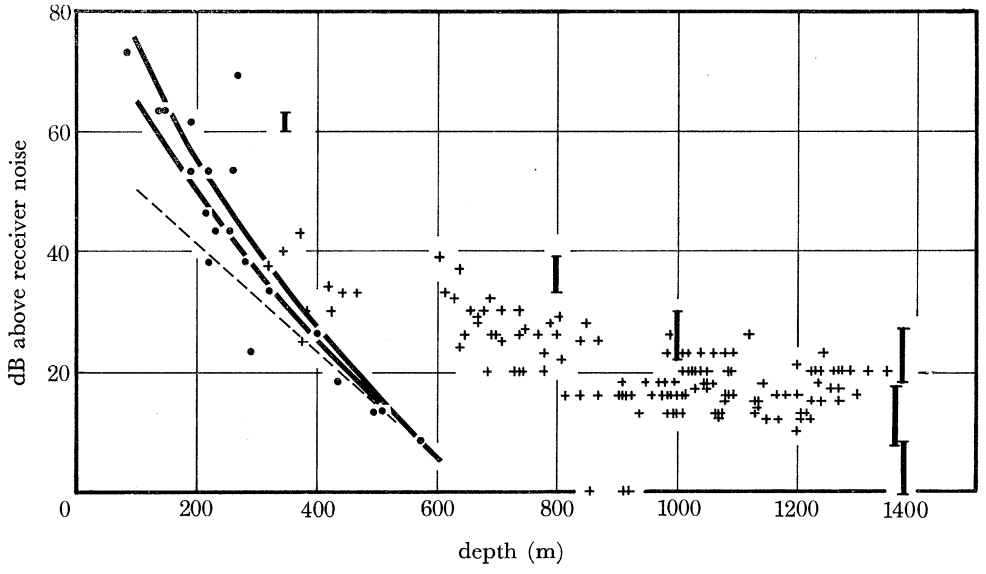

FIGURE 25. Echo strength measurements compared to calculation. At low elevations the ice mass is nearly isothermal at the melting point. The gradient of the broken line is 4.5 dB/100 m; the two curves show the effect of adding to this the loss due to spreading, according to an inverse square law and an inverse cube law. At high surface elevations the thick vertical lines show the echo strengths predicted on the assumptions given in §6(*d*).

If all the above factors are measured or calculated in decibels (R is negative in sign, all others are positive in our convention), we have the relation

$$S+R = E+A+G. \tag{29}$$

From data on the isothermal ice mass, shown in figure 25, we see that for an ice thickness of 500 m, our echo strength is 13 dB above noise level. We calculate A for an attenuation of 4.5 dB/100 m and we find from equation (2), for an inverse square law:

$$S+R = 13+45+62 = 110 \text{ dB}$$

from equation (5), for an inverse cube law:

$$S+R = 13+45+67 = 115 \text{ dB}.$$

Since the system performance is calculated to be 146 dB, this indicates that the mean reflexion coefficient is between -31 and -36 dB or, in other words, the energy reflected from the glacier bed is about one part in two thousand of the incident energy. This is much lower than the estimated reflexion coefficient of -14 dB derived in §4(*f*), and is lower than the estimated limit of -22 dB for quartz-based materials. It suggests that either the model of a simple ice-rock interface is inappropriate, or that some additional absorption takes place close to bedrock in this region.

(ii) *Cold ice mass, surface elevations above* 1000 m

All the echo strengths observed at elevations above 1000 m are shown by the crosses in figure 25. Since there are large variations of temperature with ice depth in this region, we cannot apply the treatment of the preceding paragraph. Instead we reverse the procedure, use the calculated total absorption from § 6 (*c*) and predict the echo strength by inserting the following numerical values in equation (29): $S = 146$ dB, $R = -14$ dB, A from figure 22, G from equations (2) and (5). Predicted values of E are shown by the vertical lines in figure 25 for four ice thicknesses and for each of the models of the temperature distribution for Camp Century. The upper and lower limits of the vertical lines are calculated from the two values of G, but other uncertainties are not included.

We note that for Camp Century, the temperature distribution (1), calculated from equation (27), produces a predicted echo strength about 5 dB stronger than the observed mean value, while model (2) in which the temperature rises to melting point at bedrock, produces a predicted echo 5 dB weaker than the observed mean. Finally, model (3) with a layer 200 m thick at the pressure melting point, predicts an echo strength 15 dB weaker than that observed.

It is the estimate for R which is likely to produce the biggest error in predicted echo strength. A much lower value of R, as found in the warmer ice near the coast, would have made it almost impossible to detect the echo at Camp Century even on the most favourable temperature distribution. The highest possible value of R, 0 dB, would only just raise the predicted echo power for the warm model (3) to the observed mean level at Camp Century.

The group of observations for ice thicknesses from 300 to 450 m seem to lie significantly lower than the predicted echo strength. Unfortunately, the nine points concerned all result from a period of not more than 3 h recording on 30 June 1964 over a small distance, at surface elevations from 1090 to 1280 m on the main trail from Tuto to Camp Century. There is no record of echo strength for this section on the return journey.

(*e*) *Conclusions*

(i) For ice thickness from 1000 to 1400 m (surface elevation 1400 to 1900 m), our model of temperature distribution and our estimated total absorptions match observed echo strengths within the limits of experimental errors. In particular, the effective reflexion coefficient in this zone is appreciably higher, probably by 10 to 15 dB, than that where the whole ice mass is at pressure melting point and it may be significant that the calculated basal temperature is below the pressure melting point throughout this thick inland zone.

(ii) At Camp Century a layer of finite thickness at the pressure melting point could hardly be reconciled with the observed echo strengths. Now that the temperature profile has been observed directly in the borehole, it strengthens our estimates of the other factors and hence our conclusions about reflexion coefficient and echo strengths, at other locations.

(iii) Observed echo strength for ice thickness between 300 and 950 m (surface elevations between 800 and 1350 m) suggest that mean ice temperatures are higher throughout the mass than those derived from equation (27) using the available accumulation and 10 m temperature data.

(iv) Three abnormally low values of echo strength, observed for an ice thickness near 900 m, came from the deep ice-filled valley at 91 km on the profile in figure 38. Although the echo strength was not recorded at this point on the return journey, the disappearance of the echo on

the film record confirms the validity of the low echo strength. We suggest the presence of a basal layer 100 to 200 m thick at the pressure melting point, or a low reflexion coefficient typical of the warmer ice near the coast.

(*f*) *Predicted echo powers at other locations*

If we look at the trend of measured echo strength with increasing ice thickness in figure 24 it appears that the average decrease is of the order of 2.5 dB/500 m, from 900 to 1400 m. In other words we need to add 5 dB/km to our system performance to cope with increasing ice thickness. However, this empirical result appears unlikely to hold over wide areas, owing to wide variations of surface accumulation on large ice sheets, and the resultant effect on the temperature profiles.

We have therefore based our predictions of performance on temperature profiles calculated from equation (27), using observed or likely values of the 10 m temperature and the rate of accumulation for a number of locations in Greenland and Antarctica. To be of general use the estimates should be as free as possible from equipment parameters and therefore we have assumed specular reflexion according to an inverse square law rather than diffuse reflexion according to an inverse cube law since the magnitude of the echo in the latter case depends on the pulse length. We have shown that in practical cases of interest the difference between the two is not very great; the diffuse echo is generally weaker but this need not be so for a longer pulse length.

TABLE 7. PREDICTED ECHO STRENGTHS

location	ice thickness (m)	10 m temperature (°C)	net accumulation (water equivalent cm/a)	calculated dielectric absorption (dB)	reflexion loss (−dB)	geometrical factor (dB)	calculated echo strength, dB down on transmitter power
north Greenland (1)	2800	−28.0	10	96	14	69	179
north Greenland (2)	2000	−26.0	30	60	14	66	140
central Greenland	3000	−28.0	30	84	14	70	168
Antarctica							
Byrd Station	2645	−28.5	18	83	14	68	165
Byrd Land	4200	−28.5	18	108	14	72	194
South Pole	2800	−51.0	7	62	14	69	145
Vostok	3600	−57.4	2.5	81	14	71	166

We have assumed that the product of aerial power gain and absorption cross-section in air are the same as for a single halfwave dipole at 35 MHz and we have included the power gain due to refraction. Allowance may easily be made for a higher aerial gain in other cases. Table 7 gives the assumed values of the mean annual temperature and the net annual accumulation at seven chosen locations. The total absorption is calculated as in §6(*c*) for the Westphal attentuation data given in figure 23. The last column gives the ratio of transmitter power to echo power including the inverse square loss and a constant reflexion coefficient of −14 dB at the bottom of the ice.

Since these estimates were made, Bentley & Jiracek reported (privately, 1965) that they had obtained echoes at the South Pole and the absolute strength seemed to be very close to our predicted value. In June 1966 the U.S. Army Electronics Laboratory made long range radio echo flights over Greenland and found echo strengths generally in agreement with our predictions except in the north of Greenland where we expected the echoes to be below their limit of detection, though the system performance has not been given directly. However, the error is most likely to lie in the assumed value of the annual accumulation since a higher rate of accumulation would reduce the temperature at depth, and hence the total absorption.

In December 1967 the Antarctic flights made by the Scott Polar Research Institute at the invitation of the U.S. National Science Foundation gave echo strengths in broad agreement with table 7 over a wide variety of conditions. In particular, in the vicinity of Byrd, and the vicinity of Vostok, the echo was detectable, intermittently with a system performance of 166 dB in remarkably close agreement with the strengths predicted in table 7. The 1967 echo strengths will be analysed fully elsewhere, by a development of the methods used in this section.

7. Bedrock topography, ice flow, and internal layering

The map in figure 1, and the cross-sections of the ice sheet in figure 37 present a broad picture of the ice cover in the region which was investigated. In § 6, the temperature distribution throughout the ice sheet was discussed in some detail in the light of new information provided by the echo strengths. This section discusses what fresh light can be thrown on other characteristics of the ice sheet from the results of radio echo sounding and we have included: characteristics of the bedrock; surface form of the ice sheet in relation to the bedrock topography; and internal reflecting layers within the ice sheet.

(*a*) *Bedrock topography*

The topography of this surface can be discussed on various scales. The largest features are those which may be seen on the detailed profile, printed directly from the film records in figure 38. Since the recorder film-transport mechanism was not coupled directly to the vehicle odometer, there is some variation in the relation between film movement and trail distance. This has been taken out, as far as possible, by trial-and-error adjustment of the horizontal-to-vertical scale at which the record has been printed on to paper so as to make it correspond with the scales used for the plot immediately above. In the printing machine, devised by D. L. Petrie, the film record is driven at a selected steady speed through the gate of a conventional 35 mm projector and the paper is driven at a fixed speed past a slit, 0.1 mm wide, in the image plane. Any misleading sections of record, mainly due to failure to maintain constant separation of the receiving and transmitting aerials, have been removed from this figure. Note, however, that there is still some wandering of the zero from which the echo time-delay is measured (the top edge of the broad white band) and allowance should be made for this when inspecting the smaller scale depth variations.

What topographical features do we expect to find? The bedrock of the coastal strip is well exposed; not only is there negligible vegetation but Pleistocene glaciation left little debris and this is mainly confined to the valley floors. In the Kap York District and Inglefield Land the exposures consist of the Precambrian Shield and areas unconformably overlain by stratified

rocks. The Basement complex, of coarsely crystalline metamorphic and igneous rocks, represents the northeastern part of the great Canadian-Greenlandic Shield and most of its eastern limit is obscured by the inland ice. The stratified rocks of the Thule Group consist of more than 2000 m of flat-lying sediments of late Precambrian age, loosely overlain by Lower Cambrian sediments, likely to give rise to a flat topography. A geological sketch map of the area (after Berthelsen & Noe-Nygaard 1965, p. 211) is shown in figure 26. The contact between the Basement rocks and the sediments is most notably exposed in Wolstenholme Ø (figure 27) and a good impression of the glaciated topography of the Shield may be gained from the photograph of Sukkertoppen area (figure 28) where the relief is of the order of 300 m but reaches 1000 m in isolated places.

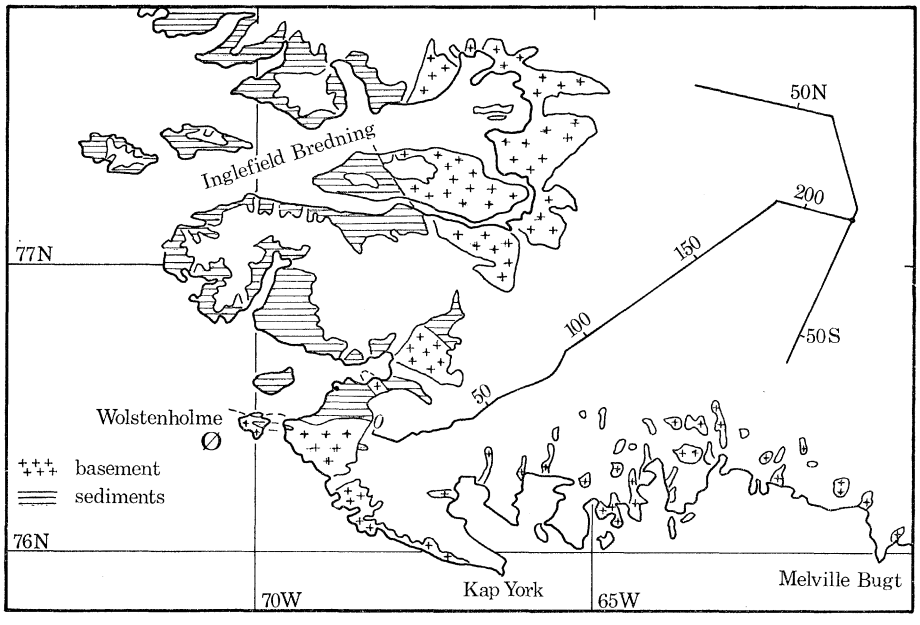

FIGURE 26. Geological sketch map (after Berthelsen & Noe-Nygaard 1965) showing, for the coastal exposures, the basement rocks of the Canadian-Greenlandic shield and the areas overlain by flat-lying sediments, without further division of rock type.

Turning to the radio echo profile, we see that the mountainous relief of about 300 m in the coastal section of the main trail, extends to the 130 km point, which is actually 45 km directly inland from the ice edge overlooking Inglefield Bredning. It is natural to associate this

DESCRIPTION OF PLATE 11

FIGURE 27. Wolstenholme Island, northwest Greenland, from the air, looking SSW. The basement rocks give rise to the generally lighter-toned areas and in particular are recognizable by the cliffs to the right, characteristic of coarsely crystalline rocks. The sediments are exposed in the foreground and to the left, where the highest point of the island lies; strata are exposed around the peaks and in the cliff faces, and the top surface is distinctly darker in tone. (Photograph, Geodetic Institute, Denmark (A. 101/68).)

FIGURE 28. Sukkertoppen area, southwest Greenland, from the air, showing heavily glaciated terrain characteristic of the coastal strip of exposed rocks. (Photograph, Geodetic Institute, Denmark (A. 150/67).)

FIGURE 29. The vertical ice front from the Etukussuks Dal in Peary Land. The annual precipitation here is low. Note the numerous dirt bands, the figure of a man, and in the foreground, the pebble-strewn plain. (Photograph, B. Fristrup, Copenhagen.)

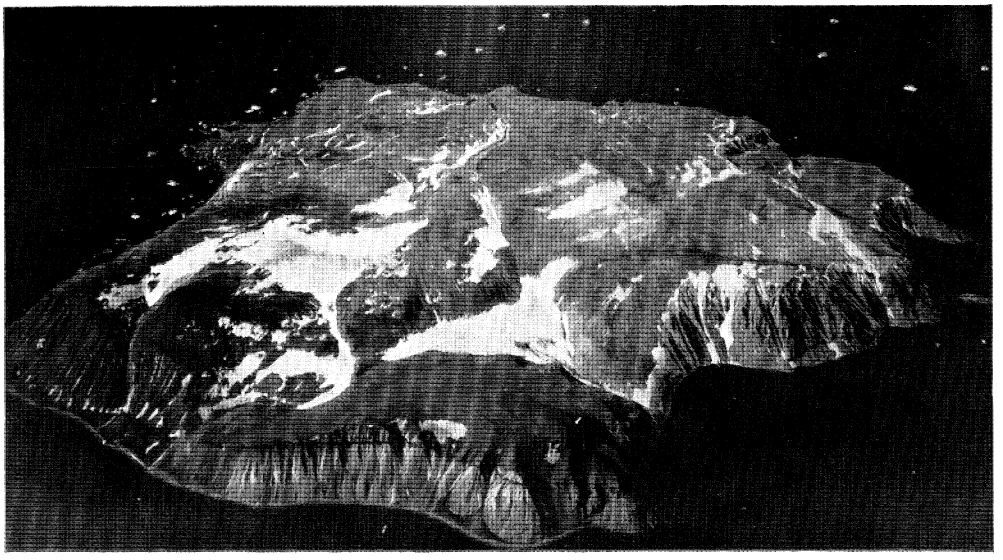

FIGURE 27

FIGURE 28

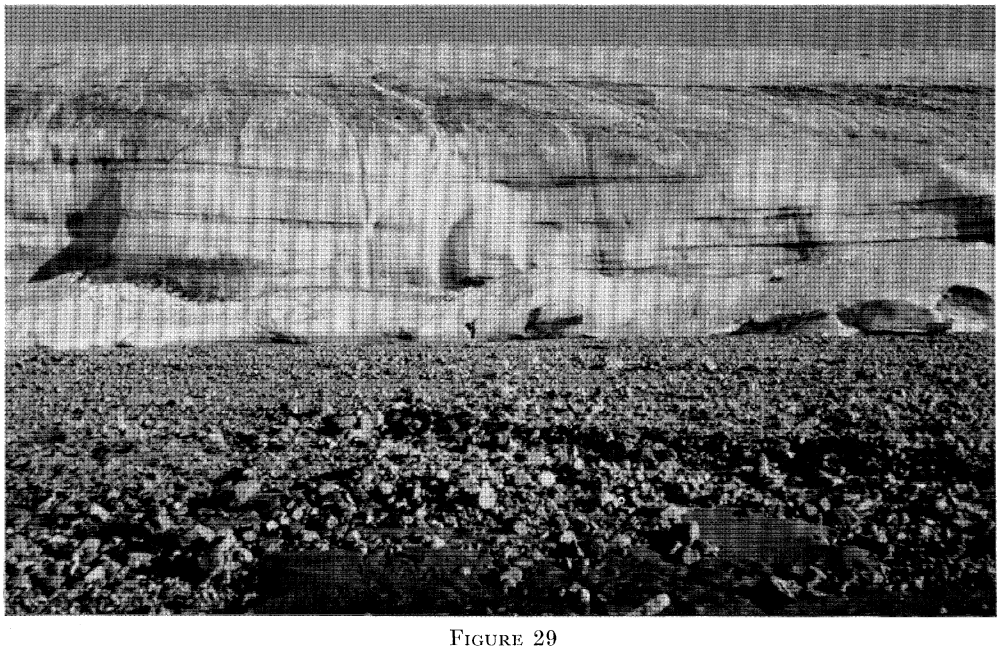

FIGURE 29

(*Facing p.* 482)

coastal section of the trail with the Basement rocks exposed along the whole coastline of Kap York and Melville Bugt and to consider if the sediments exposed around Inglefield Bredning could account for the very flat topography recorded along the remainder of the main trail, for 30 km of the southern traverse, and possibly all except the northwestern extreme of the northern traverse. Certainly the limits of these traverses stretch towards coastal regions where the exposures are wholly of Basement rocks. The inland plain, in so far as we have traced it, lies within 600 ± 100 m of sea level throughout our profiles. However, both the Basement and the sediments, where they are exposed on the southern coast of Inglefield Bredning, form striking plateaux at exactly this same level, so no definite conclusion about the composition of the plain can be drawn from its elevation above sea level.

Our only direct knowledge concerning the composition and conditions at the bottom of the ice sheet is provided by observations from the drill hole at Camp Century. The preliminary report (Hansen & Langway 1966) states that 'at a depth of 1370.5 m, ice containing silt bands and small pebbles was encountered. On 4 July, after we had drilled through 16.9 m of this material, the interface at the bottom of the ice cap was reached at a depth of 1387.4 m. The bottom material is frozen till; 3.55 m of this material was recovered.' Thus, at one point only, we know the character of the bottom surface and bearing in mind the danger of generalising from this one point, it can be suggested that the presence of till may explain the relative smoothness of the bottom of the ice in the inland regions, at least on the small scale. As mentioned in §4, we can gain some information on this from the echo fading rate and from the extension in echo duration, to be seen in figure 38. Notice that close to Camp Century the echo strength is almost constant over a distance of several kilometres, and the extension of the trailing edge of the echo is small compared to the total echo delay. Thus facets of the reflecting surface at considerable distance from the perpendicular point, and therefore at longer range, do not return significant power to the receiver and the surface behaves as smooth for this wavelength and pulse length. On the other hand, about 20 km inland of the ice edge, where the slopes of the large scale bottom features are known to be steep, we can see that the echo extends out to a range of the order of twice the perpendicular depth, and the fading in strength is deep and very rapid. In table 8 we have compared the apparent slopes of bottom features measured in three different ways: by the large-scale variation of depth and position, by the extension in range beyond the minimum (perpendicular) range, and by the maximum echo fading rate in cycles per kilometre.

The interpretation of table 8 is as follows. First, the contrast between the large-scale mountainous slopes of about 14° in column 3, and the gentler slopes of the inland plain, about 2.5°, is greater than the contrast for small features. Probably the fading rate is limited by the pulse duration as is to be expected when the extension in range is greater than the pulse length which is 40 m. The observed fading rate does not vary greatly from 50 c/km and this may be alternatively expressed as a correlation of around 10 m for horizontal displacement. One should expect the fading frequency always to be of this order unless the surface is very smooth compared to the radio wavelength, and the depth of fading will also decrease as this condition is approached. Columns 4 and 5 show that local irregularities on the bottom return power from surprisingly large angles, even in the inland plain. The angles are as great as those commonly observed at shorter wavelengths from aircraft flying over unglacierized terrain (Edison *et al.* 1960) and this suggests that the reflexion contains a diffuse component produced by irregularities of the same order of size, or smaller than, the radio wavelength, distributed on an

otherwise smooth surface. We suggest that the kind of terrain illustrated in front of the ice in figure 29 would behave in this way.

In the mountainous coastal strip it is easier to visualize that reflexions will occur at large angles to the perpendicular but the observed angles in column 5 are so large as to be limited by the aerial polar diagram in ice. From the fading depth, it seems likely that the reflexion contains a larger random component here and thus we deduce that in both regions the variations of echo power with range will be intermediate between an inverse-square law (equation (2)) and an inverse-cube law (equation (5)). Edison *et al.* (1960) reached the same conclusion by direct measurements with radio altimeters, over a wide variety of terrain, and we used these two laws as the limits when calculating the geometrical factors affecting the echo strengths in §6.

TABLE 8. ESTIMATES OF BOTTOM ROUGHNESS

Column 1. Position, defined by the scale of kilometres on the main trail.

Column 2. Ice depth (metres).

Column 3. Large features: the maximum bottom slope ± 0.5°, maintained over a distance of 500 m, to be found within 5 km each way of the position given.

Column 4. The extension in range of the echo, averaged over 500 m each way.

Column 5. Small features: the slope of facets derived from the echo extension (see §4(*d*)).

Column 6. Fading rate, the number of peaks in echo amplitude per kilometre.

Column 7. Small features: the maximum slope of facets contributing to the fading rate (see §4(*e*)).

1	2	3	4	5	6	7
213	1280	2.5°	50	16°	36	5°
191	1160	2.5°	60	18°	48	7°
173	1050	2.0°	45	16°	38	5.5°
147	950	3.5°	63	20°	53	7.5°
117	825	14.5°	65	22°	58	8°
98	760	11.5°	74	24°	60	8.5°
76	310	14.5°	100	40°	60	8.5°
26	330	9.0°	90	39°	65	9°

Some other features to be seen in the profiles may be briefly mentioned. Very steep slopes occasionally appear if there are regions from which no vertical echo is obtained. Then an observer moving horizontally will receive a single echo whose range increases hyperbolically with distance from the vertical to the echoing region. This is the situation between 80 and 86 km on the main trail where there are three hyperbolic loci representing three separated reflecting regions, duplicated with remarkable similarity on the outward and return journeys. This type of echo was characteristic of those obtained by Walford (1964) on the Brunt ice shelf and it is frequently seen on marine ultrasonic echo sounders.

Where steep bottom slopes are maintained over some distance, soundings calculated from the minimum-time echo do not correspond to the vertical depth. We are not so much concerned with the 'cosine correction' but with the fact that the result refers to a point displaced upslope and the possibility that the vertical depth at the observer is grossly different (example (*a*) in figure 30). When travelling across the narrow valley in figure 30(*b*), a minimum-time echo will never arise from within the shaded portion, though there are likely to be longer range echoes from facets in the valley bottom. Conversely, the sharply convex peak is responsible for the echo obtained the whole way from P to Q. It would clearly be an aid to interpretation to use narrow beam aerials, directed vertically, and this would at the same time be the most direct

way to limit the area of the bottom surface which is illuminated and to learn more about the smaller irregularities which are of considerable interest in the resistance to ice flow at the glacier bed.

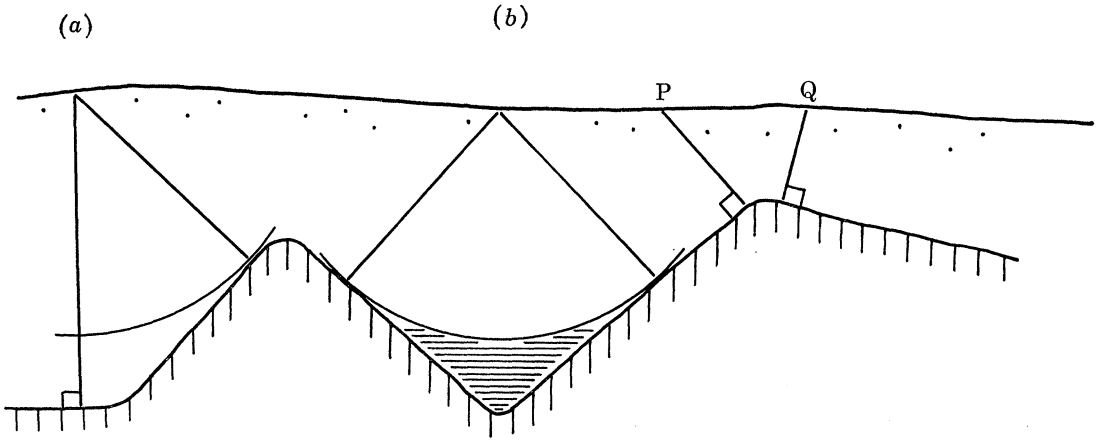

FIGURE 30. Illustrating geometrical problems of interpretation in regions of steep slopes, narrow valleys, and peaks.

(*b*) *The surface form of the ice sheet*

The surface form of ice sheets has been studied extensively over the past two decades, both theoretically and by observation. Following the suggestion by Orowan (1949) that ice could be treated as a substance with a definite yield stress, Nye (1951) developed a theory which related the surface form of glaciers and ice sheets to the flow properties of ice. From Orowan's initial simplifying assumption of a single yield stress, which led to a parabolic equation for the surface profile of ice sheets resting on a flat base, gradual improvement has been made to the theory. Instead of the assumption of a plastic yield, a realistic flow law was incorporated into a comprehensive theory by Nye (1957). Weertman (1957) derived a theoretical relationship governing the sliding velocity of ice, and this was used later by Nye (1959) to derive a surface form, allowing for variation in the velocity of ice movement from central to peripheral regions of the ice sheet. This paper also made some predictions about the effect of a subice ridge on surface slopes.

The basic relationship used in most of the thoretical papers relating the thickness H at any point on an ice sheet, to the basal shear stress τ is

$$\tau = \rho g H \sin \alpha, \tag{30}$$

where α is the surface slope.

Although in earlier papers (Nye 1952) some emphasis was placed on the need for conditions to be uniform over a distance of order H around the point of observation for this equation to apply, this restriction has frequently been ignored. Observers such as Bentley (1964) and Robinson (1966) who have attempted to make experimental checks of equation (30) have found that the relation fails to explain the detailed surface form of the Antarctic ice sheet. On the other hand, the relation does appear to provide an explanation of the broad scale form of the ice sheets of Greenland and Antarctica (see, for example, Haefeli 1961). Bourgoin (1956), on the basis of limited seismic soundings, also considered that it explained undulations of the ice sheet in Greenland.

The main difficulty which has prevented the development of the theory relating surface form to bedrock topography over short distances, has been the inadequate data on ice thickness and bedrock relief. In the past such knowledge has been derived from a series of spot soundings by the seismic shooting technique, spaced perhaps 30 to 100 km apart, and rarely made along a flow line for a continuous distance of several times the ice depth. In recent years, much more detail has been provided by frequent gravity measurements, but these indicate average ice thicknesses over a distance around the point of observation of similar order to ice thickness.

Continuous profiling of ice thickness by the radio echo sounding technique has given so much more detail of the bottom relief that a new approach to the relationship between ice surface and bedrock topography was made by Robin (1967*b*), using the surface and bottom profiles for a distance of 45 km along the traverse to the south of Camp Century. This route was laid out by Mock (1963) along the estimated flow line, and values of ice temperatures and accumulation given by Mock (1965) have provided the data necessary for a preliminary study of the problem. It is shown by Robin (1967*b*) that a much better explanation than that of earlier theories is given if one adds to equation (30) an extra term which allows for the presence of longitudinal stresses, σ_x^0, along the flow line. A simple two dimensional analysis shows that the surface slope is related not directly to these stresses, but to the stress-gradients, by the equation

$$\alpha = \left(\frac{\tau}{\rho g H}\right) - \frac{1}{\rho g}\left(\frac{\mathrm{d}\overline{\sigma_x^0}}{\mathrm{d}x}\right). \tag{31}$$

The stress gradient in the last term, in the flow direction x, is defined in terms of the mean value of σ_x^0 throughout the ice thickness where $\sigma_x^0 = \sigma_x - \sigma_y$. Collins (1968) sets out an exact solution to this two-dimensional problem and shows the approximations which are introduced using equation (31). He shows that provided bottom slopes are not too great, and in general that $\overline{\sigma_x^0} = \overline{\sigma_x - \sigma_y} \gg \frac{1}{2}\tau$, then σ_x^0 effectively represents the departure of the longitudinal stress from the weight of overlying ice.

The procedure to check equation (31) is to assume an equilibrium ice sheet and to estimate the velocity of movement, u, from

$$uH = \int_0^x \dot{a}\,\mathrm{d}x, \tag{32}$$

where $\dot{a}$ is the rate of accumulation and x the distance from the ice divide. Strain rates, $\dot{\epsilon}_x$, are then estimated on the same assumption from

$$\dot{\epsilon}_x H = \dot{a} - u(\mathrm{d}H/\mathrm{d}x), \tag{33}$$

and these are converted to longitudinal stresses $\overline{\sigma_x^0}$ using

$$\overline{\sigma_x^0} = C\,\dot{\epsilon}_x^{\frac{1}{4}} \tag{34}$$

which is an approximate form of Glen's (1955) flow law. The constant C is based on Glen's laboratory data and the temperature throughout the vertical column of ice. By determining $\overline{\sigma_x^0}$ every 220 m along the profile, one can then determine the component of slope α_F, due to the stress gradient, and defined by

$$\alpha_F \rho g = -(\mathrm{d}\overline{\sigma_x^0}/\mathrm{d}x) \tag{35}$$

This gives the series of values of α_F shown in figure 31(*c*) (reproduced from Robin 1967*b*). Each point is based on values of $\dot{\epsilon}_x$ and $\overline{\sigma_x^0}$ determined from the change of ice thickness over a distance of 880 m. The gradient, $\mathrm{d}\overline{\sigma_x^0}/\mathrm{d}x$, is taken from the change of $\overline{\sigma_x^0}$ over the same distance.

The results of this study of the southern profile are shown in figure 31. The good agreement between observed slopes and those calculated from equation (35), indicates that the concept of longitudinal stress gradients is a substantial improvement to theory in spite of the approximations: the use of mean values over distances similar to the ice thickness, the smoothing introduced by taking a running mean of α_F over five calculated points, and the final adjustment to the value of the flow velocities—this last adjustment accounts for the difference between (*c*) and (*d*) in figure 31. In contrast to these results it was shown explicitly by Mock (1968) that the available theories did not explain the observed relationship of surface form to bottom relief for the ridge at 27 km on the southern profile.

Since Robin's analysis was completed, Mock (1968) has published revised figures for accumulation in the region around Camp Century, and detailed measurements of surface strain rates and velocities are now being evaluated. The strain rate and velocity data will make a better test of equation (31) practicable. The revised accumulation figures are up to 50 % greater than the earlier ones towards the southern end of the profile in figure 31. Preliminary figures for surface velocities (S. J. Mock, private communication 1967) suggest that those used in calculating curve (*c*) are fortuitously close to the most recent observations. However, the broad conclusion that velocities are less than those indicated from the assumption of equilibrium, remains unchanged. Further study of this problem is being carried out by Mock on the basis of his additional data.

The only other section of our profile which lies for any appreciable distance along a probable flow line, is the part of the northern profile 40 to 89 km from Camp Century. Like the southern profile, this section was laid out by Mock to carry out strain rate and velocity measurements along an estimated flow line on an ice sheet. Precisely the same approach has been used as for the southern profile in order to calculate the values of α_F along this flow line. The limited data on the surface form of the ice sheet made it more difficult to estimate values of u in equation (32), but they were obtained on the basis of a map by Benson (1962) and velocities, deduced from the assumption of equilibrium, varied from 10 m/a at the 40 km point to 15 m/a at the 90 km point. Values of accumulation given by Mock (1965) were used as before, but on this profile they do not differ from the most recent figures (Mock 1968) by more than 20 %. The calculated slope variations, α_F derived from the equilibrium assumption, proved to be greater in absolute magnitude although similar in sense, to the observed variations. This may be seen in curve (*c*) of figure 32 and the values of α_F were recalculated using velocities reduced to two thirds of the value obtained from the assumption of equilibrium. This gave a considerable improvement in the fit as shown in curve (*d*) except around the 75 km point on the profile where the drop of bedrock height is so great that a fit could only be obtained by decreasing the velocity to an unreasonably small value. It is clear that equation (31) gives a good quantitative explanation of the surface form of the major part of the profile from 40 to 89 km. Since we are tackling a three-dimensional problem in terms of two-dimensional data and theory, some discrepancies are to be expected and we shall not attempt further explanation of the poor result around the 75 km point.

Budd (1967) has attempted to deal with the problem in three dimensions by applying a correction factor deduced from the strain rate in the third dimension $\dot{\epsilon}_z$, where $\dot{\epsilon}_z = \nu\dot{\epsilon}_x$ and ν is a constant of proportionality. His correction factor may be regarded as subtracting the proportion of the strain rate in $\dot{\epsilon}_x$ due to the stress system $(\sigma_x - \sigma_z)$ so that a more realistic value of the vertical strain rate $\dot{\epsilon}_y$ is made, and an improved value of $(\sigma_x - \sigma_y)$ along the flow line is

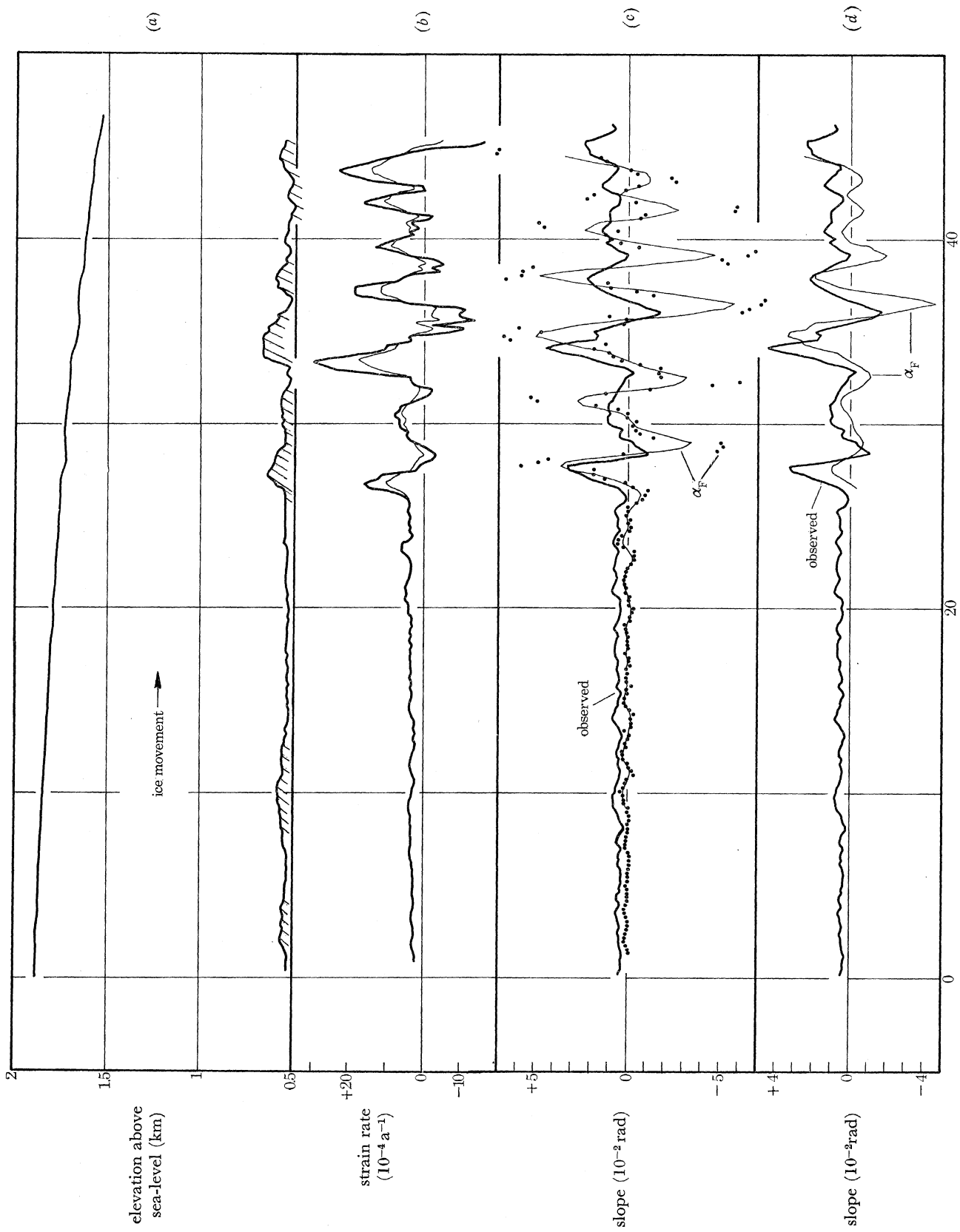

FIGURE 21. For legend see facing page

obtained. In principle the idea is useful and over the long intervals used for strain measurement on Wilkes ice dome it appears to produce some improvement in analysis. However, Budd's analysis uses only mean values of strain rates in the plane perpendicular to the flow line. The problem of how far disturbances of strain rates along one flow line affect surface slopes along adjacent flow lines has not yet been solved theoretically. We shall therefore see if our observational data provide any practical information of the effect of the third dimension.

A relevant study was made further to the south of the southern profile. Soundings were obtained along the three lines, about 8 km in length, shown in the plan in figure 33, using light vehicles and a less effective antenna system. The centre line, B in the plan, is a continuation of the southern traverse and in each case the surface form is shown in exaggerated form above the profile itself which is plotted without vertical exaggeration. Owing to the lack of reliable accumulation data along these lines, a less efficient radio echo sounding technique, and some uncertainty over the direction of flow lines, we have not calculated values of α_F here. Nevertheless, the general character of surface profiles in each of the three cases appears to be related to the bedrock profile in much the same way as along our calculated profiles, although the surface slopes differ considerably between the three lines. Profile C is not more than 500 m to the west of profile B (that is less than the ice thickness) but immediately downstream from the steep slope on B is a rising surface which is absent from profile C. Surface slopes on profile A (which lies from 600 to 2500 m to the east of profile B) appear to be explicable in terms of equation (31) and the bedrock profile, although profile A differs greatly in detail from B. We conclude from these results that bedrock irrgularities modify the surface slopes along the flow line, and that effects transverse to the flow line are of secondary importance, although such effects must be present.

In contrast to the southern traverse, the route for the first 40 km to the north of Camp Century runs roughly along the 1880 m contour, as may be seen from figures 1 and 38. The lack of any relationship similar to that obtained along the flow lines, is apparent when one studies the bottom irregularities along this section of the profile and attempts to relate them to surface form. We are therefore led to a similar conclusion to the prevous paragraph, namely that the field evidence suggests that the primary factor causing local variations of surface elevation is the bedrock relief along the line of ice flow.

We shall now consider the data on the main trail from Tuto to Century, a profile recorded not because it lay along either flow lines or contours, but because it provided as safe a route as practicable. For this reason it tends to be near the crest of a broad ridge running from the inland ice sheet towards Camp Tuto. Owing to the tendency of ice to flow off to the sides of such a ridge, it is believed that velocities of ice movement along the broad crest of the ridge are relatively low. This in turn leads to absence of crevasses, the prime safety factor which led to the selection of the route. A rough estimate, based on the probable drainage basin (Benson 1962), suggests that velocities along the inland half of this route are likely to be of the order of 5 m/a, similar to velocities within 20 km of Century on the southern profile.

FIGURE 31. (*a*) Profile of the upper and lower surfaces of the ice sheet along an estimated line of ice flow for 46 km to the south of Century. (*b*) Estimated strain rates, $\dot{\epsilon}_x$, along the same profile. The heavy line is calculated from equation (33) on the steady-state assumption. The thin line is based on one half the velocities of ice movement calculated from the steady-state assumption. (*c*) Observed surface slopes (heavy line) compared with the calculated slope variations, α_F. The points show individual results from equation (35) based on the change of ice thickness between soundings 880 m apart. The continuous thin line is the running mean over five points. (*d*) The same as (*c*) using one half the velocity of ice movement for the southern half of the profile.

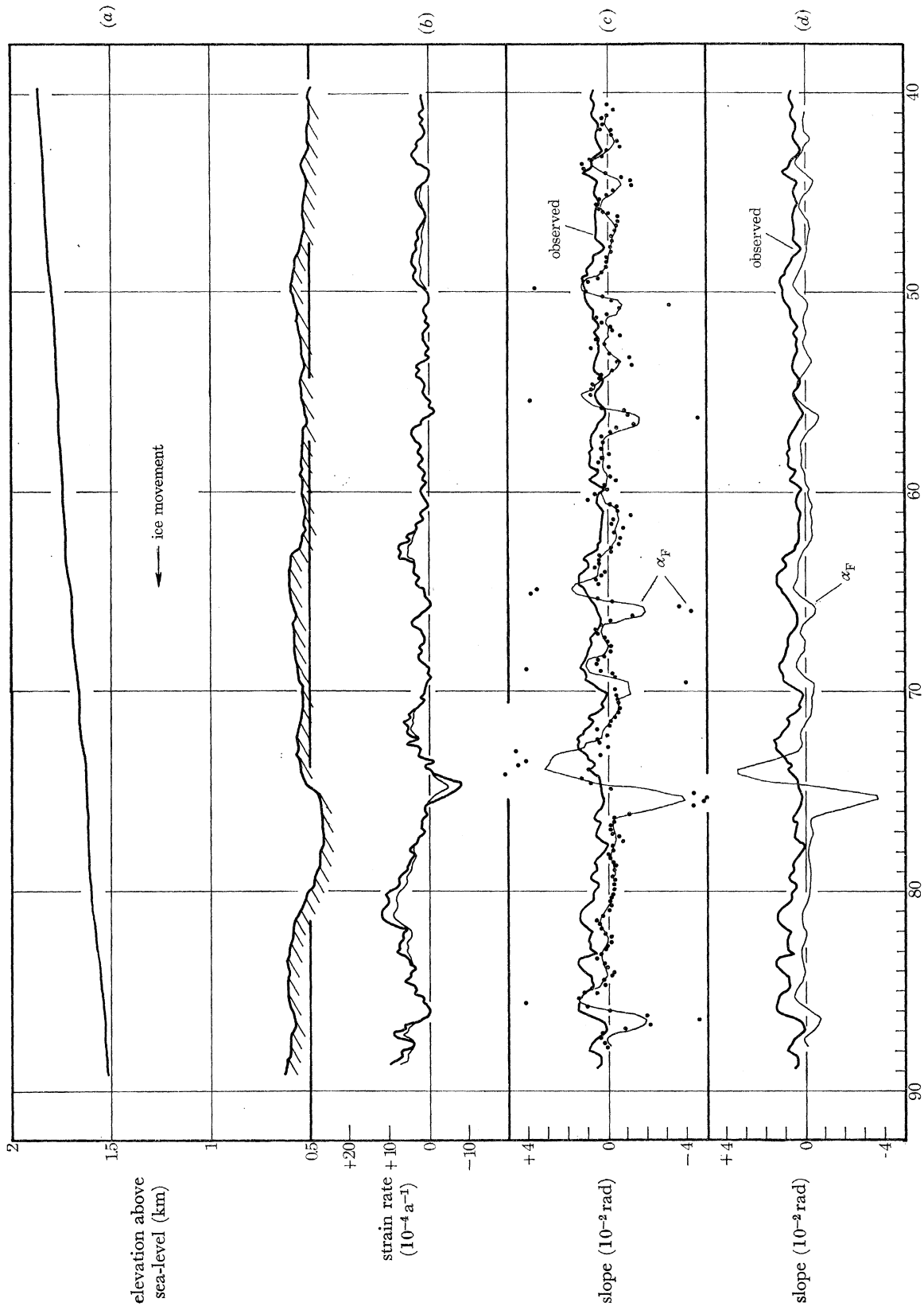

FIGURE 32. The same as figure 31, for a section of the northern traverse, 40 to 89 km from Century. The thin line in (*b*) and the calculated slopes in (*d*) are based on velocities of ice movement reduced to two thirds of the calculated steady-state values. This fits the magnitude of the observed surface slopes best, except at the 75 km point.

From 220 to 195 km on the main trail, both the map and the steep surface slope (figures 1 and 38) suggest that the profile lies close to the line of ice flow. Changes of bedrock relief on this section are small and this, together with relatively low movement of ice, produce a fairly uniform surface profile. From 195 to 108 km, surface slopes are less than those from 220 to 195 km, possibly because the route lies on one side of the ridge, but more probably because the height of the ridge is controlled by the slopes off to either side, rather than the flow of ice down the line of the ridge. This is emphasized by the weak control of surface slopes exerted by the large variations of bedrock relief between 130 and 108 km. From 108 to 90 km slopes steepen considerably and appear more subject to control by the bedrock relief, and hence seem likely to lie along a flow line.

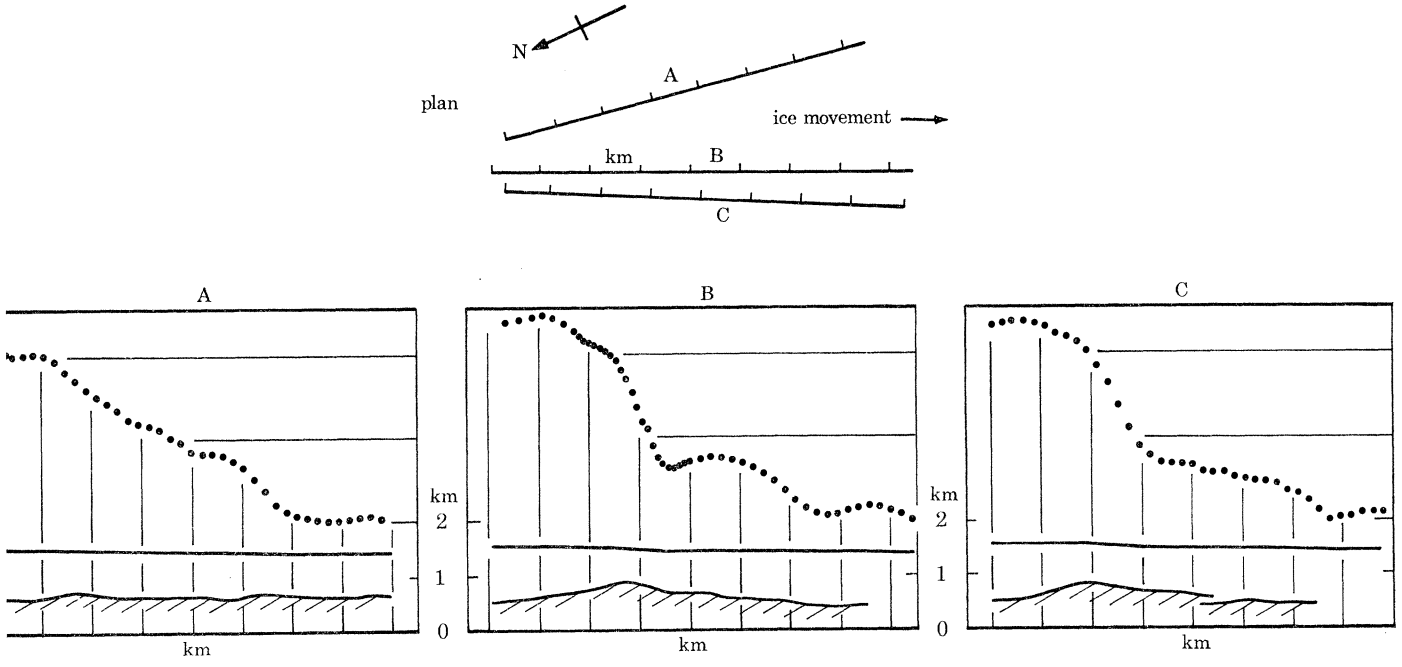

FIGURE 33. The plan at the top shows the disposition of three traverses A, B, C, each about 8 km in length beyond the end of the southern traverse profile plotted in figure 38. The top and bottom surfaces of the ice are shown at a 1 : 1 scale, without vertical exaggeration, in the lower part of each of the three cross sections. The ice surface variations are shown immediately above in exaggerated form by the individual aneroid altimeter readings plotted on an expanded vertical scale: the horizontal lines here are at 50 m intervals.

For the coastal section, from 100 km to Tuto, it has been possible to obtain greater details of surface relief from the combination of an unpublished series of route maps, produced by the U.S. Army, with the surface elevation data of our profile. The form lines given in figure 2 are at approximately 100 m intervals and although accuracy is low, the map gives a general idea of surrounding relief which is much more varied than further inland. From 100 km towards Camp Tuto, the route at first tends to run downslope approximately on a flow line (normal to contours) until at 80 km it reaches a locally high point due to a col between two hills. From there until a slight valley around 64 km the route is downslope, mostly within 45° of the flow lines, although by 64 km the flow appears to have turned to the northwest, normal to the course. Then follows a rise to 60 km corresponding to a rise of bedrock, then downslope to another valley draining to the northwest at about the 50 km point. Thereafter the route changes frequently

and cannot be said to follow a flow line with any certainty until the last 5 km into Camp Tuto. Over the section from 15 to 50 km from Tuto, the relationship of surface form to bedrock relief is certainly not that found on a flow line: eight out of nine of the tops of hills on the upper surface correspond to underlying peaks of the subglacial relief. The only exception is the broad rise centred around 31 km, which appears to be due to a col between two hills on either side of the route. Thus in this sector where ice movement is low and approximately normal to the mean route, the surface relief along the line of the profile reflects the underlying relief almost directly but at a reduced scale. From 5 to 15 km the route is variable, crossing slopes on the side of the main ridge at varying angles, so the lack of apparent relationship with bedrock relief is not surprising.

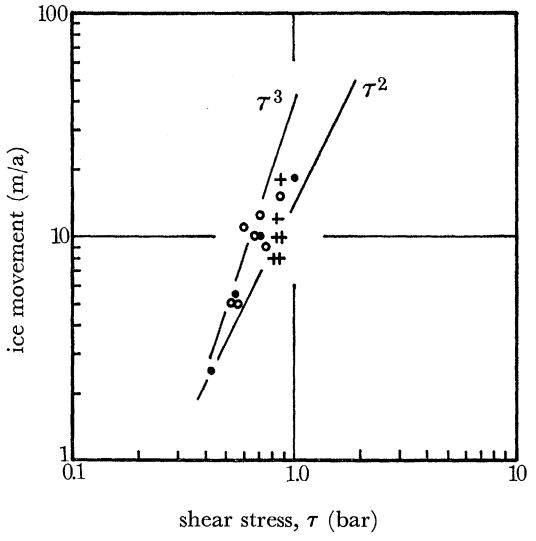

FIGURE 34. Double logarithmic plot of the basal shear stress against mean ice velocity, from table 9. ●, Values from the southern traverse; ○, other points where the estimated basal temperature is below the melting point; +, points where the basal ice is believed to be at the pressure melting point.

(c) *Regional slopes and basal shear stress*

In equation (31) we saw that the surface slope is due to two terms, the first of which (α_τ say) is due to the basal shear stress while the second (α_F) is caused by longitudinal stress gradients. The latter term varies considerably over distances of the same order of magnitude as the ice thickness, but since $\overline{\sigma_x^0}$ in practice can rarely exceed ± 3 bar, over long distances the mean value of α_F must tend towards zero. Consequently, if we wish to determine the value of the basal shear stress, we can do this most accurately by taking a mean value over a distance which is long compared with the ice thickness. Alternatively if we assume that variations of α_τ along a flow line are of much smaller magnitude than α_F, then by drawing a smoothed surface profile we can determine values of α_τ from the smoothed curve, while departures of the actual profile from the smoothed profile are primarily due to the term α_F, as is evident from figures 31 and 32.

We have determined the values of τ shown in table 9 by the above procedure. Horizontal distances from 2 to 10 km have been used to determine the mean slopes for ice thicknesses from 180 to 1350 m. Smooth surface profiles were drawn by eye to eliminate effects of longitudinal stresses, that is, to eliminate the slope components, α_F. The shear stresses have been

calculated only for those sections of profiles lying along, or close to, the estimated direction of ice flow. Values of τ have been calculated from

$$\tau = \bar{\rho} g \bar{H} \bar{\alpha}_\tau,$$

where the bars indicate that mean values of the parameters have been used.

Also shown in table 9 are the estimated velocities of ice movement, the 10 m temperature, and the basal temperature which, apart from the measured value of −13 °C at Camp Century, is estimated from the calculations described in §4.

TABLE 9. SHEAR STRESSES AT THE BASE OF THE ICE SHEET IN NORTHWEST GREENLAND

position in figures 1 and 38 (km)	mean slope over the whole distance (rad)	mean ice thickness (m)	τ (bar)	estimated mean ice velocity (m/a)	ice temperature (°C)	
					10 m mean	basal estimate
Southern traverse						
0–10	0.0037	1311	0.43	2.5	−24	−13
10–20	0.0049	1272	0.55	5.5	−23	−13
20–30	0.0067	1197	0.71	10	−23	−13
30–40	0.0103	1108	1.01	18	−22	−13
Northern traverse						
30–50	0.0066	1296	0.76	9	−25	−8
50–60	0.0063	1225	0.68	10	−24	−7
60–70	0.0061	1139	0.61	11	−24	−6
70–80	0.0071	1130	0.71	12.5	−23	−6
80–87	0.0101	980	0.87	15	−22	−6
Main trail						
210–220	0.0045	1322	0.53	5	−24	−13
200–210	0.0050	1256	0.56	5	−23	−13
96–101	0.0118	796	0.82	8	−17	−7†
93–103	0.0129	782	0.88	8	−17	−7†
73–78	0.0278	350	0.88	18	−14	−7†
52–56	0.0253	400	0.85	12	−1	0
2.2–4.7	0.0528	179	0.85	10	−1	0
2.9–4.7	0.0500	196	0.88	10	−1	0

† According to the discussion of absorption in §6, the deep ice in this region of the main trail is warmer than according to equation (27) on which the estimates in this column are based.

In two regions where there was some uncertainty over how to draw a smoothed surface profile, mean values of α_τ were calculated over two different distances around the same central location. The resultant values of τ differed by 4 % in one case and 7 % in the other, and this gives an indication of the maximum errors likely to arise from uncertainty over the effect of longitudinal stresses. Further errors may be due to the profile not following the line of ice flow, but deviations of 20 and 30 degrees introduce errors of only −6 and −13 % respectively. Although a precise value of the errors in τ is not practicable, an estimate of 10 % for the standard error appears reasonable. However, errors in the value of ice velocity and temperature shown in table 9 are much larger. The velocity of ice movement is based on the available maps and Mock's preliminary comments (see p. 487) and many of the estimates could be in error by a factor of two, but along the southern profile it seems from Mock's comments that the relative and absolute values should be correct to within ±30 %. In figure 34 we show a

double logarithmic plot of estimated velocity against basal shear stress and the straight lines represent $u \propto \tau^2$ and $u \propto \tau^3$. For the southern profile at least, it is not surprising that the relation between velocity and movement lies between these limits, but the pattern of the remaining values also appears to be within these same limits, which is perhaps surprising in view of the wide range of basal temperatures. Weertman (1957) predicted a relationship, $u \propto \tau^{2.5}$ but this is not significant in the present situation since his formula was based on basal sliding in which regelation was present. The basal temperature is -13 °C at Camp Century and there is no possibility of regelation.

Even if the detailed reasoning may be wrong, it is satisfactory to find that a frequently assumed relation between basal shear and velocity of movement is confirmed. It is particularly surprising to find no indication of a major variation of τ with the basal temperature, since the experiments of Glen (1955) indicated that strain rates at -13 °C should be an order of magnitude lower than those at -1 °C. However, a wide selection of surface profiles for polar and temperate glaciers (Robin 1964) indicates a surprising degree of uniformity of profile, irrespective of ice temperatures. Thus, in spite of Glen's results, it still appears that one can assume basal shear stresses do not vary widely in nature. This was previously suggested by Nye (1952) when he found that a value of $\tau = 0.88$ bar fitted an observed surface profile across the whole of central Greenland.

Summarizing our conclusions on the surface form of the ice we can say that:

(1) Along a line of flow, equation (31) explains surface slopes satisfactorily. Neglect of transverse strain rates does not appear to introduce serious errors.

(2) Where the route is normal to the line of ice flow, that is approximately along a contour, the relationship between bedrock relief and surface relief is not obvious.

(3) Where the route lies along a centre of outflow, there is direct correspondence, but at a reduced scale, of the surface hills and valleys to subglacial features.

(4) The velocity of ice movement increases in proportion to the square or cube of the basal shear stress.

(5) The basal shear stress shows no obvious dependence on basal ice temperatures.

(*d*) *Distribution of reflecting layers within the ice sheet*

An unexpected phenomenon found on the records was the presence of a number of relatively weak reflexions from within the ice mass (figure 4(*d*)). Although our equipment was not designed specifically to study these internal reflexions the records provide evidence which may guide future investigations and some results were obtained relevant to our understanding of the mechanism of ice flow.

Internal echoes from the ice mass were found on the records taken between Tuto and Century starting at 77 km from Tuto on the outward journey, while on the return journey they ceased at a distance of 70 km from Tuto. The internal echoes tend to be most frequent and strongest between 90 and 160 km along this route, although they occur intermittently up to Century. On the southern traverse they were present as far as 46 km from Century, but a changed aerial system for light vehicles reduced the system performance beyond that point, so that their absence over the last 16 km may not be significant. On the northern traverse they were present from Century for 44 km then were conspicuously absent except for one weak occurrence at 84 km even though the equipment parameters were not changed.

Thus, in terms of height above sea level, they were detected on the Tuto to Century trail when the surface elevation was higher than 1 km above sea level, and were strongest between 1.3 and 1.6 km elevation, and still present at 1.9 km. They were present down to 1.6 km on the southern traverse and may have extended further. On the northern traverse they ceased below 1.8 km except for the one weak occurrence around 1.5 km.

The depth beneath the surface at which discrete echoes were recorded started at a minimum of 275 m. Usually there was a continuous return of energy from shallow depths so that discrete echoes could not be identified with any regularity at depths less than 350 to 400 m. Beyond these depths, to around 550 m, internal echoes were frequent in all those areas where they were present. The maximum depth at which an internal echo was clearly present was 720 m, at the 117 km point on the Tuto to Century profile, the ice thickness being 920 m at this point.

Internal echoes from within polar ice masses have since been discovered in the Antarctic, both by the University of Wisconsin, at the South Pole and Byrd Stations in 1965, and at depths down to 2000 m over a wide area of eastern Antarctica by the Scott Polar Research Institute–U.S. National Science Foundation flights in 1967.

TABLE 10. REFLEXION COEFFICIENT OF LAYERS OBSERVED IN GREENLAND

traverse	from Tuto (km)	depth of reflecting layer (m)	G (dB)	A (dB)	E (dB)	S (dB)	R (dB)
Tuto to Century	77.0	580	56	23	20	146	−47
	78.7	450	54	18	23	146	−51
	80.0	610	56	24	23	146	−43
	84.8	355	52	14	24	146	−56
	90.3	445	54	17	16	146	−59
	97.5	500	55	19	16	146	−56
	100.1	500	55	19	16	146	−56
	200.6	420	53	9	13	146	−70
	from Century (km)						
south from Century	5.9	430	53	11	10	146	−72
	9.2–13.8	430	53	11	10	146	−72
	15.6	425	53	11	7	146	−75
	18.0	445	54	12	5	146	−75
	19.3	450	54	12	5	146	−75
	20.4	450	54	12	2	146	−78
	21.5	440	54	11	11	146	−70
	22.6	455	54	12	3	146	−77
	23.7	450	54	12	6	146	−74
	24.4	455	54	12	0	146	−80
	25.1	440	54	11	6	146	−75
	27.1	410	53	10	6	146	−77
	28.8	440	54	11	2	146	−79
	30.6	445	54	12	3	146	−77
	31.5–33.4	450	54	12	7	146	−73

(*e*) *Reflexion characteristics of internal echoes*

We can make useful estimates of the reflexion coefficients of the observed layers by following the procedures of §6(*a*), but rearranging equation (29) to give the reflexion coefficient R:

$$R = E+A+G-S, \tag{36}$$

where the right-hand terms are defined on pp. 477, 478. The dielectric absorption is calculated from the estimated temperature–depth profiles and as we are dealing mainly with the upper, and therefore colder, layers of ice the mean absorption loss per unit of depth is less than for the bottom echoes. Unfortunately, an accurate record of echo strength is not available, since the attenuator setting on the receiver was set to bring the echo from the ice/rock interface to a satisfactory intensity. Since the internal reflexions were usually recorded at lower intensities than those from bedrock, and in many cases they were present only intermittently along the record, we have taken their echo strength above noise level to be the same as the receiver attenuator setting. This should be correct to within 5 dB for the weaker echoes from greater depths, and table 10 gives a guide to the reflexion coefficients.

TABLE 11. CALCULATED LAYER THICKNESSES TO GIVE VARIOUS REFLEXION COEFFICIENTS FOR A HORIZONTAL LAYER OF CLEAR ICE WITHIN A GENERAL MEDIUM OF BUBBLY POLAR ICE

depth (m)	bubble pressure w (atm)	density difference, bubbly and clear ice	required layer thickness (cms) (for λ = 5 m in ice)					
			R=50 dB	R=60 dB	R=70 dB	R=80 dB	R=90 dB	R=100 dB
120	10	0.010	63	20	6.3	2	0.6	0.2
320	30	0.0033	190	57	19	6	2	0.6
520	50	0.0020	—	100	31	10	3	1.0
720	70	0.0014	—	142	45	14	5	1.4
1020	100	0.0010	—	—	63	20	6	2.0
1320	130	0.00077	—	—	82	26	8	2.5
2020	200	0.00050	—	—	126	40	13	4.0

TABLE 12. CALCULATED REFLEXION COEFFICIENTS WHICH WOULD BE DETECTABLE ABOVE THE NOISE LEVEL, AT REPRESENTATIVE SITUATIONS IN ANTARCTICA

The same wavelength and aerial system assumed as in table 10, but a system performance, S = 160 dB, which is more in line with the equipment used during the S.P.R.I.–N.S.F. flights made in December 1967

	mean annual temperature (°C)	depth of layer (m)	G (dB)	A (dB)	(R) (dB)
vicinity of Byrd	−30	500	54	10	−96
		1000	60	20	−80
		1500	63	33	−64
		2000	66	53	−41
vicinity of South Pole	−50	500	54	3	−103
		1000	60	6	−94
		1500	63	12	−85
		2000	66	24	−70

The internal reflexions have the character of weak specular reflexions of slowly varying intensity and appear to be caused by layers of wide areal extent approximately parallel to the surface. This is apparent from the constant range as echoes fade away or strengthen. The alternative hypothesis that echoes originated from diffuse scattering centres within the ice can be rejected, since the characteristic change of range due to vehicle movement over such centres was not present.

Although a number of reflecting horizons may be present at one location, the duration of each individual echo is short and appears to be governed by the length of the transmitter pulse, rather than by the thickness of the layers causing the reflexion. This puts an upper limit on the

thickness of the reflecting layer of around 20 m. To specify a lower limit, we need to consider the discussion in §4(*h*) and the observed reflexion coefficients in table 10.

To estimate possible values of $\delta\rho$, the density change between adjacent layers in the ice, let us assume that the reflecting layers consist of pure ice of relative density 0.92 and the surrounding material consists of bubbly ice. We can make a rough estimate of the density of bubbly ice at any depth by assuming that the air bubbles become trapped in the firn when the density becomes 0.82, and that at greater depths, the air in the bubbles is compressed to a pressure equal to the weight of overlying ice, w, in atmospheres. We then have

$$\delta\rho = 0.10/w \tag{37}$$

to a good approximation if one atmosphere refers to the atmospheric pressure at the level at which air bubbles become trapped. We shall assume this to be 920 mbar for our calculation, so that each 10 m of ice corresponds closely to 1 atm load, except in the lower density layers near the surface. Then using equation (16) we find the thickness of single layers of clear ice required to produce any reflexion coefficient, from

$$l = (\lambda\sqrt{R})/(\pi\,\delta\rho). \tag{38}$$

The required layer thicknesses for stated values of the reflexion coefficient and a wavelength of 5 m in ice (approximately 35 MHz) are shown in table 11 but this formula does not hold when the layer thickness approaches $\frac{1}{4}\lambda$.

When tables 10 and 11 are compared, we see that we could readily explain the reflexion coefficients for the observations south of Century in terms of a single layer of clear ice varying in thickness between approximately 10 and 20 cm. However, on the main trail from Camp Tuto to Camp Century, between 1.3 and 1.6 km above sea level, the required layer thicknesses become too great for equation (38) to apply. Nor would a single sharp interface between clear and bubbly ice have a sufficient density contrast at the depths involved to produce the necessary reflexion coefficient. A number of ice layers could produce a random but additive effect and in §4(*h*) it is suggested that 40 random layers, each having $\delta\rho = 0.01$ could produce a coefficient of -40 dB. However, at 500 m depth our probable value of $\delta\rho$ is 0.002, so it is difficult to explain greater reflexion coefficients than -53 dB at 500 m depth on this model. There remains the possibility that the first three reflexion coefficients in table 10 are too large due to an underestimate of the absorption and/or echo strength terms, or that some different type of discontinuity caused the reflexion of energy.

The reflexions from 1 to 2 km depth in the Antarctic are now known to be of considerable areal extent and (referring to table 12) they could be explained by a single layer of clear ice of the order of 20 cm in thickness, or by the combination of a number of layers of one quarter that thickness, in a zone 20 or 30 m thick.

(*f*) *Possible causes of internal reflexions*

Of all possible causes of internal reflexions, variations of density between various layers seem to provide the most satisfactory explanation both quantitatively and qualitatively. At a frequency of 35 MHz, we are dealing with the component of permittivity which depends on the structure of the individual H_2O molecules and their relation within the crystal lattice. We expect that neither the grain size, nor the orientation, nor the dislocation density, will affect this though we must allow that the anisotropy of the individual grain is somewhat uncertain

on present knowledge. Nor do we expect the impurity content to affect it until the proportion is such that it behaves as a macroscopic mixture of two dielectrics. To consider one specific example: a layer of volcanic ash, whose relative permittivity will be assumed to be 4.8, if mixed in the proportion of p : 1 with ice, is expected to cause a change in refractive index from pure ice of $0.4p$, using simple dielectric mixing formulae. By the same method as previously, the power reflexion coefficient for a layer of thickness l within the pure ice is

$$R = (0.4\pi pl/\lambda)^2. \tag{39}$$

Thus layers of ice containing 10 % of ash and of thicknesses 1 and 5 cm would have reflexion coefficients of -74 and -60 dB respectively. Four layers of ash, for which thickness and ice content are not yet available, have been reported at 1.5 km depth in the borehole at Byrd Station (National Science Foundation 1968). It should be noted that such ash layers may have an indirect influence on the permittivity, through their effect on the albedo and thus on the surface melting of the snow.

TABLE 13. STRUCTURAL FEATURES OBSERVED OVER THE ENTIRE 411 m DEEP CORE FROM SITE 2, GREENLAND

		observations less than 70 m depth				observations below 70 m depth			
feature	thickness (mm)	numerous	common	present	rare	numerous	common	present	rare
thin ice layers	1–2	.	×	.	.	.	×	.	.
thick ice layers	3–5	.	.	×	.	.	.	×	.
ice wedges	10–25	.	.	×	.	.	.	×	.
ice glands	30–100	.	.	.	×	.	.	.	×
depth hoar layers	10–20	.	×	.	.	.	.	.	?
wind crusts	1–2	.	×	.	.	.	.	.	?
relative light transmission	variable	×	.	.	.	×	.	.	.
definite indications of melt	5–20	.	.	×	.	.	.	×	.
slight indications of melt	5–20	.	.	×	.	.	.	×	.

The most detailed study of the deep stratigraphy of a polar ice sheet is that of Langway (1967) who has used a variety of techniques to examine the cores available from 'site 2', approximately 100 km to the east of Century at an elevation of 2 km. The mean annual temperature at site 2 is -25.4 °C and the net annual accumulation averages 42.3 cm of water equivalent. Conditions are thus similar to those around and south of Century. Langway made a continuous examination of the top 110 m of core and examined sample sections of core down to a depth of 411 m. The results are summarized in table 13, reproduced directly from Langway (1967).

In general, one can assume that the ice layers, ice wedges, and ice glands refer to clear ice which is surrounded by bubbly ice. The features described as definite indications of melt, and slight indications of melt, refer to 'horizontal strata, usually 5 to 20 mm thick, of relatively lighter appearing material commonly, although not always, having larger subrounded grains than the material on both sides'. In regard to relative light transmission he states: 'It was learned during this study that the relative amount of light transmitted through a firn-ice core segment is related to the density of the sample.' It is thus clear that many variations of density occur

in the upper layers of the ice sheet, but such variations should become smaller with depth as predicted by equation (37). This equation suggests that the range of density variation to be expected at 100 m depth is about 0.01, compared with variations of 0.02 observed by Langway at a similar depth.

The reflexion coefficient of the internal reflecting layer south of Century, where it is present, has a mean value of -75 dB (table 10) which requires an ice layer 9 cm thick on our model of the density variations. Since the reflexion was observed intermittently along the profile, this appears to be consistent with Langway's note that ice glands 30 to 100 mm thick are rare at all depths. The thinner ice features, and other layering effects listed by Langway, appear sufficient to explain the almost continuous return of energy from the surface down to 300 m.

On the basis of oxygen isotope ratios, net annual accumulation, and dissolved chemical constituents, Langway concludes that the climate around A.D. 934, corresponding to a core depth of of 411 m, was similar to the warm period in the first half of this century, but that the climate cooled down from A.D. 934 until A.D. 1783, after which a warming trend commenced. The estimated age of the prominent reflecting horizon which we discuss in the following section is close to that from 411 m depth in 'site 2' borehole. The formation of a prominent reflecting horizon of such an age could therefore result from warm spells similar to those of 1921, which produced an ice layer 4.5 cm thick at 'site 2', the thickest ice layer in the top 110 m of the core.

The geographical distribution of observed internal reflexions also appears consistent with the idea that they are produced by denser ice layers. The absence of reflexions over the first 70 km from Camp Tuto is consistent with the absence of density changes in the ice mass since we have suggested in §6 (*b*), that in this region the ice is isothermal and close to the pressure melting point. Thus there is an absence of bubbly polar ice, owing to the elimination of bubbles during the transformation from firn to ice, as in temperate glaciers. The frequent occurrence of internal reflexions between elevations of 1.3 and 1.6 km is explicable, as it is in this borderline zone that greatest fluctuations of surface melting are likely between cold and warm decades.

The presence of reflexions at Camp Century, and more significantly in the Antarctic, call for more unusual phenomena which are able to produce ice layers at such locations. At Century, or Byrd Station in Antarctica, one can postulate a rare climatic warming which might soak the surface firn layers with water to a sufficient extent to reduce the bubble content. However, the presence of an ice layer 20 cm thick and 1 km deep at the South Pole is much more difficult to accept. At this depth we are dealing with ice deposited on the surface at least 10 ka ago, possibly 15 ka ago. One naturally thinks of climate as the most likely cause of ice layers, but even under present-day conditions, iced crusts 1 mm thick are found near the surface at the South Pole (Giovinetto 1960). It is possible that a slow process could cause a thin ice layer to grow in thickness whilst within the mass of firn and ice, since we have 10 ka for the process to operate. Alternatively one could postulate surface processes, such as a rare layer of volcanic ash causing melting on or just below the surface, and causing formation of clear ice layers. A final possiblity is that in some areas there may have been no net accumulation over a period of years, and the prolonged exposure to the surface environment caused clear ice to form. This would have occurred at many tens of kilometres from the South Pole, to which the ice has now been transported by the general movement.

(g) Reflecting horizon along the southern profile

In figure 36 internal reflexions are plotted for the profiles to the south of Camp Century and for a distance of 43 km there is a continuity in the depth of echoes (with the exception of two points around 6 and 8 km, and four points near the southern end) which suggests that they represent a continuous layer which at one time formed the surface of the ice sheet. According to Langway and our own interpretation, this layer will have resulted from an exceptionally warm spell of weather around the time of its formation. Since the layer increases in depth southwards, as does the accumulation, whereas the total ice thickness decreases in this direction, we must check numerically to see if the data is consistent with the simultaneous formation of an ice layer over the whole zone of the profile.

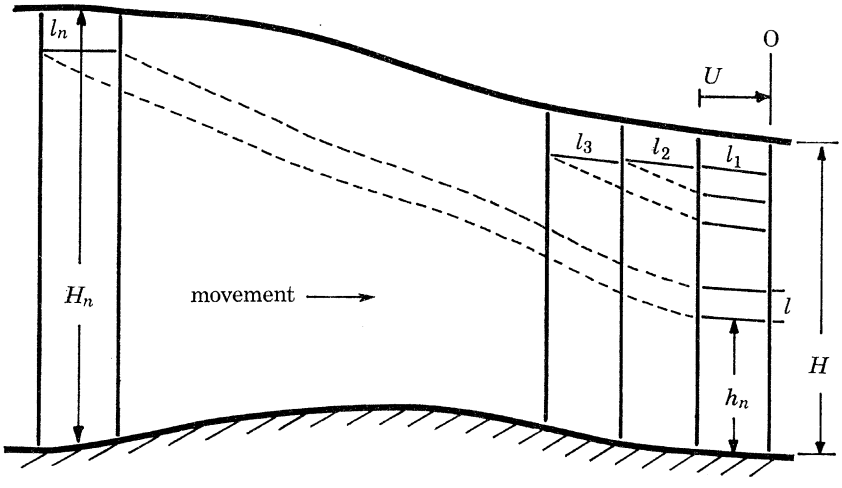

FIGURE 35. Illustrating the transport and vertical deformation of layers of ice of thickness l_n laid down upstream from the point of observation, O. The ice movement in the previous 100 a is U, the total thickness is H, and h is the height of any layer above bedrock.

The thicknesses of annual layers at varying depths in an ice sheet have been discussed by Nye (1963). Using as basic assumptions that the vertical plastic strain rate along any vertical line in the ice is uniform at any instant, and that there is no bottom melting, he concludes that the thickness of any layer l, of initial thickness l_n is given by

$$l/l_n = h_n/H_n, \tag{40}$$

where h is the height of the layer above bedrock at the location being considered, and H_n is the height above bedrock at which the layer of thickness l_n was deposited. All layer thicknesses and heights must be given in equivalent solid ice thicknesses to correct for the effect of density variations (see figure 35).

In order to apply equation (40), we assume that the ice sheet is in a steady state, so that its thickness is constant at any point. We use equation (32) to calculate velocities of ice movement from accumulation figures given by Mock (1965). The velocities range from 3 m/a at Century (given by Weertman 1968) increasing to 7 m/a at the 20 km point, and 23 m/a at 44 km. However, the accumulation itself is taken from a more recent paper (Mock 1968) since this is based on numerous stake measurements, unlike the earlier paper based on pit studies.

We start by assuming that the layer was laid down 1 ka ago, and then use step by step

calculations for time intervals of 100 or 200 a, as appropriate, to evaluate equation (40). This is done as suggested in figure 35, by calculating first

$$h_1 = H - l_1(H/H_1),$$

then

$$h_2 = h_1 - l_2(h_1/H_2),$$

and

$$h_n = h_{n-1} - l_n(h_{n-1}/H_n). \qquad (41)$$

We thus determine a value for h_n for ice deposited on the surface 1 ka ago. We have plotted the calculated elevation of the reflecting layer in figure 36, allowing a correction for the lower density layers near the surface.

For comparison we have also made a separate set of calculations on the assumption that the ice sheet is not moving, and is building up steadily at a rate equal to the net accumulation at each point as given by Mock (1968). On this assumption, the ice in the reflecting layer at Camp Century would be 930 a old and this same age has been used for the whole profile in figure 36 to provide a comparison of observed internal reflexions with the corresponding depths calculated from the two assumptions—steady state equilibrium and static, but increasing, ice sheets. When we remember that the ages used for calculating the two models were chosen in order to tie in with the observed layer depth near Camp Century, it is immediately apparent that our steady state model provides much the best fit with the observed reflecting horizon along the whole profile. On this model the calculated depth does not differ from observed depths by more than 6 % at any point, and the agreement of calculated depth between 40 and 43 km is within 2 % of that calculated. The general validity of the steady state model and the figures for accumulation rates and velocities of movement of ice thus seem well justified.

There appears to be a small systematic difference between the depths of the reflecting layer observed on the outward and return journeys so we have assessed these results separately. We have selected one measurement of layer depth per kilometre of traverse and determined the difference between the observed depths and the computed layer depths at the same points, using the steady state model. On the outward journey we have 19 observed depths available, differing from calculated layer depths by $+10 \pm 14$ m standard deviation. For the return journey 5 days later, the mean difference of the 36 observations available was -1 ± 12 m. The systematic difference between the outward and return journeys is probably due to an instrumental effect, and lies within estimates of accuracy given in §5. Since the total thickness of the layer deposited in the interval between 900 and 1000 a ago is shown by our calculations to range between 28 and 32 m we can say that the results suggest that the reflecting layer was formed at the surface of the ice sheet 1033 a before our observations in 1966 if we use results for the outward journey, or 997 a using the return journey. On the basis of Langway's (1967) work, it appears reasonable to assume that the layer was formed in a single season, probably within a warm spell of a few days duration. The standard deviation of the layer depth, relative to the calculated 1000 a surface, is then not relevant to the errors in age determination except that the standard deviations are consistent with the hypothesis that layer formation took place during a very short period.

The mean age of the reflecting layer, based on the mean observed depths of both outward and return journeys, is 1009 a ago or A.D. 957. The principal error in this dating depends on how closely the 3-year mean values used for the net accumulation (Mock 1968) agree with the long term mean over the 1000 a in question. In the absence of other criteria, one would used standard

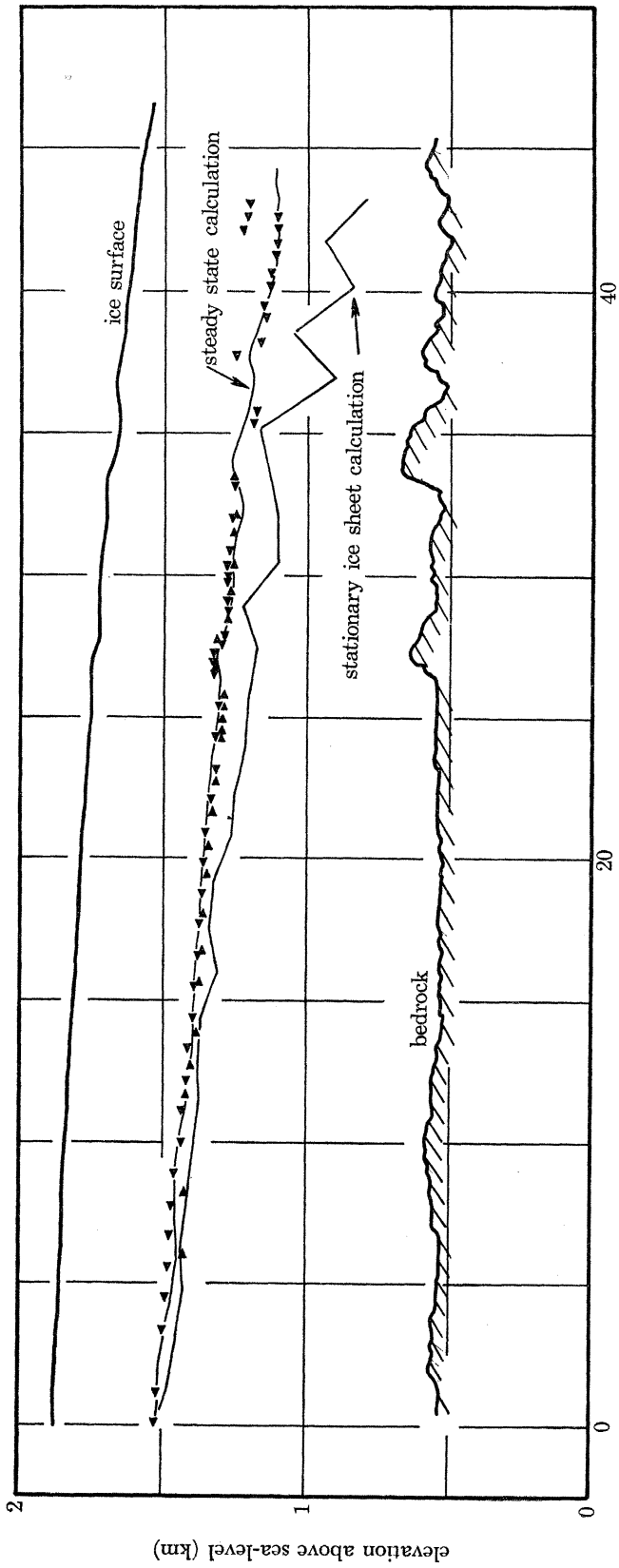

FIGURE 36. Showing the reflecting horizon on the southern profile from Century. The triangles mark individual layer positions measured from the radio echo film, on both outward and return journeys, the point of the triangle indicating the direction of travel. The lines are based on the two methods of calculation described in §7 (*g*).

deviations for similar areas, to make the appropriate estimates. From stratigraphical analysis covering 70 a accumulation at site 2, Langway (1967) gives the average net annual accumulation as 40.6 ± 12.5 cm water equivalent. Thus his figure for standard deviation in a single year is 31 % of the annual average accumulation and the error of the mean derived from a random 3 a period is likely to be around 18 %, equivalent to an uncertainty of the order of 200 a in the estimated age of our reflecting layer.

TABLE 14. CAMP CENTURY ACCUMULATION (MOCK 1968)

time interval	method	accumulation rate (water equivalent, cm/a)	reference
1964–47	firn stratigraphy	31.2	Crozas *et al.* (1966)
1964–47	fission products	31.2	Crozas *et al.* (1966)
1962–55	firn stratigraphy	31.8 ± 5.7	Mock (1965)
1964–1800	^{210}Pb	$32 + 3$	Crozas & Langway (1966)
1965–1876	firn stratigraphy	36.7	Mock (in preparation)
1966–63	trend surface	35	Mock (1968)

However, a better estimate can be obtained by comparing the mean value of accumulation over a 3 a period, with mean values over longer periods. Table 14, reproduced from Mock (1968), shows values for the accumulation rate at Century derived by different observers from different types of observation covering different periods. The value of 35 cm of water equivalent per year is that used in our calculations, and we see that this is about 5 % lower than the figure derived from firn stratigraphy over a period of 89 a, and from 10 to 12 % above the other figures. On the basis of this table one would estimate our probable error in dating our reflecting horizon as 100 a or less. Langway (1967) considers that accumulation rates in A.D. 934 were similar to the present but that they fell to perhaps 25 % smaller around A.D. 1773. However, below 100 m depth he has sampled only a few short sections of core in the site 2 borehole, so this is not as reliable as conclusions based on the upper 70 m. We conclude that our reflecting layer was formed at the surface of the ice sheet during a period of perhaps a few days of warm weather around A.D. 957 ± 100 a.

Another aspect of the reflecting layer which warrants more detailed investigation is a study of the way in which it is deformed when the ice sheet flows over subglacial ridges. The calculated and observed deformations around 28 km and from 33.5 to 35.5 km appear to be in good agreement, but there is no evidence in the observations of the calculated dip in the reflecting horizon around 32.5 km.

Detailed studies of vertical deformations will be possible on the extensive records of the S.P.R.I.–N.S.F. Antarctic flights made in 1967. The value of the present study is its confirmation that the reflecting horizons appear to be formed at the surface of the ice sheet practically simultaneously over wide areas. Their subsequent deformation can therefore be related to the existing surface form of the ice sheet and to known irregularities of bedrock, so that we have a very powerful method of seeing how the ice has deformed during flow. Another useful conclusion from this study, is that in the deformation of the reflecting layer resulting from ice flow, the steady state model of the ice sheet offers a much superior explanation to a static model.

Two principal agencies made this work possible. The Paul Instrument Fund (administered by the Royal Society, the Institute of Physics & the Physical Society, and the Institution of

Electrical Engineers) provided the whole cost of development of the apparatus during the uncertain early years until the end of 1964. The logistic backing for the field work in Greenland was managed entirely without any responsibility falling upon ourselves, by the U.S. Army Research Support Group, through the good offices of A. H. Waite (late U.S. Army Electronics Laboratory) and J. N. Rinker, U.S. Army C.R.R.E.L. We hope that the extent of our debts is evident from this paper.

REFERENCES

Auty, R. P. & Cole, R. H. 1952 *J. Chem. Phys.* **20**, 1309–1314.
Bailey, J. T. & Evans, S. 1968 *British Antarctic Survey Bulletin* no. 17, 1.
Bailey, J. T., Evans, S. & Robin, G. de Q. 1964 *Nature, Lond.* **204**, 420–421.
Beckmann, P. & Spizzichino, A. 1963 *The scattering of electromagnetic waves from rough surfaces.* London: Pergamon Press.
Benson, C. S. 1962 *U.S. Army S.I.P.R.E. Res. Rep.* no. 70, 93 pp.
Bentley, C. R. 1964 In *Research in geophysics* (ed. H. Odishaw), vol. 2, pp. 355–389. Cambridge, Mass.: M.I.T. Press.
Bentley, C. R. & Jiracek, G. R. 1965 *J. Glaciol.* **6**, no. 44, 319.
Berthelsen, A. & Noe-Nygaard, A. 1965 In *The precambrian* (ed. K. Rankama), vol. 2, pp. 113–262. New York, etc.: Interscience Publishers.
Booker, H. G., Ratcliffe, J. A. & Shinn, D. H. 1950 *Phil. Trans.* A, **242**, 579–607.
Bourgoin, J. P. 1956 *Ann. Géophys.* **12**, 75–83.
Brocas, J. & Delwiche, R. 1963 *J. Geophys. Res.* **68**, 3999–4000.
Budd, W. 1967 *Int. Assoc. Sci. Hydrol. Publ.* (in the press). Presented to Commission of Snow and Ice, Berne 1967.
Clarke, G. K. C. 1966 *U.S. Army C.R.R.E.L. Res. Rep.* no. 191.
Collins, I. F. 1968 *J. Glaciol.* **7**, 199–204.
Cooper, R. I. B. 1948 *Proc. Phys. Soc. Lond.* **61**, 40–47.
Crozas, G. & Langway, C. C. jun. 1966 *Earth Planet. Sci. Lett.* **1**, 194–196.
Crozas, G., Langway, C. C. jun. & Picciotto, E. 1966 *Earth Planet. Sci. Lett.* **1**, 42–48.
Cumming, W. A. 1952 *J. appl. Phys.* **23**, 768–773.
Edison, A. R., Moore, R. K. & Warner, B. D. 1960 *I.R.E. Trans. Antennas and Propagation*, **AP-8**, 246–254.
Evans, S. 1963 *Polar Rec.* **11**, 406–410, 795.
Evans, S. 1965 *J. Glaciol.* **5**, 773–792.
Evans, S. 1967 *Polar Rec.* **13**, 413–420.
Evans, S. & Smith, B. M. E. 1969 *J. Sci. Instrum.* (2), **2**, 131–136.
Glen, J. W. 1955 *Proc. Roy. Soc. Lond.* A **228**, 519–538.
Giovinetto, M. B. 1960 *Columbus, Ohio St. Univ. Res. Found.* Project 825, Rep. 2, part 4.
Haefeli, R. 1961 *J. Glaciol.* **3**, 1133–1150.
Hansen, B. L. & Landauer, J. K. 1958 *Int. Assoc. Sci. Hydrol. Publ.* no. 47, 313–317.
Hansen, B. L. & Langway, C. C. jun. 1966 *Antarctic J. U.S.* **1**, 207–208.
Jenssen, D. & Radok, U. 1961 *Int. Assoc. Sci. Hydrol. Publ.* no. 55, pp. 112–122.
Jenssen D. & Radok, U. 1963 *J. Glaciol.* **4**, 387–397.
Jiracek, G. R. 1965 Unpublished M.Sc. (Geophysics) thesis. Madison, University of Wisconsin.
Kaye, G. W. C. & Laby, T. H. 1959 *Tables of physical and chemical constants and some mathematical functions*, 12th ed. London: Longmans.
Kuroiwa, D. 1956 *Int. Assoc. Sci. Hydrol. Publ.* no. 39, pp. 52–63.
Lamb, J. 1946 *Trans. Faraday Soc.* **42** A, 238–244.
Lamb, J. & Turney, A. 1949 *Proc. Phys. Soc. Lond.* B **62**, part 4, 272–273.
Langway, C. C. jun. 1967 *U.S. Army Cold Regions Res. Engng. Lab. Res. Rep.* no. 77.
Mock, S. J. 1963 *Int. Assoc. Sci. Hydrol. Publ.* no. 61, pp. 147–153.
Mock, S. J. 1965 *U.S. Army Cold Regions Res. Engng. Rep.* no. 157.
Mock, S. J. 1967 *U.S. Army Cold Regions Res. Engng. Rep.* no. 233.
Mock, S. J. 1968 *J. Glaciol.* **7**, 59–76.
National Science Foundation 1968 *Antarctic J. U.S.* **3**, 45.
Nobles, L. H. 1960 *U.S. Army S.I.P.R.E. Tech. Rep.* no. 66.
Norton, K. A. *et al.* 1955 *Proc. Inst. Radio Engrs., N.Y.* **43**, 1354–1361.
Nye, J. F. 1951 *Proc. Roy. Soc. Lond.* A **207**, 554–572.
Nye, J. F. 1952 *Nature, Lond.* **169**, 529–540.
Nye, J. F. 1957 *Proc. Roy. Soc. Lond.* A **239**, 113–133.
Nye, J. F. 1959 *J. Glaciol.* **3**, 493–507.

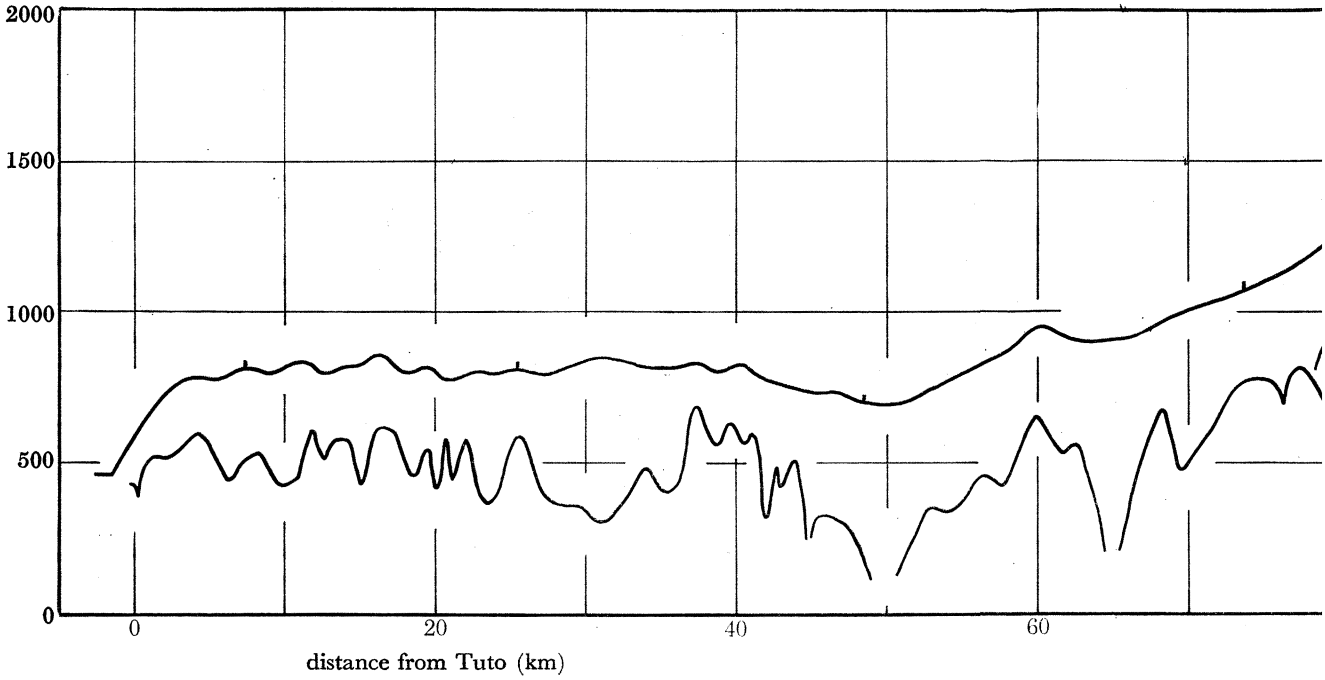

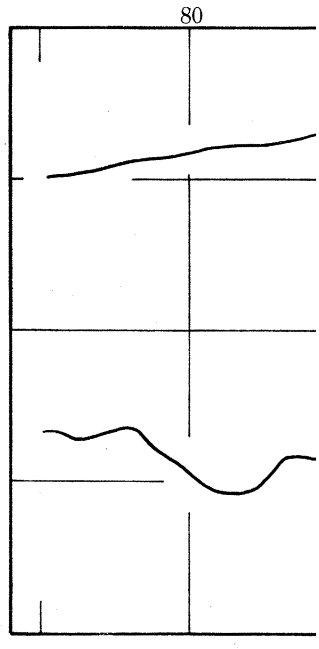

FIGURE 37. Cross sections through the ice sheet, showing the upper and lower surfaces along the routes in figure 1. The elevations are given in metres above sea level and the vertical scale is exaggerated twenty times compared to the horizontal scale. Above: the main trail scaled in kilometres from Tuto to Century. To the right; the northern and southern traverses from Century scaled in kilometres north or south respectively. The most prominent internal reflecting horizon is included in these.

main trail, Tuto to Century

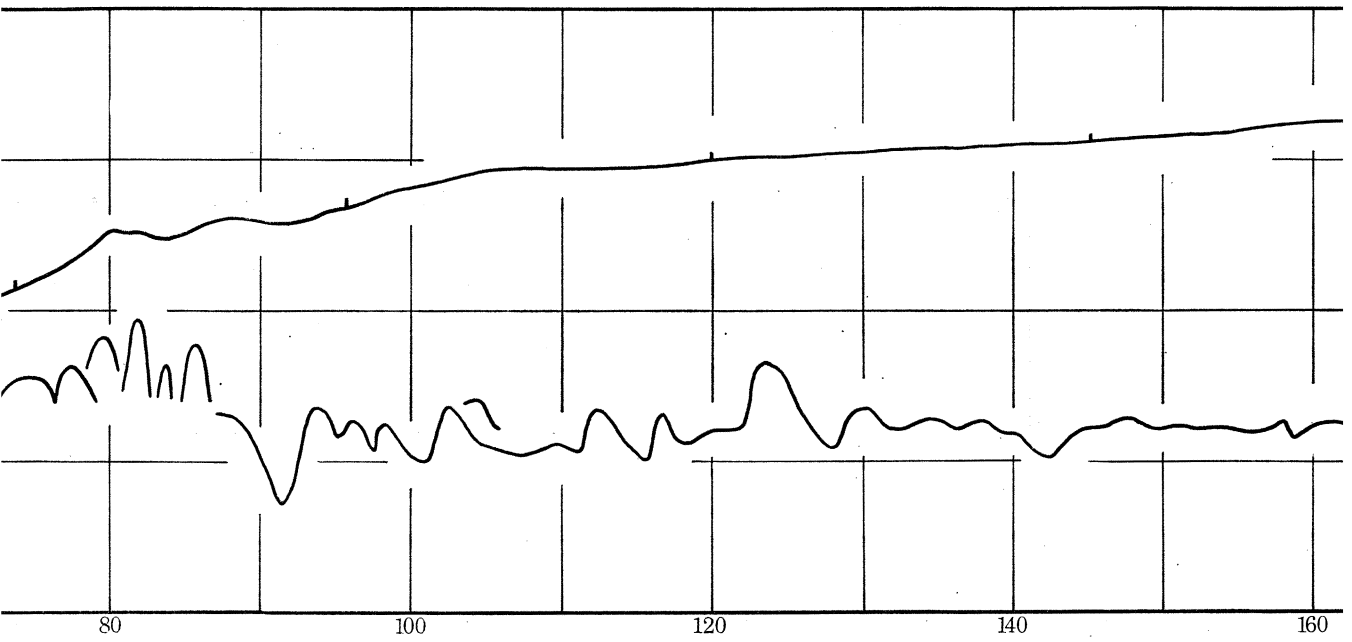

northern traverse

distance from Century (km)

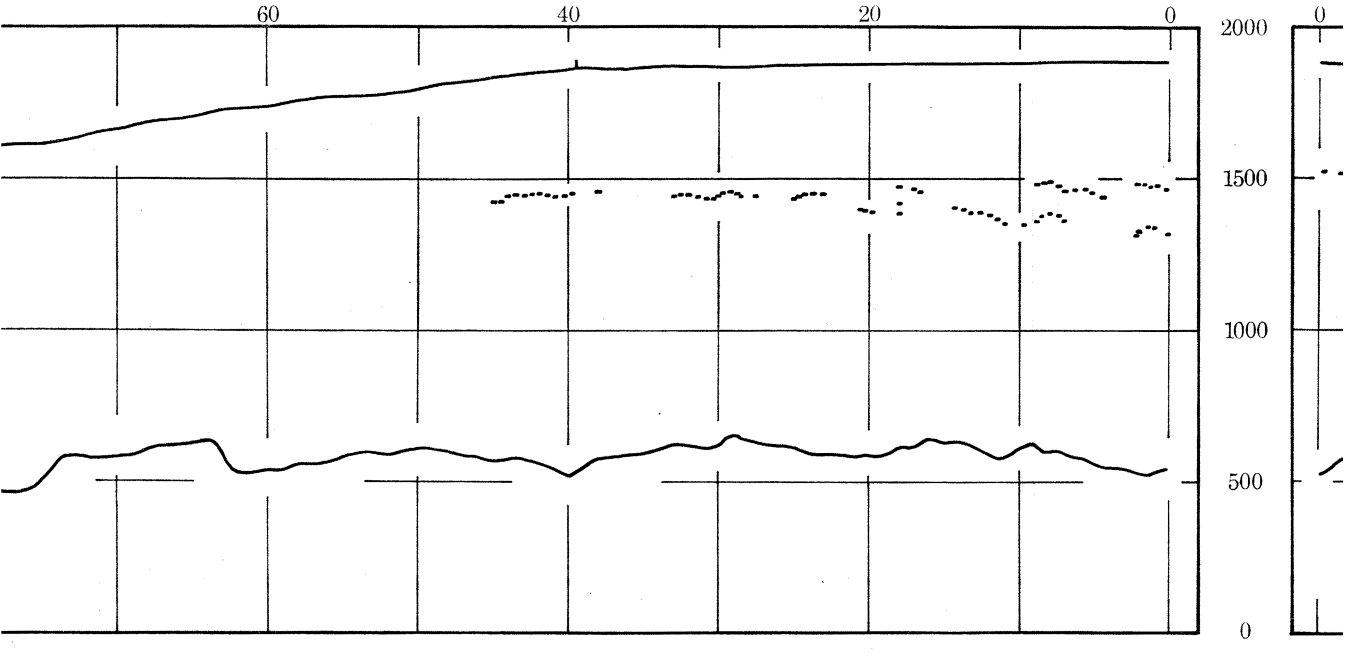

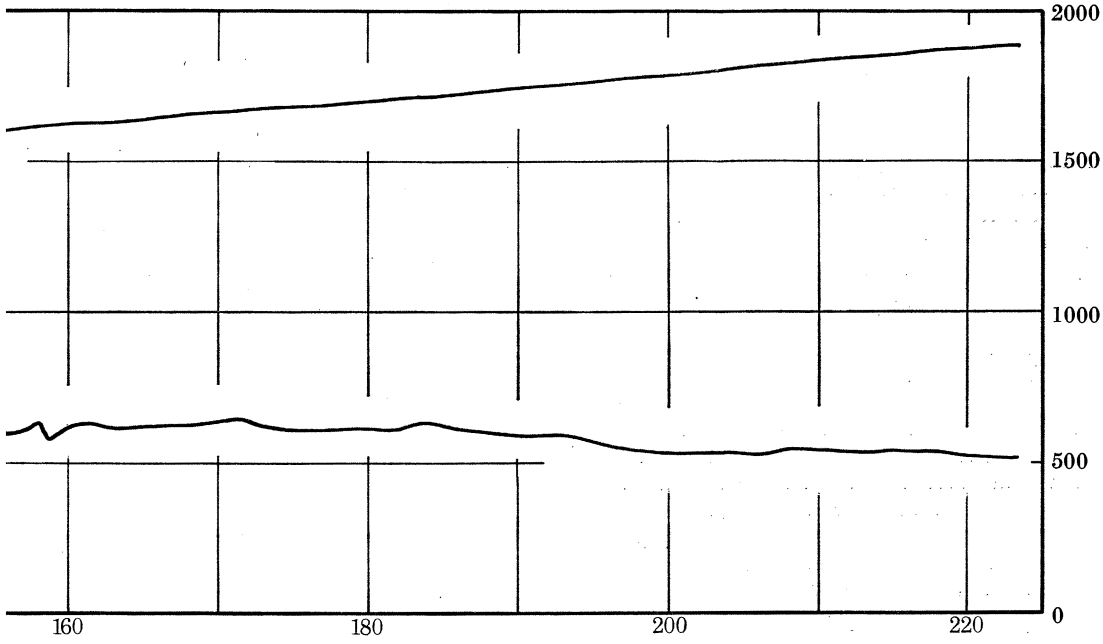
2000
1500
1000
500
0
160
180
200
220

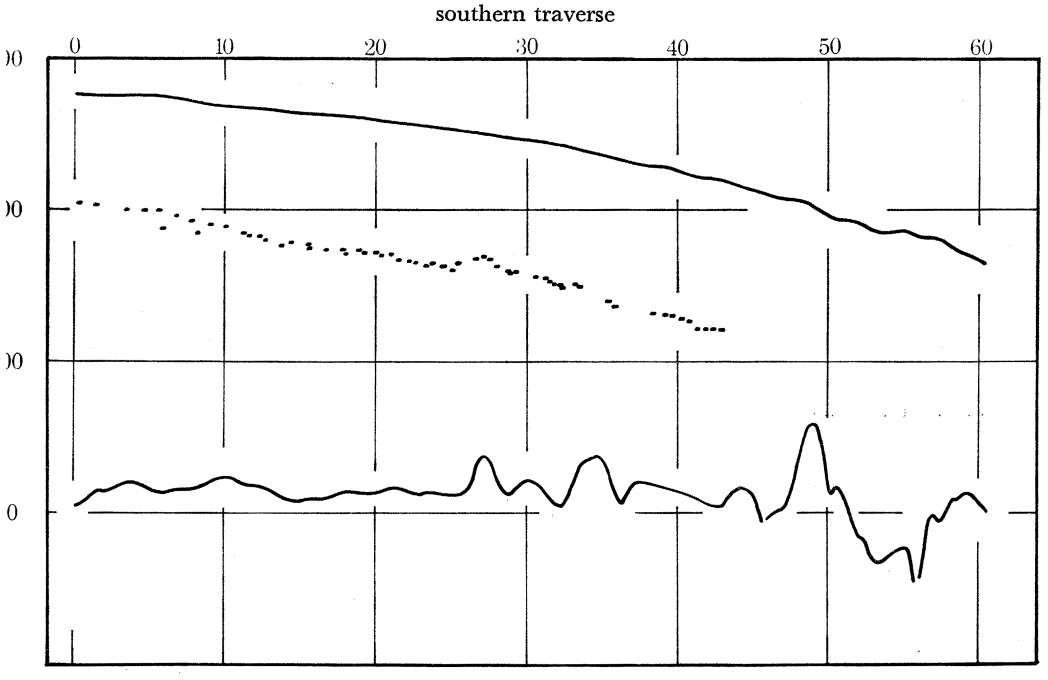
southern traverse
0
10
20
30
40
50
60

(*Facing p.* 504)

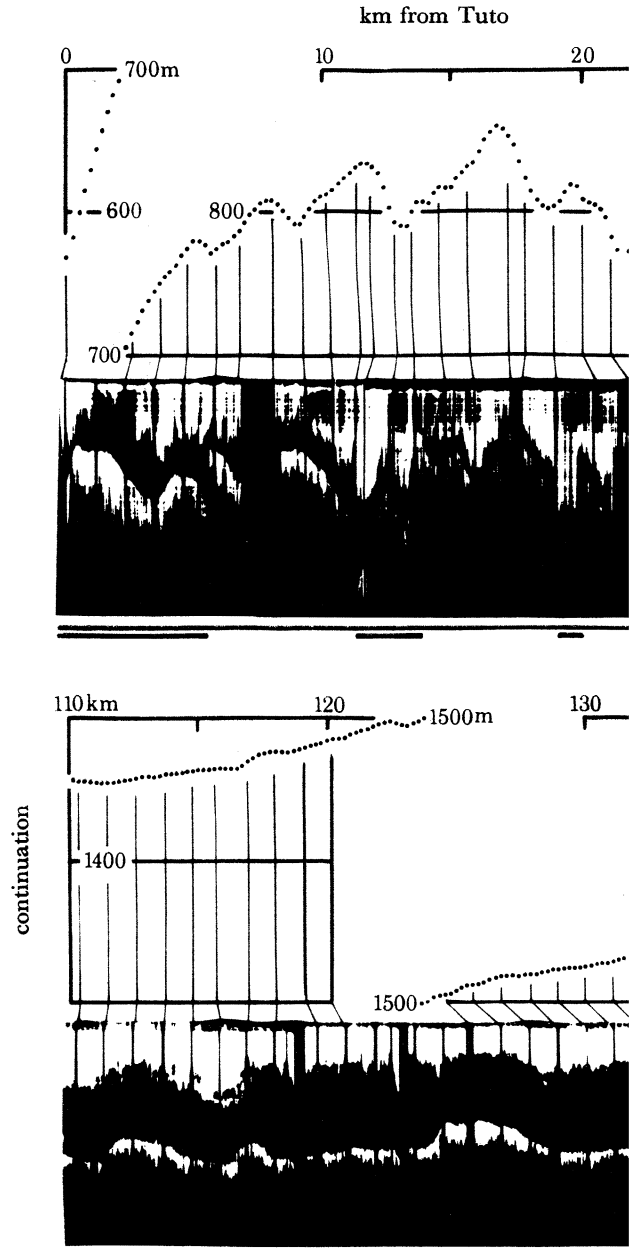

FIGURE 38. Detailed snow surface topography correlated with direct prints from the radio echo film records. Each elevation point represents a single reading of the aneroid altimeter. They are spaced horizontally at 220 m intervals along the trail and this representation faithfully conveys our knowledge of the smallest surface features. Individual points have been correlated with specific marks on the print below as explained in §7 (*a*). The scale of microseconds echo delay is given at the right hand end of each print. Note that the zero from which the echo time delay is to be measured at any point along the print should be identified with the top of the broad white band of clutter echoes. On the top print, between 0 and 86 km from Tuto on the main trail, there were changes in the time base sweep velocity used in the recording oscilloscope and these are indicated by the code below the print. For one bar the microsecond time scale should be halved and for two bars divided by four, so that the total sweep time is then about four microseconds. Internal echoes cannot be seen in this reproduction except near 150 km on the main trail and between 0 and 10 km on the northern traverse.

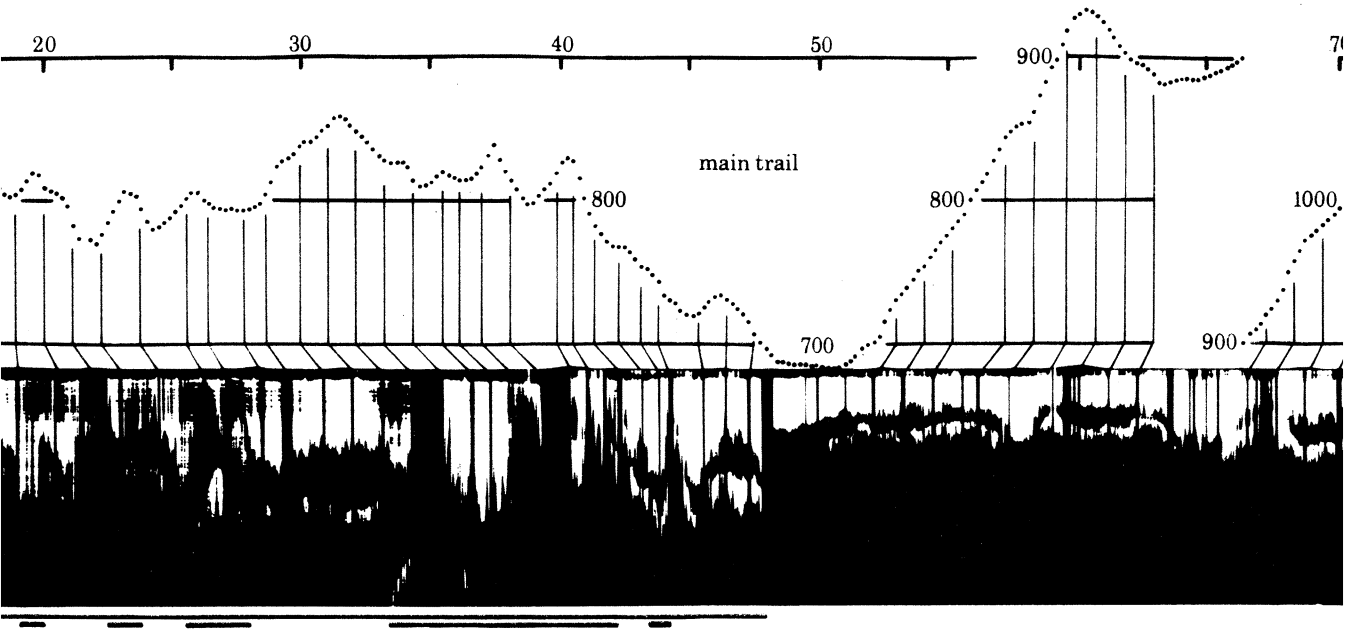
20
30
40
50
900
main trail
800
800
1000
700
900

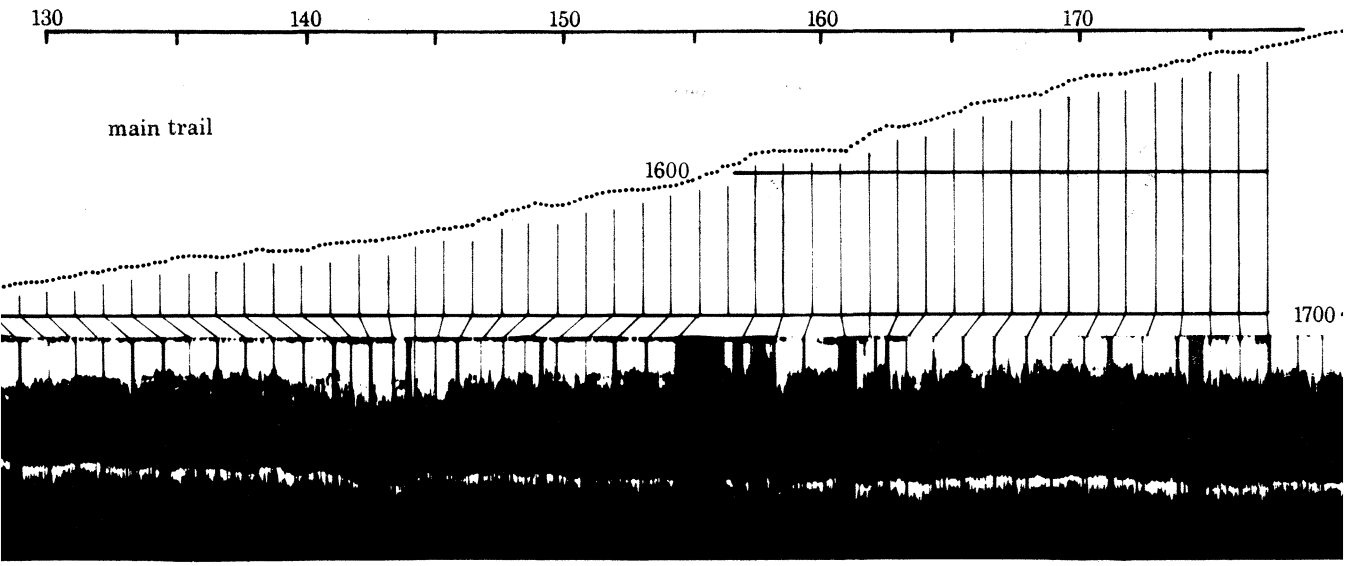
130
140
150
160
170
main trail
1600
1700

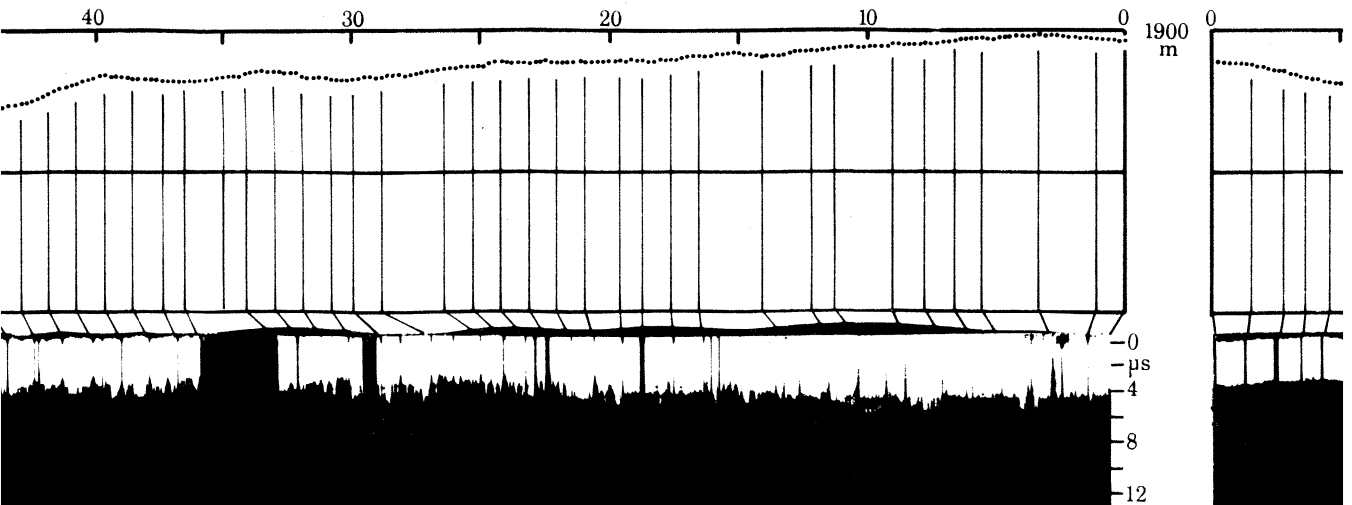
40
30
20
10
0
1900
m
0
0
μs
4
8
12

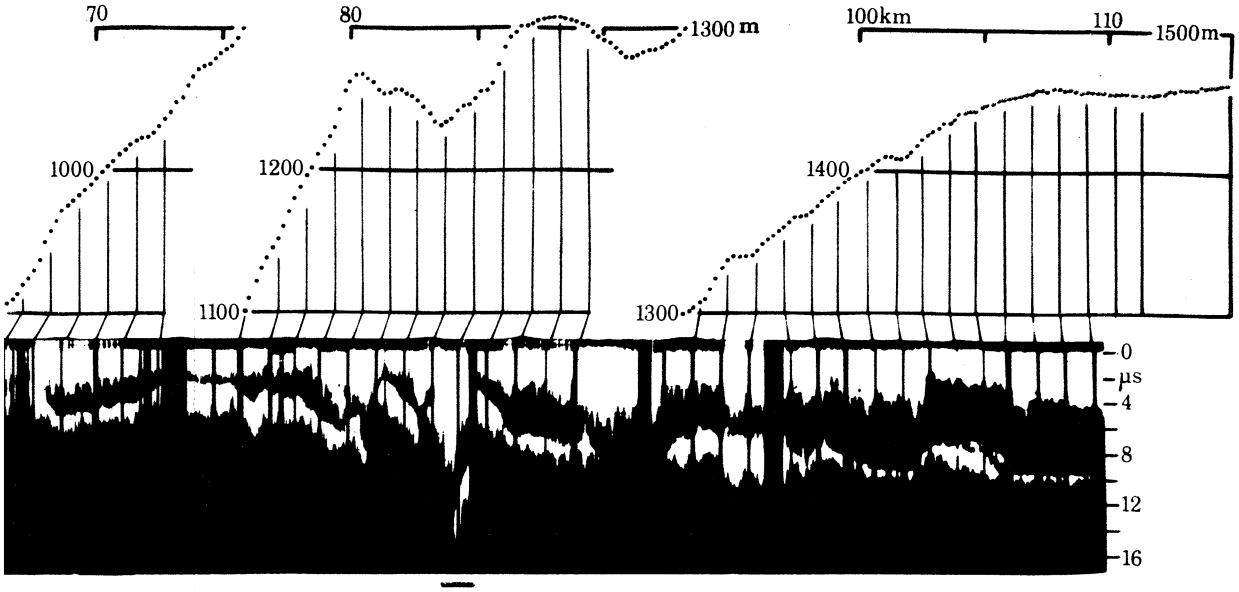

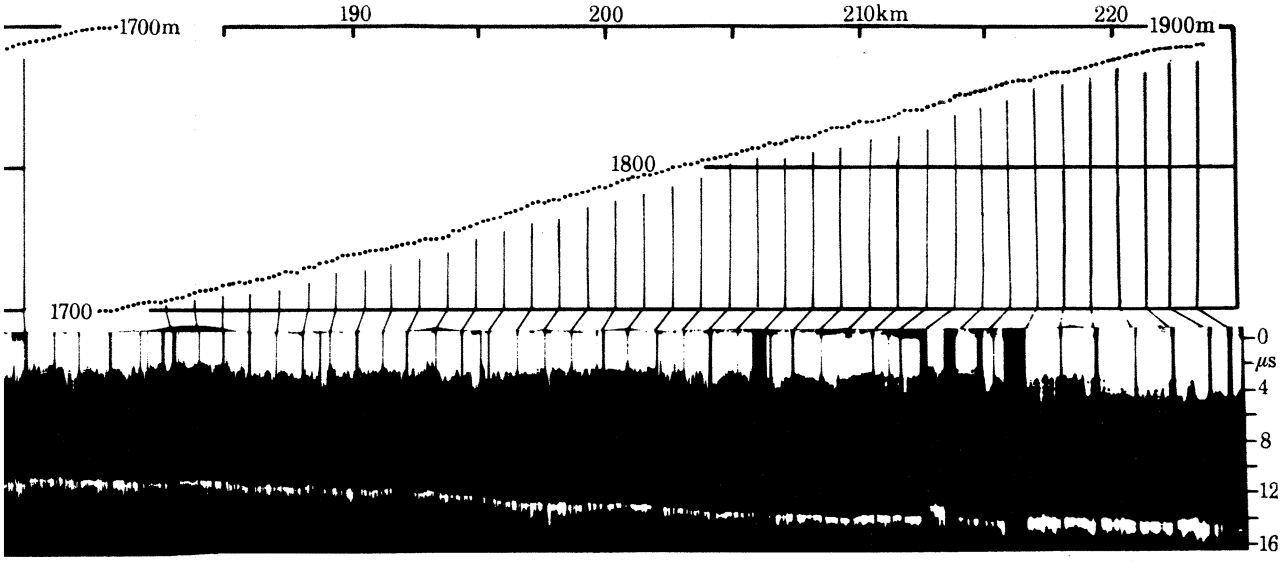

km from Century

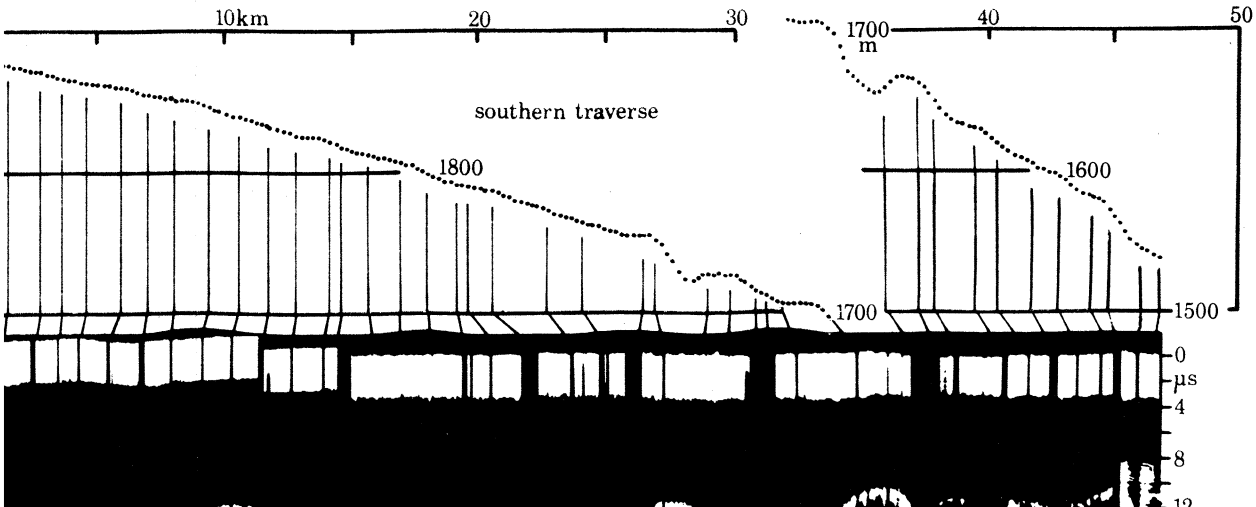


8
12
16

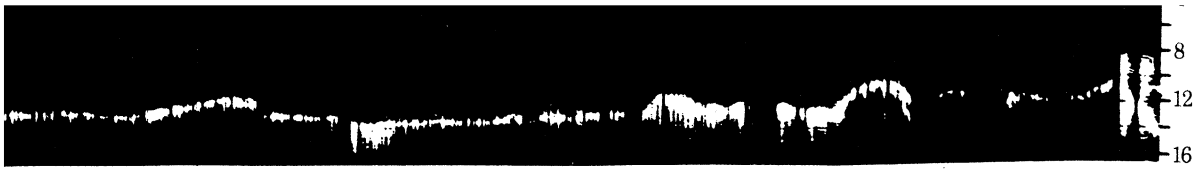

(*Facing p.* 505)

Nye, J. F. 1963 *J. Glaciol.* **4**, 785–788.
Orowan, E. 1949 *J. Glaciol.* **1**, 231–240.
Parkhomenko, E. I. 1967 *Electrical properties of rocks*. New York: Plenum Press.
Patterson, W. S. B. 1955 *Meddr Grønland* **137**, no. 1, 1–12.
Pearce, D. C. & Walker, J. W. 1967 *J. Geophys. Res.* **72**, no. 22, 5743–5747.
Radok, U. 1959 *Nature, Lond.* **184** (suppl. no. 14), 1056–1057.
Rice, S. O. 1945 *Bell Syst. Tech. J.* **24**, 46–156.
Rinker, J. N. 1965 *Polar Rec.* **12**, 403–405.
Robin, G. de Q. 1955 *J. Glaciol.* **2**, 523–532.
Robin, G. de Q. 1958 *Norwegian–British–Swedish Antarctic Expedition* 1949–52. *Scientific results*, vol. 5, *Glaciology* III. Oslo: Norsk Polarinstitutt.
Robin, G. de Q. 1964 *Endeavour* **23**, no. 89, 102–107.
Robin, G. de Q. 1967*a* *Annals I.G.Y.* **41**, 52.
Robin, G. de Q. 1967*b* *Nature, Lond.* **215**, no. 5105, 1029–1032.
Robinson, E. S. 1966 *J. Glaciol.* **6**, no. 43, 43–54.
Schytt, V. 1955 *U.S. Army S.I.P.R.E. Rep.* no. 28.
Schytt, V. 1958 *Norwegian–British–Swedish Antarctic Expedition*, 1949–52. *Scientific Results*, vol. 4, *Glaciology* II*C*, pp. 113–152. Oslo: Norsk Polarinstitutt.
Stratton, J. A. 1941 *Electromagnetic theory*. New York and London: McGraw-Hill.
Von Hippel, A. R. (ed.) 1954 *Dielectric materials and applications*. Cambridge, Mass.: Technology Press of M.I.T.; New York: John Wiley and Sons; London; Chapman and Hall.
Waite, A. H. 1966 *Can. J. Earth Sci.* **3**, 887–892.
Walford, M. E. R. 1964 *Nature, Lond.* **204**, 317–319.
Walford, M. E. R. 1965 Unpublished Ph.D. thesis. University of Cambridge (Scott Polar Research Institute).
Walford, M. E. R. 1968 *J. Glaciol.* **7**, no. 49, 89–94.
Weertman, J. 1957 *J. Glaciol.* **3**, no. 21, 33–38.
Weertman, J. 1968 *J. Geophys. Res.* **73**, 2691–2700.
Yoshino, T. 1961 *Antarctic Record (Tokyo)*, no. 11, 228–233.
Zotikov, I. A. 1961 *Inform. Bull. Soviet Antarctic Exped.* no. 28, 16–21.

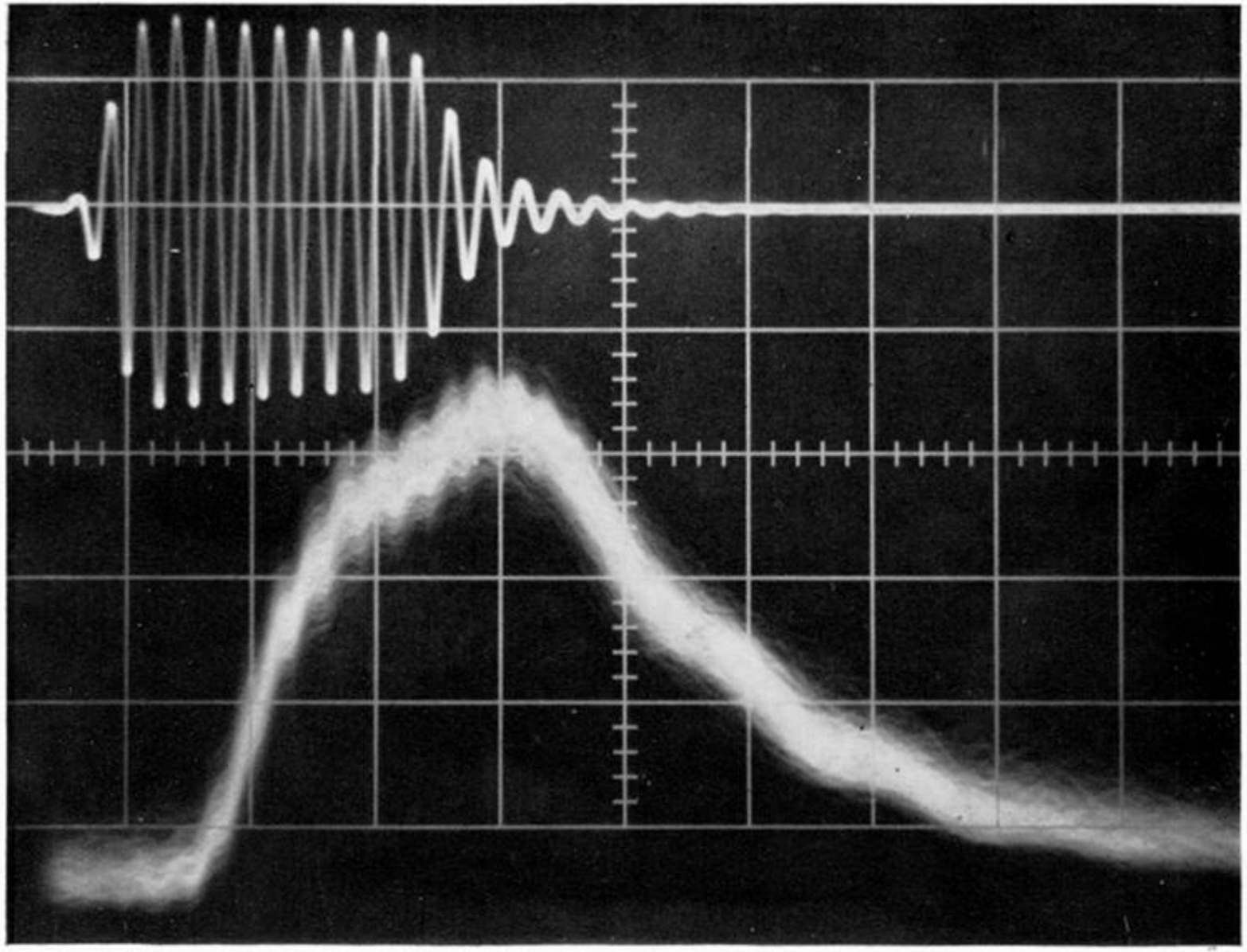

FIGURE 3. At the top, a direct oscillogram of the transmitter output feeding a dummy load. Below: the same pulse, on the same time scale, after attenuation to 15 dB above the input noise level and passage through the receiver. The horizontal scale occupies a total of 1 μs and the vertical scale of volts is arbitrary. The rise time, t_r, is defined as the time for the power to increase from 10 to 90 % of its peak value, and similarly for the fall time, t_f.

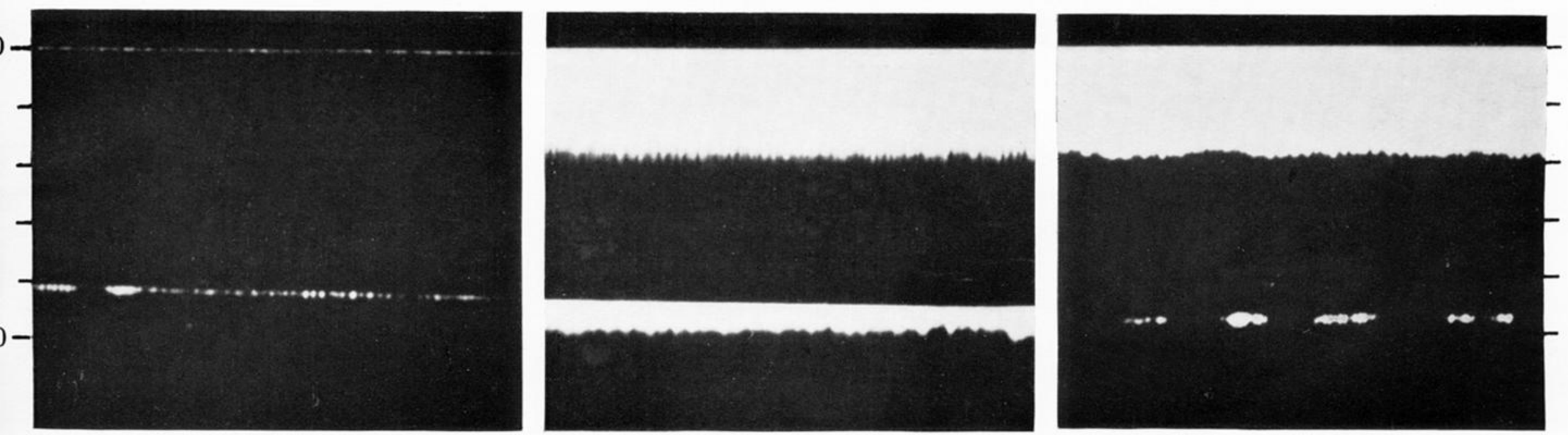

(*a*)

(*b*)

(*c*)

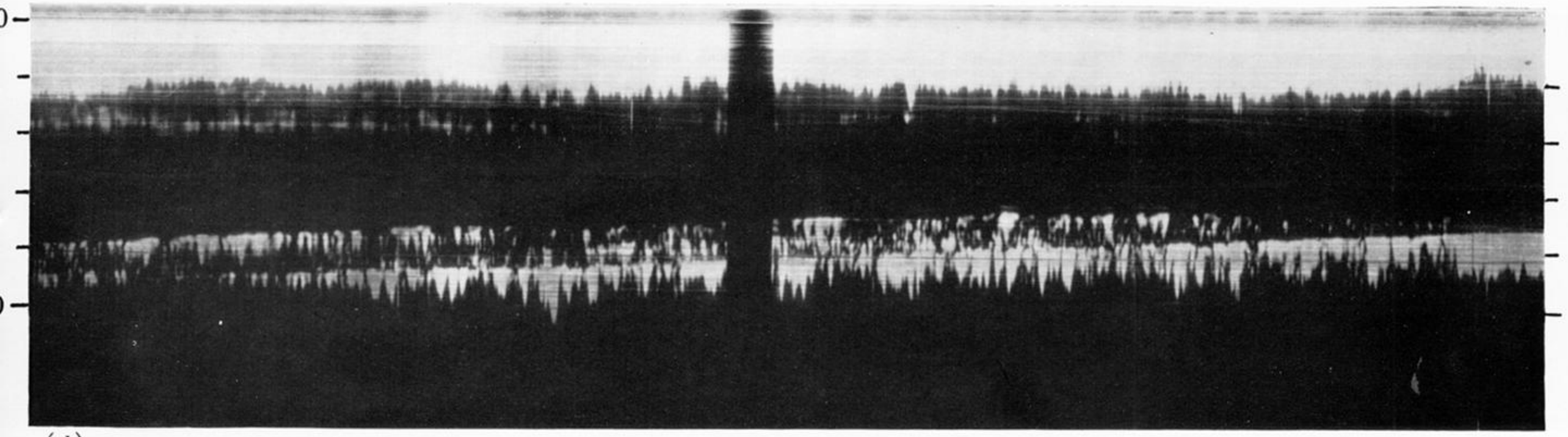

(*d*)

FIGURE 4. Sample echoes recorded on a moving vehicle. Echo delay is measured in microseconds vertically downwards from the zero which marks the arrival of the transmitter pulse at the receiver. (*a*) Single echo at approximately constant range, strength approximately equal to the transmitter break-through. (*b*) Strong clutter echoes following the transmitter pulse, a strong bottom echo showing the sharp leading edge and a varying trailing edge (*c*) Illustrating how a very intermittent bottom echo may be safely recognized by the continuity of the pattern in which it appears. (*d*) A sequence of echoes showing clutter, an isolated layer, and two or more bottom surfaces, both rough, and presumably seen at different angles to the vertical.

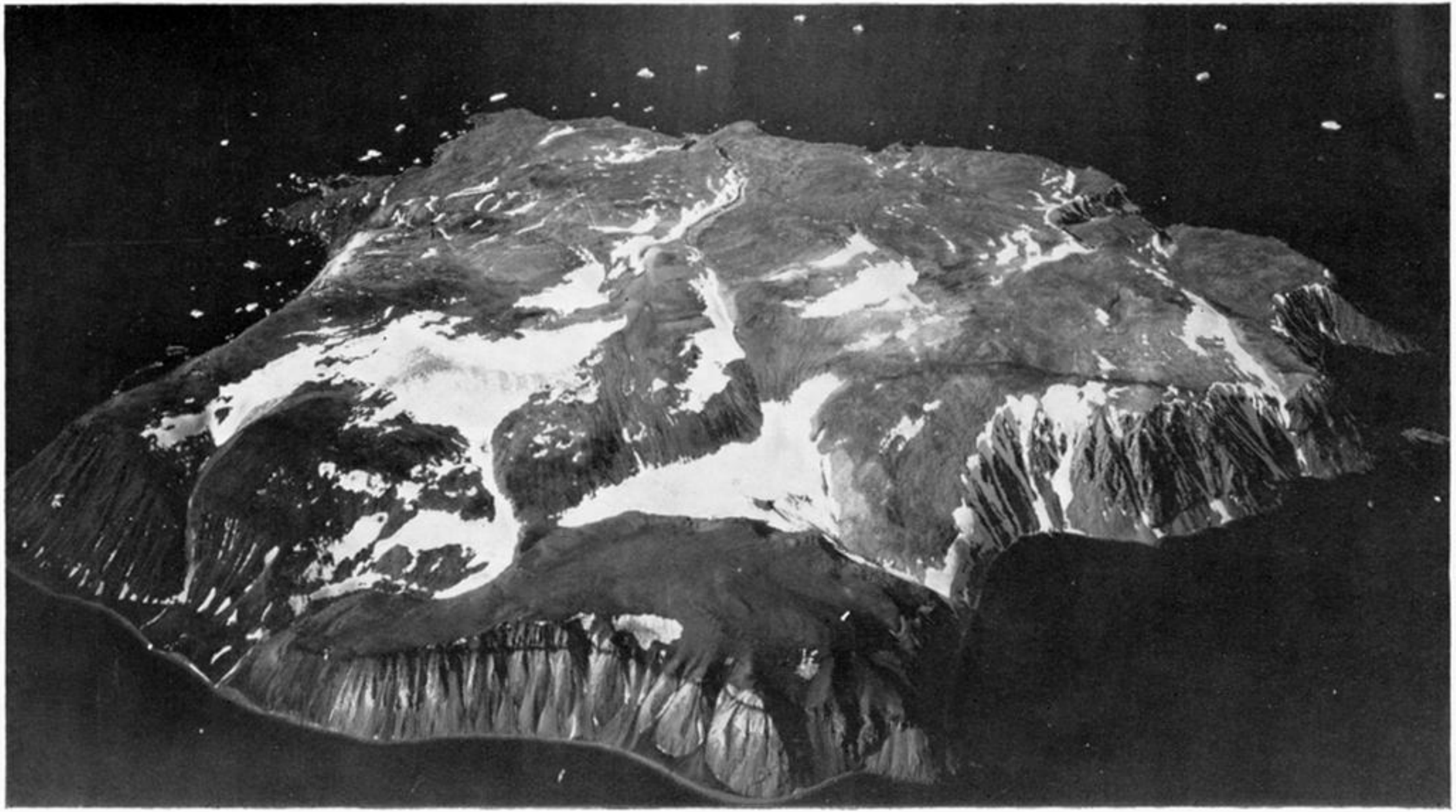

FIGURE 27

FIGURE 28

FIGURE 29

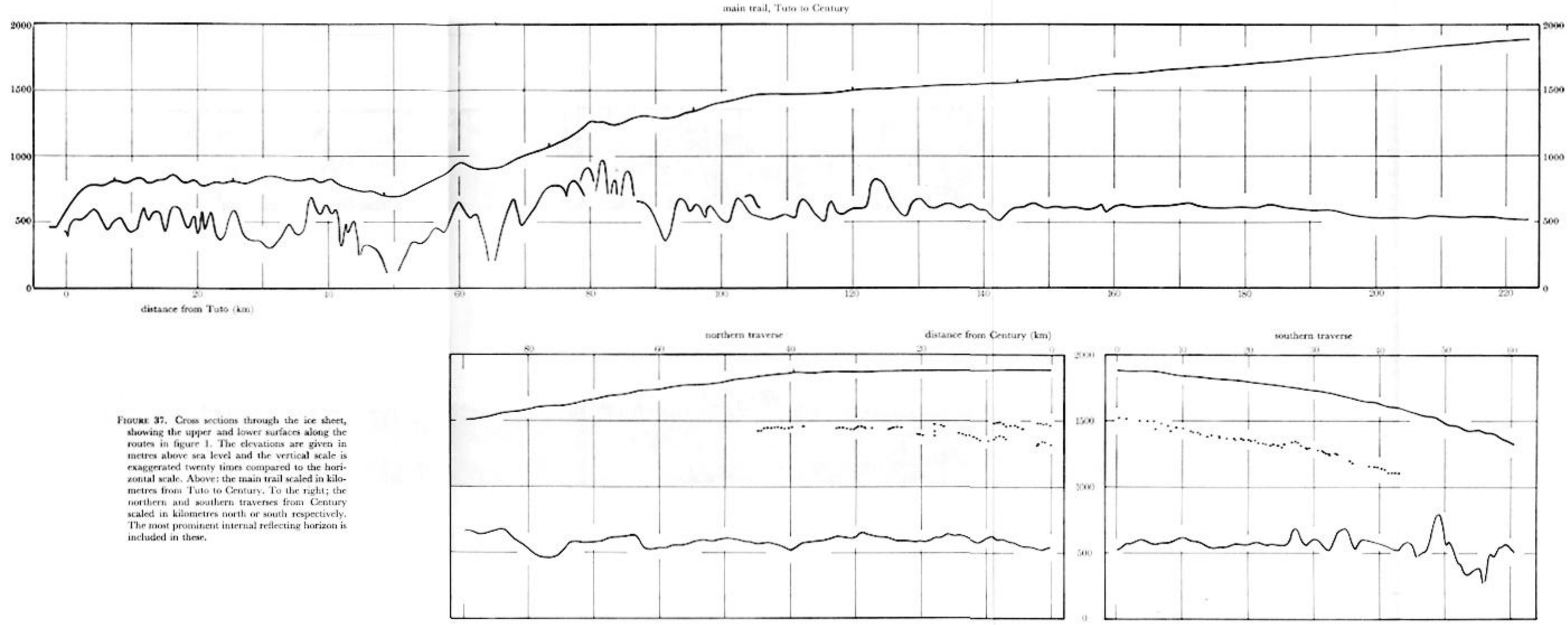

FIGURE 37. Cross sections through the ice sheet, showing the upper and lower surfaces along the routes in figure 1. The elevations are given in metres above sea level and the vertical scale is exaggerated twenty times compared to the horizontal scale. Above: the main trail scaled in kilometres from Tuto to Century. To the right; the northern and southern traverses from Century scaled in kilometres north or south respectively. The most prominent internal reflecting horizon is included in these.

(Facing p. 504)

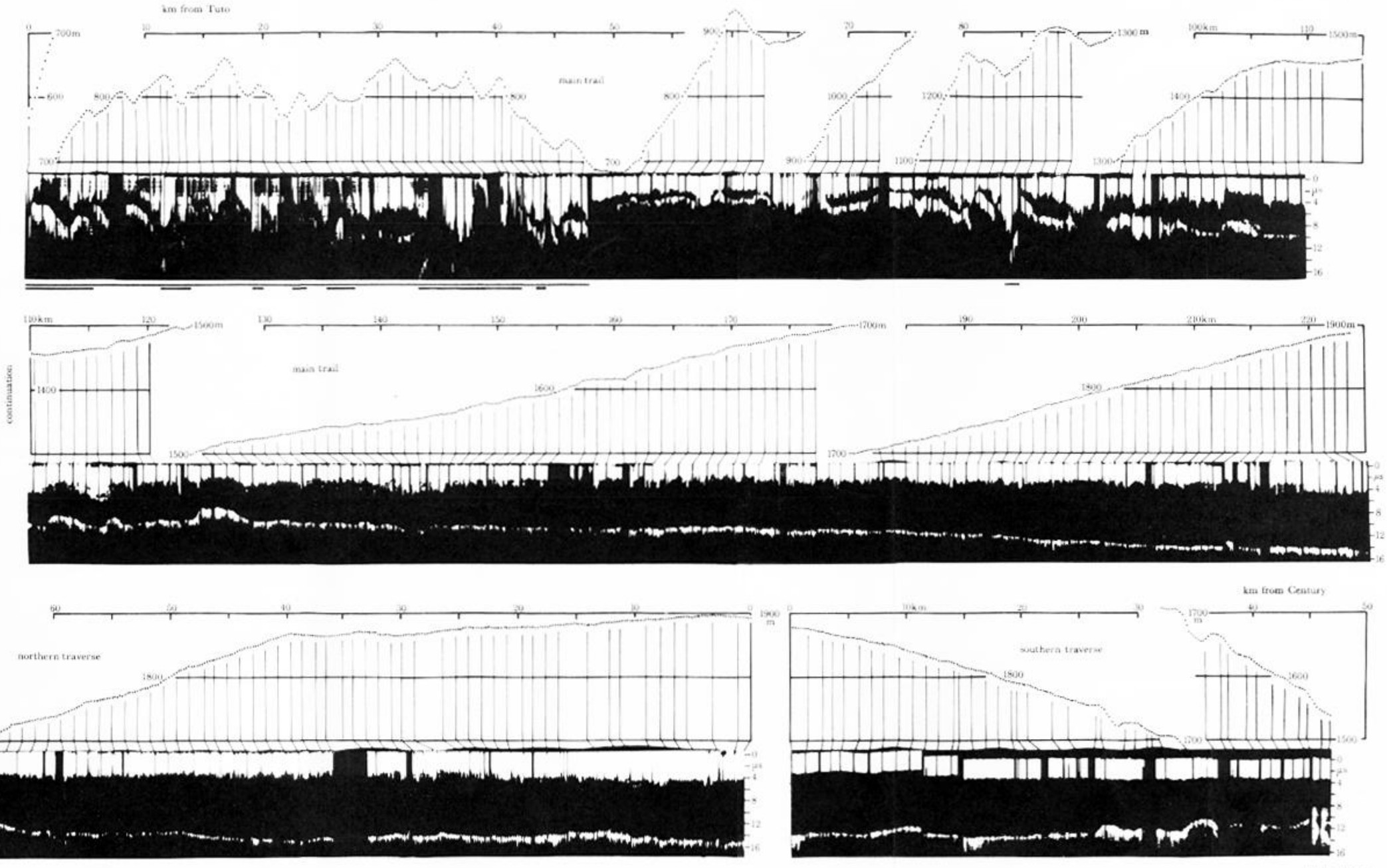

FIGURE 38. Detailed snow surface topography correlated with direct prints from the radio echo film records. Each elevation point represents a single reading of the aneroid altimeter. They are spaced horizontally at 220 m intervals along the trail and this representation faithfully conveys our knowledge of the smallest surface features. Individual points have been correlated with specific marks on the print below as explained in §7 (a). The scale of microseconds echo delay is given at the right hand end of each print. Note that the zero from which the echo time delay is to be measured at any point along the print should be identified with the top of the broad white band of clutter echoes. On the top print, between 0 and 86 km from Tuto on the main trail, there were changes in the time base sweep velocity used in the recording oscilloscope and these are indicated by the code below the print. For one bar the microsecond time scale should be halved and for two bars divided by four, so that the total sweep time is then about four microseconds. Internal echoes cannot be seen in this reproduction except near 150 km on the main trail and between 0 and 10 km on the northern traverse.

(Facing p. 393)